A KINETIC STUDY OF CHROMIUM ETCHING

BY

SATYAJIT NIMU GANGULI P.Eng

Department of Chemical Engineering
McGill University, Montreal Quebec

A thesis submitted to the Faculty of Graduate Studies and Research in partial fulfillment of the requirements for the degree of Master of Engineering.

McGill University
Montreal, Quebec

March, 1988

ISBN 0-315-46022-9

A KINETIC STUDY OF CHROMIUM ETCHING

S.N. GANGULI

ABSTRACT

The kinetics of the solid-liquid reactions occurring during the etching of chromium metal with an alkaline potassium permanganate solution was studied.

A rotational etcher was developed to determine the intrinsic rates of reaction. The characteristics of the chromium surface namely surface roughness, metal thickness uniformity and oxide composition along with the etchant solution parameters : [NaOH]; [$KMnO_4$]; [Cr^{+6}]; and temperature were investigated in order to determine the reaction mechanism and the intrinsic rate expressions.

The experimental results showed that the etching of chromium follows two consecutive solid - liquid reactions. The first reaction is related to the dissolution of the oxide layer and is governed by the following rate law:

$$r_1 \text{ (mmol Cr/m}^2\text{-s)} = 4.05 \times 10^8 \exp[-5.01 \times 10^4 / RT]\ C_{NaOH}$$

The second reaction is related to the dissolution of the underlying chromium metal and the intrinsic rate expression for this reaction at 43^0C is :

$$r \text{ (mmol Cr/m}^2\text{-s)} = 3.91\ C_{KMnO_4^-} - 53.61 C_{Cr^{+6}}$$

SOMMAIRE

L'étude a consisté en une analyse de la cinétique des intéractions solide - liquide lors du processus d'attaque chimique du chrome par un solution de permanganate de potassium alkaline.

Une graveuse rotative a été conçue pour déterminer les niveaux intrinséques des réactions propres à la solution. Plus particuliérement, l'étude a porté sur la charactérisation du chrome au niveau de la rugosité de surface, de l'épaisseur du métal et la composition de l'Oxyde de chrome, et au niveau des facteurs chimiques c'est-à-dire [NaOH], [$KMnO_4$], [Cr^{+6}] et la température en relation avec le niveau de réaction chimique du metal.

Les résultats expérimentaux ont démontrés que l'attaque chimique du chrome découle de deux réaction solide-liquide consécutives. La premiére réaction qui est reliée à la dissolution de l'Oxyde (Cr_2O_3), est définie par l'expression suivante:

$$r_1 \ (\text{mmol Cr}/m^2\text{-s}) = 4.05 \times 10^8 \exp[-5.01 \times 10^4 / RT] \ C_{NaOH}$$

La dieuxieme réaction quant à élle est reliée à la dissolution de couche inférieure de chrome est définé par cette seconde formule à 43 ^{0}C:

$$r \ (\text{mmol Cr}/m^2\text{-s}) = 3.91 \ C_{KMnO_4^-} \ 53.61 C_{Cr^{+6}}$$

ACKNOWLEDGEMENTS

I would like to thank the management at IBM Canada Ltd Bromont Manufacturing Plant for allowing me the opportunity to conduct this research using their extensive resources. I would particularly like to thank my manager Jean Dufresne for allowing me to take the necessary time off from work in order to conduct the research work.

I would like to express my sincere appreciation to my research supervisor Dr. Dimitrios Berk for his technical guidance and valued advice during the course of the experimental research.

I would like to give special mention to Clement Fortin of IBM Bromont's Quality Laboratory for his work in producing the S.E.M. cross sections used in chapter 4 of this thesis. Also Mike Safoniuk for his effort in producing the polished chromium tiles used in the etching experiments and the members of the reaction engineering research group : David Mulligan and John Sarlis for their technical input.

I would like to thank IBM Canada Ltd and the Natural Sciences and Engineering Research Council of Canada for their financial support.

Finally I would like to thank my family and friends for their support during the course of my research work.

TABLE OF CONTENTS

		Page
Chapter 1. Introduction		1
Chapter 2. Characterization of the Etchable Surface		
2.1	Introduction.....	6
2.2	Materials and Methods	6
2.3	Results and Discussion	12
2.4	Conclusions	20
Chapter 3. Kinetic Study of Chromium Etching		
3.1	Introduction.....	24
3.2	Materials and Methods	25
3.3	Results and Discussion	28
3.4	Conclusions	55
Chapter 4. Chrome and Copper Etch Profiles		
4.1	Introduction	57
4.2	Materials and Methods	58
4.3	Results and Discussion	61
4.4	Conclusions	72
Chapter 5. Overall Conclusions and Recommendations		78
References		82
Appendicies :		
A.1	Data for Chapter 2	84
A.2	Data for Chapter 3	88
A.3	Data for Chapter 4	97
A.4	Statistical Analysis of Data	98

LIST OF FIGURES

		Page
1.1	Levels of Metallurgy on a Ceramic Substrate ..	3
2.1	Thickness Measurement Grid Pattern	9
2.2	Calculation of Surface Roughness	10
2.3	Metal Thickness Variation of Base Cr on Glass.	13
2.4	Metal Thickness Contour of Base Cr on Glass ..	13
2.5	Metal Thickness Variation of Cu on Glass.....	14
2.6	Metal Thickness Contour of Cu on Glass	14
2.7	Metal Thickness Variation of Top Cr on Glass .	15
2.8	Metal Thickness Contour of Top Cr on Glass ...	15
2.9	Comparison of Surface Roughness of Cr and Cu on Glass Slides and Ceramics	17
2.10a	ESCA Broadscan of Chrome on Ceramic	19
2.10b	ESCA Broadscan of Chrome on Glass	19
2.10c	ESCA Broadscan of Chrome Tile	19
2.11a	ESCA Scan of Chrome Region on Ceramic	21
2.11b	ESCA Scan of Chrome Region on Glass	21
2.11c	ESCA Scan of Chrome Region on Tile	21
2.12a	ESCA Scan of Oxygen Region of Cr on Ceramic...	22
2.12b	ESCA Scan of Oxygen Region of Cr on Glass	22
2.12c	ESCA Scan of Oxygen Region of Cr on Tile	22
3.1	Variation in Amount of Cr Etched with Time ...	29
3.2	Variation of Cr Etch Rate with Agitation Rate.	32
3.3	Variation of Cr Etch Rate with Surface Roughness	34
3.4	Variation of Surface Roughness with Etch Time.	36
3.5	Pourbaix Diagram of MnO_4^{-1} / Cr System	40
3.6	Variation in Initial Rate with Concentration of NaOH	44
3.7	Variation of Initial Etch Rate with [NaOH]: Experimental vs Models	46
3.8	Variation in Cr Etch Rate with Concentration of $KMnO_4$	47
3.9	Variation in Cr Etch Rate with Concentration of Chrome	48
3.10	Variation in Cr Etch Rate with [$KMnO_4$]: Experimental Versus Models	50
3.11	Variation in Cr Etch Rate with [CrO_4^{-2}]: Experimental Versus Models	51
3.12	Arrhenius Plot for Initial Rate vs Temperature	53
3.13	Arrhenius Plot for Cr Rate vs Temperature	54
4.1	Comparison of Etch Profiles	70

LIST OF PLATES

		page.
Plate 3.1	Chrome Tile Surface After 60 sec Etch	38
Plate 3.2	Chrome Tile Surface After 300 sec Etch	38
Plate 4.1a	Spray Etched Electrodes at Etch Times of Cr/Cu/Cr of 60/30/60 Seconds	63
Plate 4.1b	Etched Electrodes at Etch Times of Cr/Cu/Cr of 60/30/60 Seconds	63
Plate 4.2	Etched Electrodes at Etch Times of Cr/Cu/Cr of 60/60/60 Seconds	64
Plate 4.3	Etched Electrodes at Etch Times of Cr/Cu/Cr of 30/90/30 Seconds	64
Plate 4.4	Etched Electrodes at Etch Times of Cr/Cu/Cr of 30/30/30 Seconds	66
Plate 4.5	Etched Electrodes at Etch Times of Cr/Cu/Cr of 30/30/60 Seconds	66
Plate 4.6	Etched Electrodes at Etch Times of Cr/Cu/Cr of 90/60/90 Seconds	67
Plate 4.7	Etched Electrodes at Etch Times of Cr/Cu/Cr of 90/90/30 Seconds	67
Plate 4.8	Etched Electrodes at Etch Times of Cr/Cu/Cr of 90/90/90 Seconds	68
Plate 4.9	S.E.M. Cross Section of 25 um Electrode Spray Etched at Cr/Cu/Cr Etch Times of 60/30/60 Sec.	71
Plate 4.10	S.E.M. Cross Section of 25 um Electrode Rotationally Etched at Cr/Cu/Cr Etch Times of >30/<30/>30 Seconds	73
Plate 4.11	S.E.M. Cross Section of 50 um Electrode Rotationally Etched at Cr/Cu/Cr Etch Times of >30/<30/>30 Seconds	74
Plate 4.12	S.E.M. Cross Section of 25 um Electrode Rotationally Etched at Cr/Cu/Cr Etch Times of >30/>60/>30 Seconds	75
Plate 4.13	S.E.M. Cross Section of 50 um Electrode Rotationally etched at Cr/Cu/Cr Etch Times of >30/>60/>30 Seconds	76

NOMENCLATURE

r_i : Initial rate in mmol Cr / m^2-s

r : Rate of Cr etching in mmol Cr / m^2-s.

C_a : Concentration of NaOH in etchant (mol /L)

C_b : Concentration of KMnO in etchant (mol/L).

C_c : Concentration of Cr in etchant (mol/L).

U : Undercut - which is defined as the difference between the resist width (Wr) and the metal width (Wm).

Ra : Surface roughness (μm).

T_1 : Top chrome etch time (s).

T_2 : Copper etch time (s).

T_3 : Base chrome etch time (s).

CHAPTER 1

INTRODUCTION

The use of alumina ceramics as chip carriers in component manufacturing is a well-established technology. In the last several years the advances in integrated circuit fabrication has led to a cheaper silicon chip; thus the cost of packaging has become greatly influenced by the cost of fabricating the ceramic substrate. In response to this, new packaging techniques have been developed to reduce the cost of the substrate chip carrier. For example, methods such as Tape Automated Bonding [1] employ chemically etched copper fingers embedded in a polymer film as the chip carrier instead of an alumina ceramic. Another method uses plastic molded technology [2] which involves the use of epoxy resin molded to a lead frame chip carrier. However several limitations to these methods such as low I/O count and inefficient heat dissipation, keep the ceramic substrate chip carrier still a viable technology.

One way to reduce the cost of the ceramic chip carrier is to understand in greater depth the various processing stages involved in the manufacturing of the substrate. With the understanding comes process improvement leading to yield improvement and reduction in rework and recycle.

The chemical etching of metals is an established process in the engraving, the metal finishing and the microelectronics industry. In the production of metallized ceramic substrates, it is one of the most important processing steps since the final circuit dimensions are defined at this stage. The first

step in the manufacturing of metallized ceramic substrates is to coat the ceramic with three layers of metal as shown in figure 1.1. The chromium 600-1300 Å thick forms the protective (top chrome) and adhesion (base chrome) layers for the copper (> 70 000 Å thick) which is the metal that forms the final circuit on the substrate. Etching of the metal layers is usually performed in a spray etcher. This type of etcher uses spray action to deliver the etchants to the substrate surface where the dissolution of the unprotected metal takes place. The dissolved metal ions are then transferred to the bulk etchant solution.

The ceramic substrate which forms the physicial interface between the microchip and the printed circuit board is produced by a photo lithographic process which essentially consists of the following steps:

1. Deposition of three metal layers (Cr^0, Cu^0, Cr^0) by a low pressure sputtering technique. The ceramics after this step are called blanket ceramics.
2. Application of photosensitive resin and exposure of this resist layer through a mask using U.V. light. At this stage the substrate has resin that is polymerized where circuitry is present and unpolymerized in the unexposed areas. The exposed resin is more resistant to the chemical etchants than the unexposed resin.
3. Development of the resist. In this step, the unpolymerized resin is removed leaving behind a substrate ready to be etched to obtain the final circuit pattern.

There are several solid-liquid reactions occurring in the etch process: The dissolution of chromium with an alkaline potassium permanganate solution and the dissolution of

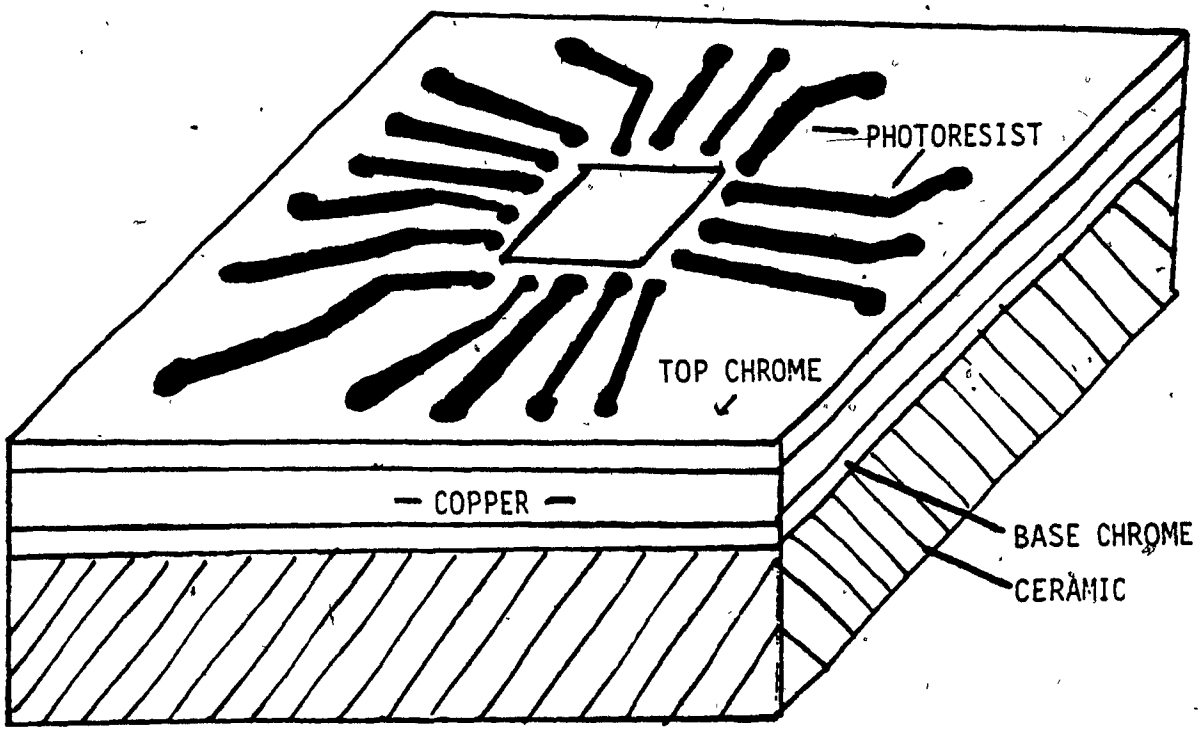

Figure 1.1 Levels of Metallurgy on a Ceramic Substrate.

copper with a ferric chloride etchant solution. Although the kinetics of the reaction of copper with ferric chloride are known [3,4,5], that of chromium with a potassium permanganate etchant is not an extensively studied reaction. Kinetic rate data for this reaction, which is not only important to the etching of metallized ceramics, but also in the production of chromium photomasks [6], and in the etch-back process for metal finishing [7], is non-existant in the open literature.

The objectives of the research work are as follows:

1. To investigate the properties of the etchable surface such as metal thickness uniformity, surface roughness, and oxide composition, which will directly influence the rate of etching.
2. To develop an understanding of the mechanism when chromium metal reacts with an alkaline solution of potassium permanganate.
3. To determine the intrinsic rate laws for the reactions taking place during chromium etching by defining the effects of the [NaOH], [$KMnO_4$], [Cr^{+6}], and temperature on the etch rate.
4. To compare the dimensional profiles of the circuit electrodes when the etching is carried out in a spray etcher and in the rotational etcher developed in this project.

With the information obtained from meeting the research objectives the etching of metallized ceramic substrates which takes place at IBM Canada's Bromont manufacturing plant will be completely defined. The understanding of the process will be at a point where process windows can be redefined in order to improve the product yield and enable the implementation of a

continuous chemical control system that automatically adjusts the etchant parameters to maintain optimal etch rates.

The contents of this thesis are divided into three distinct chapters. Chapter 2 is devoted a discussion on the characterization of the metal surfaces. Chapter 3, is devoted to the kinetic study of chromium etching. The reaction mechanisms for the dissolution of the metal as well as the intrinsic rate laws are determined based on experimental data. The properties of the etchant solution and the physical properties of the etchant system that affect the etch rate are also investigated. Chapter 4 is devoted to the application of the results in Chapters 2 and 3 to the etching of actual circuit patterns. Statistical models are proposed to describe the effect of the chromium and copper etch times on the resist undercut.

CHAPTER 2

CHARACTERIZATION OF THE ETCHABLE SURFACE

2.1 Introduction

The purpose of this chapter is to discuss the properties of the metal surface that can influence the rate of chromium etching. The measurement of surface roughness is made to determine how the roughness of the virgin ceramic affects the thickness variation and roughness of the deposited metal layers. ESCA (Electron Spectroscopy for Chemical Analysis) is used to determine the composition of the oxide layer that is known to exist on the surface of chromium and its approximate thickness. In summary the objectives of the investigation described in this chapter are to characterize the etchable surface in terms of :

a. The surface roughness of the metallized layers on ceramic and glass.

b. The uniformity in the metallization of Cr^0 and Cu^0.

c. The composition and approximate thickness of the oxide layer on the chromium surface.

2.2 Materials and Methods.

A. Metallized Substrate Preparation.

The experiments in this research work used two types of chromium sources :

1) Chromium tiles (99.99 % pure) which were

purchased from Aysar Co. and polished to the desired surface roughness;

2) Metallized ceramics used in the experiments of this section and in the modeling experiments of chapter 4.

Alumina ceramics (28mm x 28mm x 1.2mm) and glass slides were metallized at about 250°C and 1 mtorr at IBM Bromont Manufacturing plant using a standard production scale ULVAC Sputter machine. The machine is designed to metallize three layers of metal on the same substrate. Firstly the base chrome layer is deposited to provide adhesion between the copper layer and the ceramic. Secondly, a copper layer which is about 100x thicker than the base chrome layer is deposited. Finally, another chomium layer is deposited on top of the copper to provide oxidation protection of the copper and to provide a layer onto which photoresist can adhere. Glass slides were metallized in the same manner. The thin metal films on the glass slides have a lower surface roughness (and consequently less background noise during thickness measurement) than metallized ceramics.

B. Thickness Measurement.

An Alpha Step 200 profiler described in [8] was used to measure the variation in the thickness of the deposited metal films on the glass slide. After deposition of the three metal layers, a grid pattern was painted onto the surface of the top chrome by means of a fine brush. Apeizon Wax (a petroleum distillate) was used to protect the metal under the grid lines. After the grid was formed, the slide was dipped in concentrated HCL (37% /w) to remove the unprotected chromium

lines exposing the copper surface. After the part was rinsed with distilled water and air dried, it was dipped in trichloroethylene to remove the wax. The thickness of the undissolved, exposed chromium lines was measured at the 25 intersection points on the grid shown in figure 2.1. Five measurements were made at each point from different directions to get a statistical average. A similar procedure was used to measure the thickness of the copper and bottom chrome. The unprotected copper layer was removed with concentrated HNO_3. The Alpha Step 200 was calibrated using standards that have the same range in thickness as the thickness being investigated (500-1500 Å and 65-80$\times 10^3$Å). The accuracy of the instrument was 2%.

C. Surface Roughness Measurement.

The Alpha Step 200 profiler was used to measure the surface roughness of the following:

a. Ceramic, base Cr^0 on ceramic, Cu^0 on base Cr^0, top Cr^0 on Cu^0.

b. Glass slide, base Cr^0 on glass, Cu^0 on base Cr^0, top Cr^0 on Cu^0.

c. Chromium tiles at various degrees of polishing.

The instrument is equipped with a 21mg stylus which records the height of the peaks and valleys of the surface of the metal. In each sample 10 readings were taken at random areas over the sample surface. For these measurements the scan time was set at 8 s and the scan length at 400 μm. The arithmetic average of the surface was determined by averaging all the deviations from the arithmetic mean height (figure 2.2).

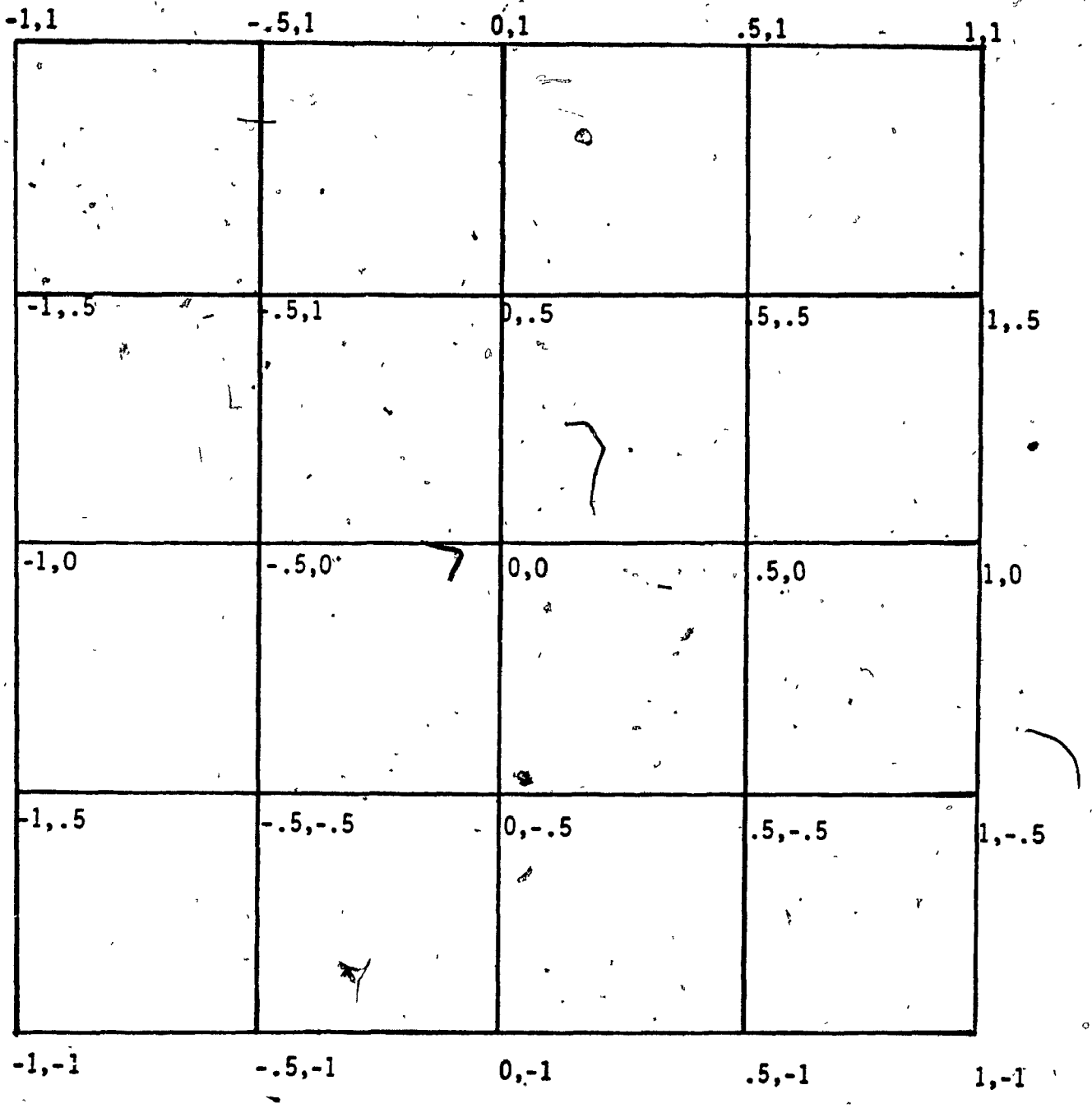

Figure 2.1 Thickness Measurement Grid Pattern.

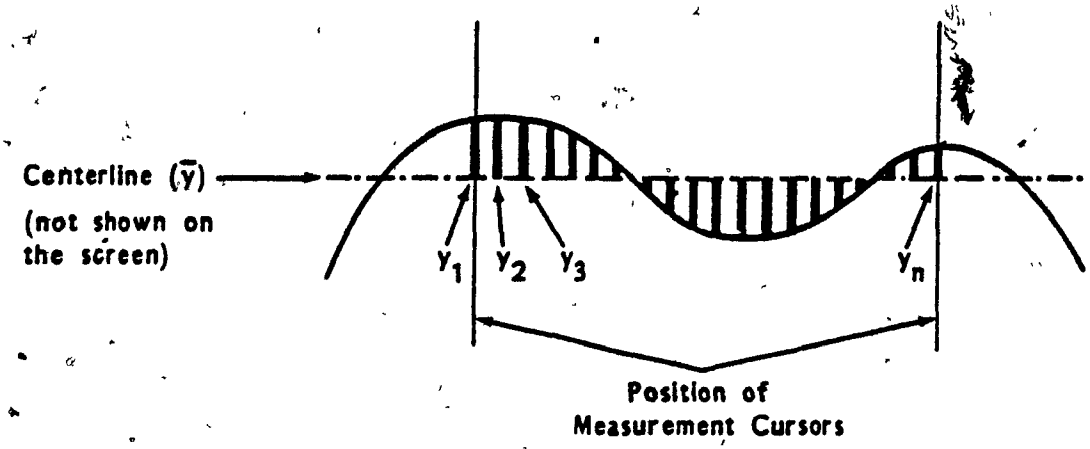

$$Ra = \frac{y_1 + y_2 + y_3 + \cdots + y_n}{n}$$

where

y_1 through y_n = the absolute value of the difference between the profile height and $\bar{y}$ for each point between the measurement cursors. (This is the deviation from the centerline.)

$\bar{y}$ = the profile heights at the points between the measurement cursors summed together and divided by n. (The profile heights are relative to the first point of the scan.)

n = the number of points between the measurement cursors.

Figure 2.2 Calculation of Surface Roughness.

D. Determination of Chromium Oxide Composition.

The nature and composition of the oxide on the chromium surface was determined using ESCA. The actual measurements were performed at the "Groupe de Recherche et Technologie des Couches Minces" at Ecole Polytechnique in Montreal. The samples being tested were:

Base chrome on ceramic (B2);

Top chrome on glass (G1);

Pure chromium tiles (T1).

In addition to a broadscan of each sample surface at 0 to -1000 eV binding energies, a scan from -537 to -525 eV for the oxygen peaks, and a scan from -568.4 to -581.6 eV for the chromium / chromium oxide peaks were done.

Using the information from the scan results, which are described in terms of the percentage of the total scan area related to a specific element, for the oxygen and chromium region, the ratio of oxygen to chromium in the oxide was obtained from the following equation:

$$\frac{n_O}{n_{Cr}} = \frac{I1}{I2} \frac{S2}{S1} \qquad (2.1)$$

where I1 and I2 : Area of the peak for oxygen and chromium.
S1 and S2 : Sensitivity factor for oxygen and chromium.

Samples of metallized ceramics were produced using the the procedure described in 2.2A. The samples were not cleaned by any degreasing solvent nor by any degassing prodecure so as not to disturb the oxide layer on the surface.

2.3 Results and Discussion

A. Metal Thickness Variation

The purpose of these experiments was to study what thickness irregularities can exist on sputter deposited metals. Glass slides were chosen as the substrate for deposition because of their relative smooth surfaces. In fact no significant thickness variation was measured on the unmetallized glass slide. The results of the variation of the thickness of sputtered copper and chromium layers are shown in figures 2.3 through 2.8. Figures 2.4, 2,6 and 2.8 show the thickness contours on the 28mm by 28mm substrate surface.

Inspection of the contours shows that the base chrome and copper have a similar surface topograpy while the top chrome is deposited unevenly onto one side. This last observation was made on several samples taken randomly from a sputter carrier. The minimum thickness in all three cases is at an edge of the part that is in contact with the track of the carrier. This is a metal strip that holds the parts in the sputter carrrier during metal deposition. It seems that shielding of the substrate by the track results in an uneven deposition of the

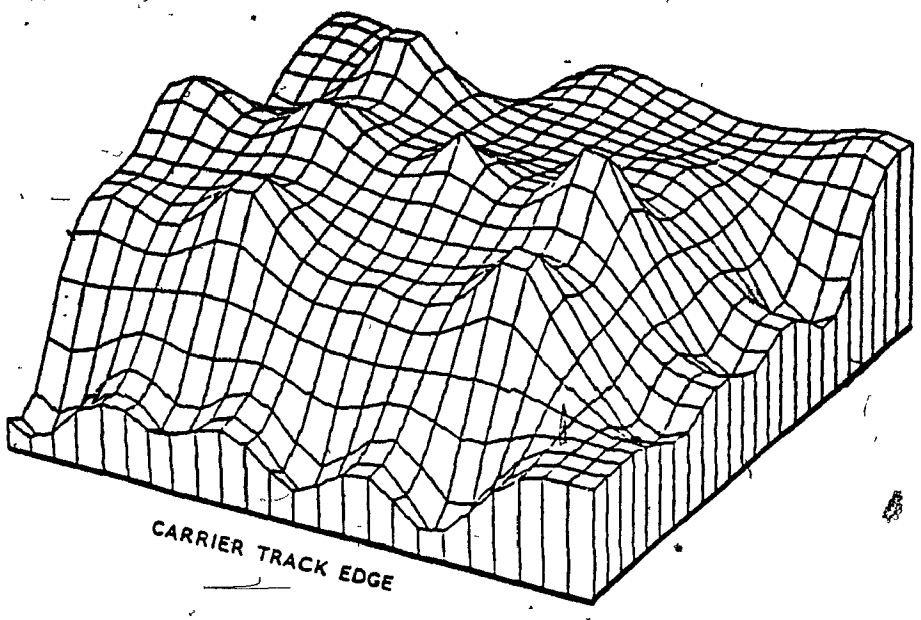

Figure 2.3 Metal Thickness Variation of Base Chrome on Glass.

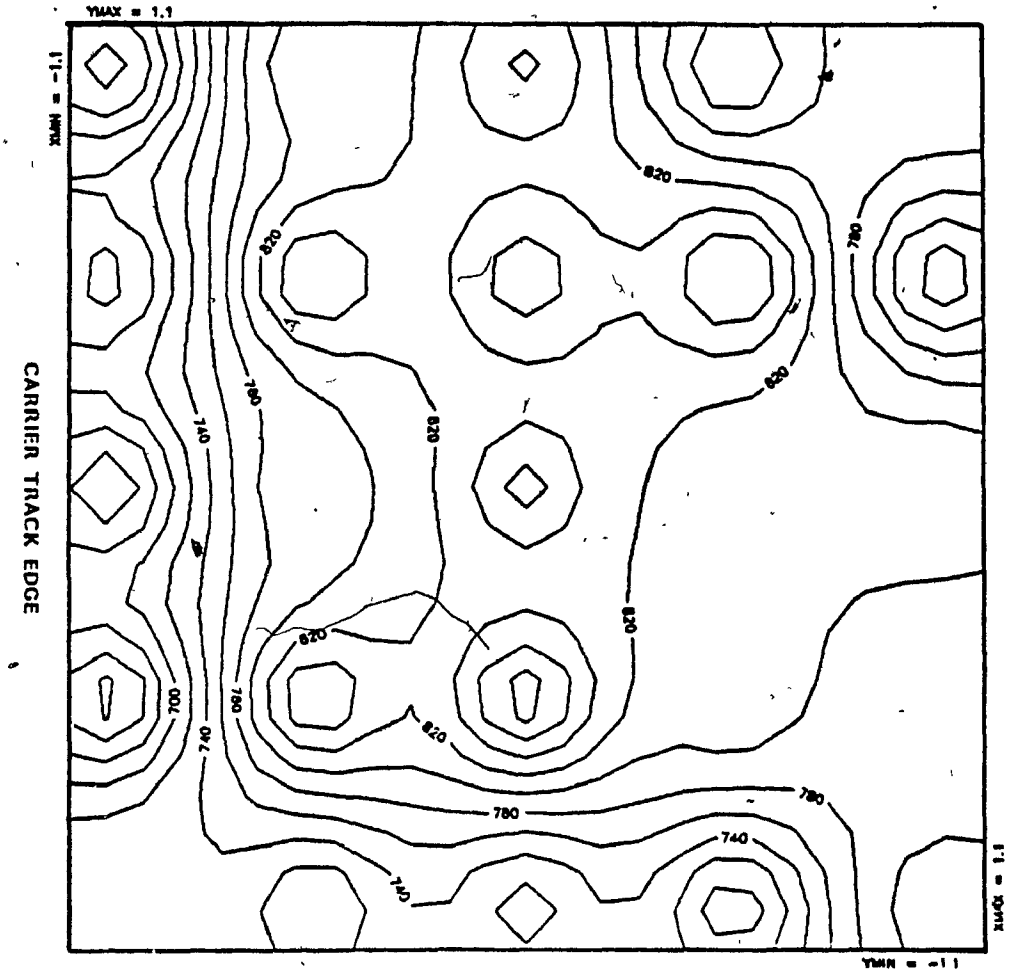

Figure 2.4 Metal Thickness Contour of Base Chrome on Glass. (Contour Interval = 20 Angstroems)

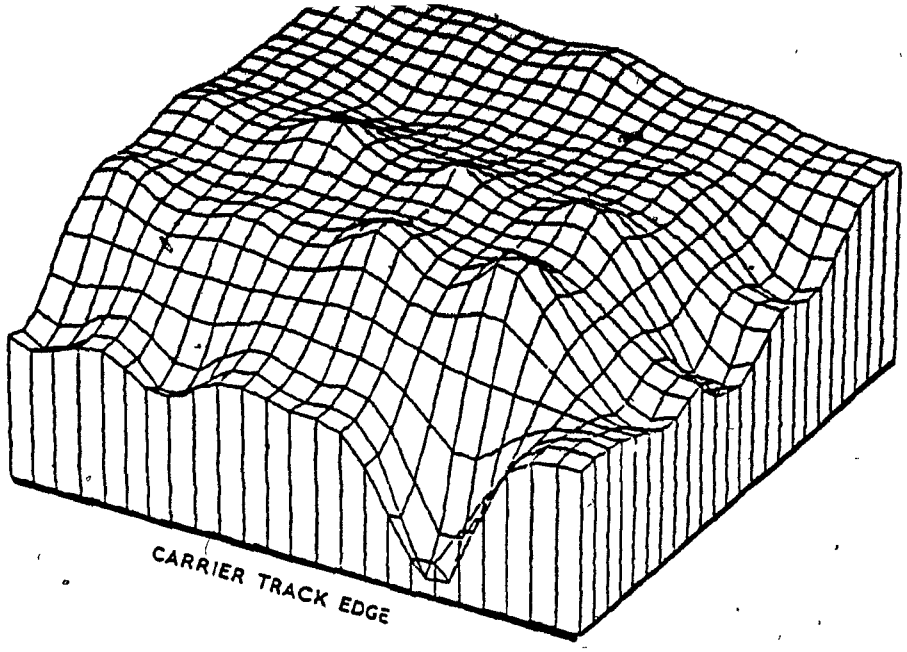

Figure 2.5 Metal Thickness Variation of Copper on Glass.

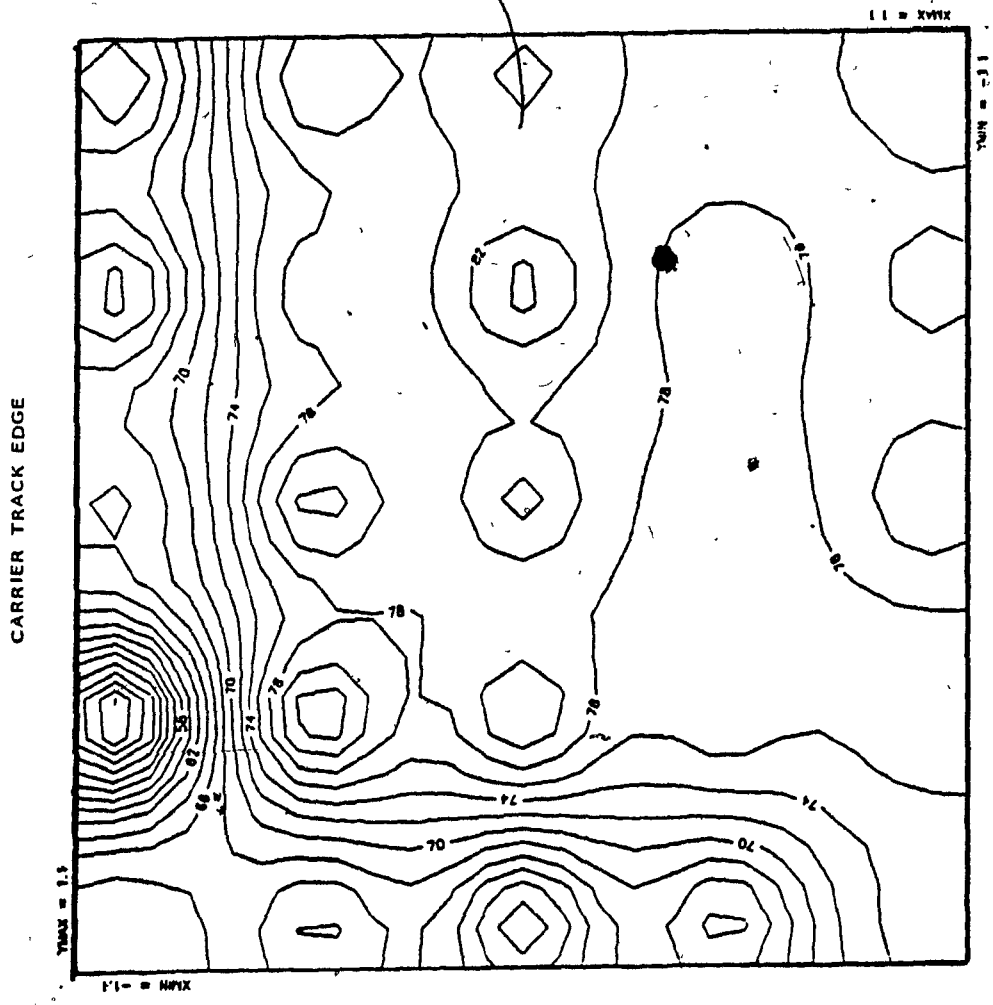

Figure 2.6 Metal Thickness Contour of Copper on Glass.
(Contour Interval = 2 KiloAngstroems)

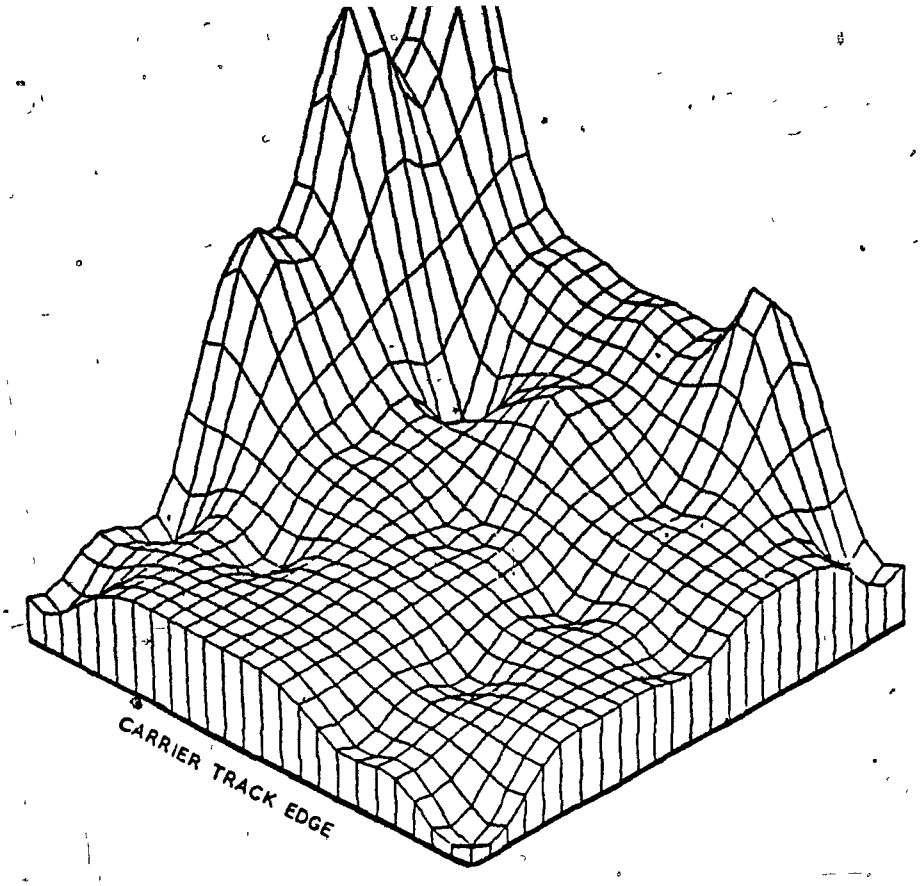

Figure 2.7 Metal Thickness Variation of Top Chrome on Glass.

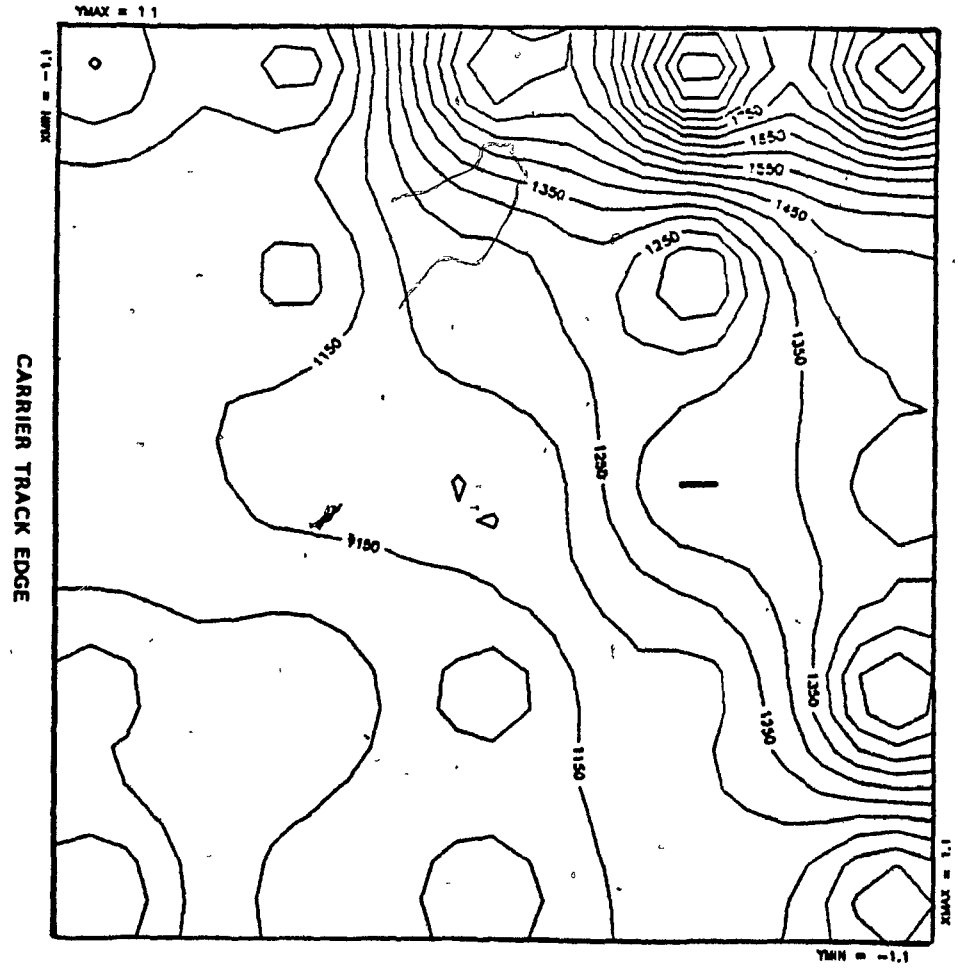

Figure 2.8 Metal Thickness Contour of Top Chrome on Glass.
(Contour Interval = 50 Angstroems)

metal. The average thickness for the top chrome, copper and base chrome are 1224 Å, 74 kÅ, 776 Å respectively. The respective standard deviations are 295 Å, 11 kÅ, and 85 Å. The range in thickness is respectively : 1070 Å, 42 kÅ, and 237 Å.

Figures 2.3, 2.5, and 2.7 give a 3 dimensional qualitative depiction of the metallization on the surface. The base chrome has the roughest appearance over the entire surface while the top chrome is open to more random metallization over the surface than the other two layers. The random metallization may be occurring while sputtering the base chrome layer but the deposition of the copper has the effect of smoothening out some of the peaks on the base chrome surface. The copper has the most uniform appearance over the surface because during sputter deposition. The Cu^0 molecules grow on the surface in columns and the thickness of the Cu^0 is 100 times that of chromium thus any surface imperfections or irregularities during deposition are less likely to stand-out.

B. Surface Roughness Variation.

The surface roughness of the deposited metal layers on ceramic and glass are compared in figure 2.9. As expected, the ceramic before metallization has a higher surface roughness than the copper and top chrome layers. Both the ceramic and glass slide metallization show similar roughness variations with the metallized layers. There is a negligible increase in roughness (3%) with the metallization of chromium on the ceramic and a 70% increase with chromium on glass. Statistically the roughness value between the virgin ceramic and the base chrome is equivalent but the difference in roughness between glass and base chrome on glass is

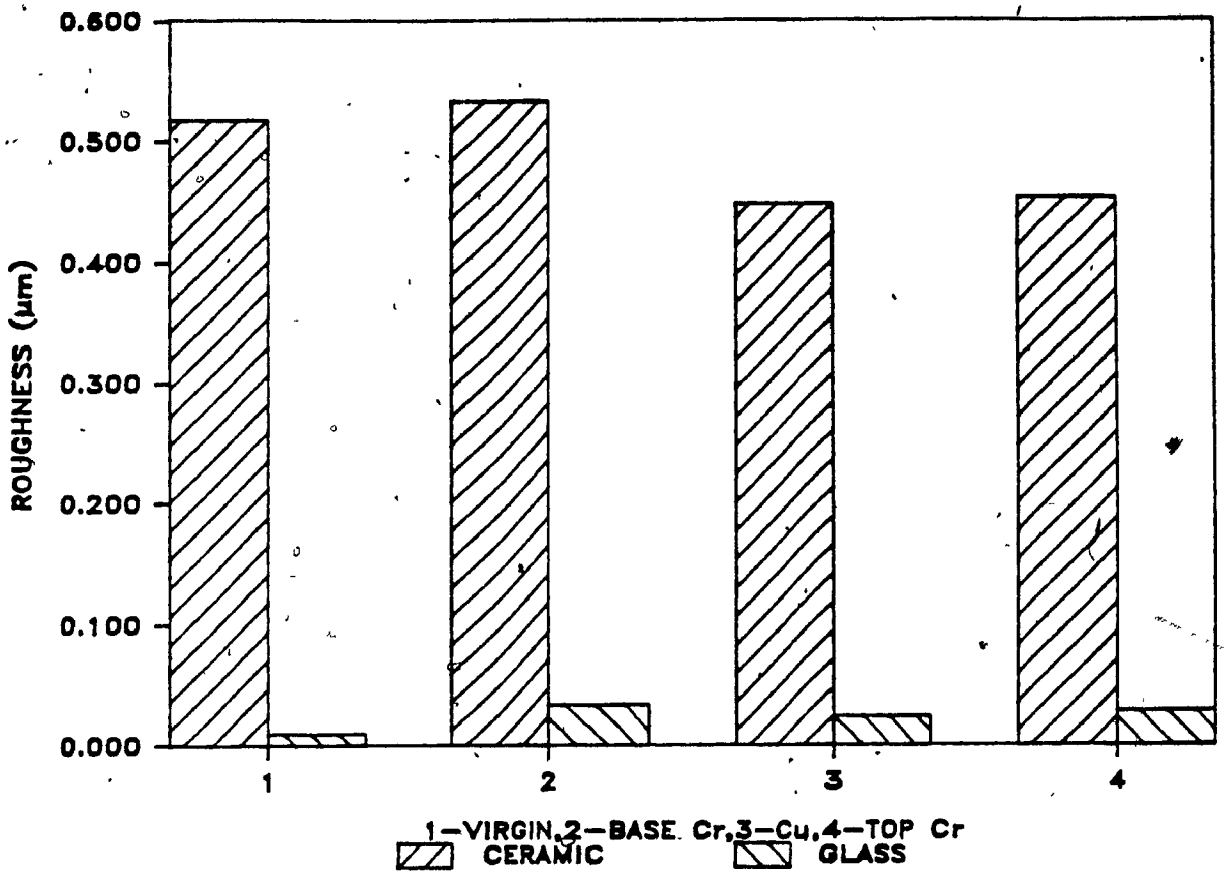

Figure 2.9 Comparison of Surface Roughness of Cr and Cu on Ceramic and Glass.

significant. This last result is apparent in figure 2.3 that in fact the base chrome is very rough on the smooth glass surface. With the application of the copper layer on chrome, the roughness decreases by a stastically significant 15% on ceramic and 30% on glass. This shows that the copper layer due to its higher thickness does indeed make the surface more uniform on both ceramics and glass. The top chrome layer shows an increase in surface in roughness by 8% on glass and 1% on ceramic, however the roughness is still lower than the base chrome layer. In both the ceramic and glass surfaces the mean roughness between the copper and top chrome layers are equivalent at a 95% confidence level.

C. Analysis of Oxide Composition.

ESCA was used to determine the composition of the chromium oxide layer exisiting on the surface of chromium and to determine the approximate thickness of this layer. The knowledge of the oxide composition will help in formulating the reaction mechanism occurring during chromium dissolution (to be discussed in chapter 3).

Figures 2.10a, 2.10b, and 2.10c, depict a broadscan of the various chromium surfaces for the elemental composition of the surface. Comparison of figures 2.10a, 2.10b, and 2.10c for chromium on ceramic, chromium on glass, and pure chromium tile respectively, show that the elemental composition of the surfaces are similar. The major components on the surface are the Cr^0 peaks at -45eV and -577eV and the oxygen peaks at -531eV and -743eV.

The presence of carbon in large quantities was mainly due to adsorbed hydrocarbons on the surface. The silicon peaks in

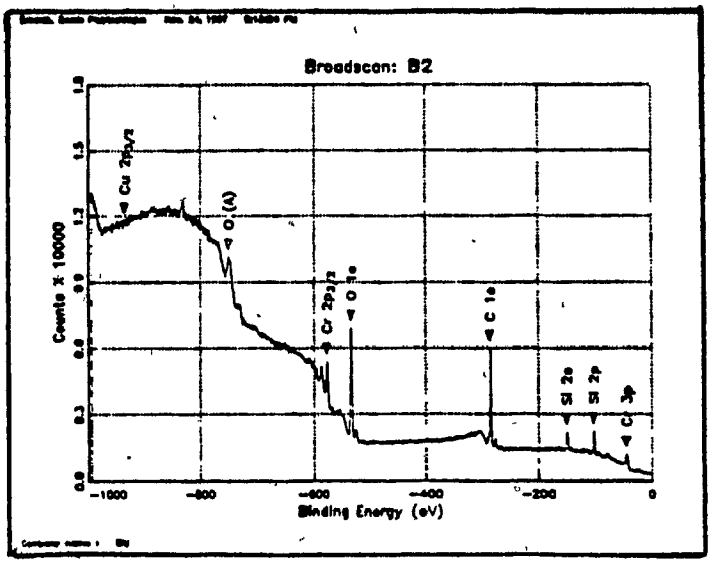

Figure 2.10a

ESCA Broadscan of Chrome on Ceramic.

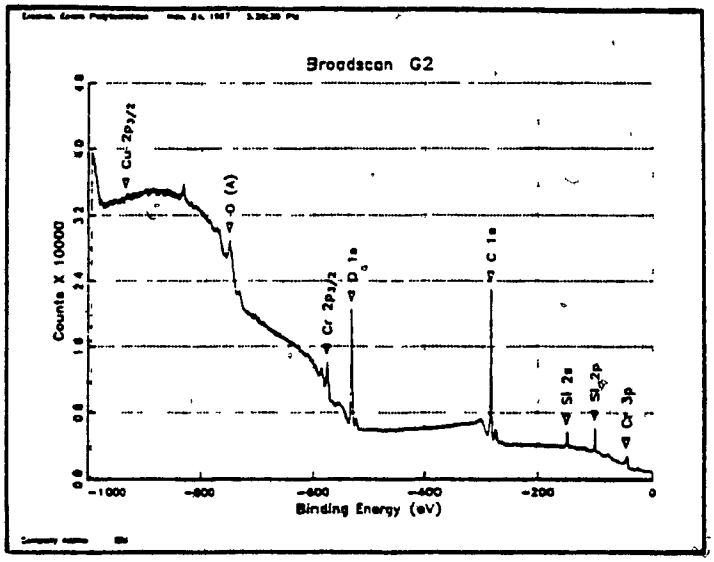

Figure 2.10b

ESCA Broadscan of Chrome on Glass.

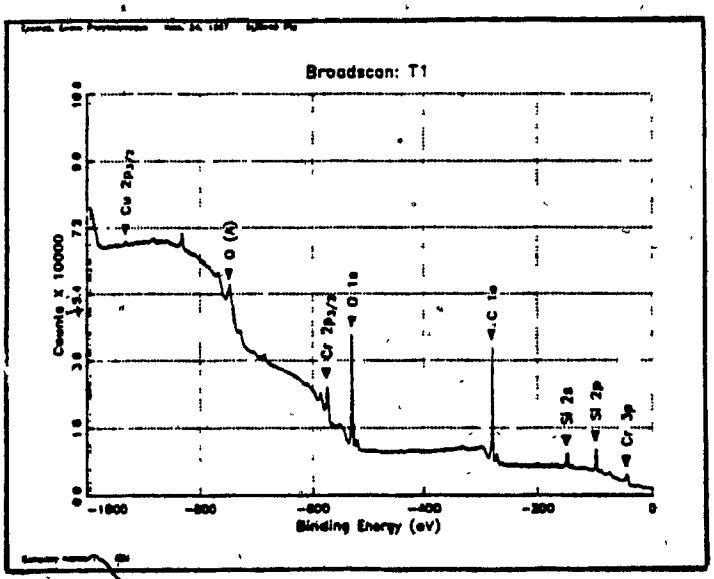

Figure 2.10c

ESCA Broadscan of Chrome Tile.

each scan are due to the silica in the ceramic and glass and in the case of tiles, they arise from residues from the polishing paper.

Figures 2.11a, 2.11b, and 2.11c show the scan region for chromium. In all three scans there are 2 peaks of chromium. The first which occupies 85% of the peak area is at -577eV and is related to chromium bonded to oxygen. The second peak at -574.5 eV occupying 15% of the peak area is related to Cr metal.

To determine the Cr^0-O bonding ratio a scan of the oxygen region was done and the results are shown in figures 2.12a, 2.12b and 2.12c for Cr^0/ceramic, Cr^0/glass, Cr^0 tile, respectively. Two peaks are observed, one is a peak that occupies 80% of the peak area and is related to oxygen bonded to carbon at -532.6 eV. The second peak occurs at -530 eV and occupies 20% of the peak area. This peak is related to oxygen bonded to chromium.

The peaks of oxygen at -531eV and that of chromium at -577eV are interrelated. Using a sensitivity factor of 1.5 and 0.66 for the chromium (Cr(O)) and oxygen (O(Cr)) scans respectively, and equation 2.1, the O - Cr^0 ratio was found to be approximately 1.5 in all three surface scans. This result indicates that within a 10% degree of error of the instrument, that the composition of the oxide is Cr_2O_3.

The approximate thickness of this layer is at least 50 Å since the depth of the x-ray penetration in the sample is in the order of 50 Å.

D. Conclusion

The surface roughness of the sputtered metals is totally

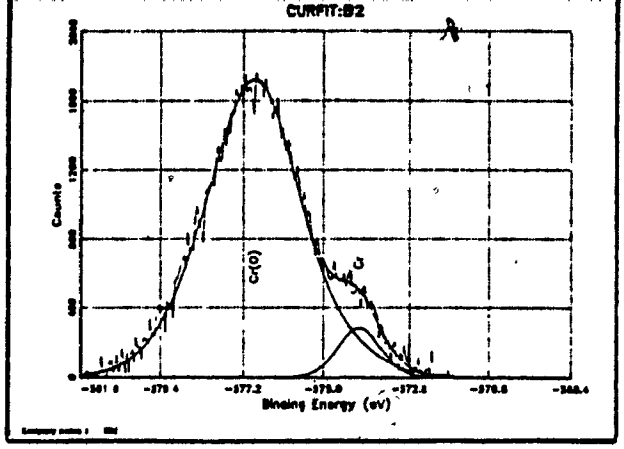

Figure 2.11a

ESCA Scan of Chrome Region on Ceramic.

Experiment type : XPS
Region : Cr $2p_3$
Sensitivity factor : 1.5
number of peaks : 2

Cr(0) : Energy position : -576.96
FWHM : 3.00
Area : 5731.0
Relative area : 0.9368

Cr : Energy position : -574.14
FWHM : 1.20
Area : 377.0
Relative area : 0.0616

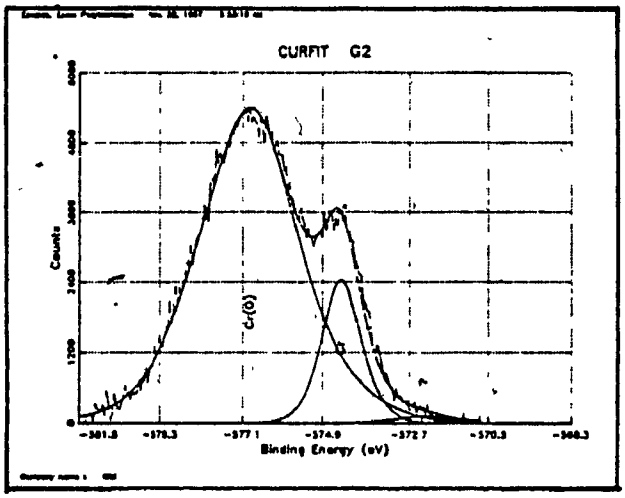

Figure 2.11b

ESCA Scan of Chrome Region on Glass.

Experiment type : XPS
Region : Cr $2p_3$
Sensitivity factor 1.5
number of peaks : 3

Cr(0) : Energy position : -576.93
FWHM : 3.10
Area : 18646.4
Relative area : 0.8448

Cr : Energy position : -574.68
FWHM : 1.17
Area : 3243.2
Relative area : 0.1484

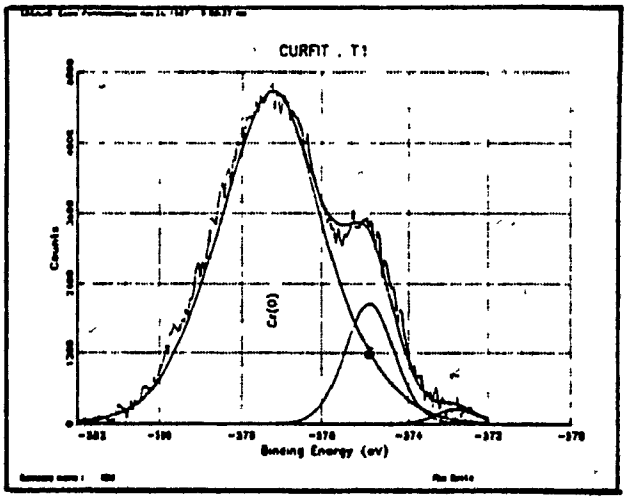

Figure 2.11c

ESCA Scan of Chrome Region on Tile.

Experiment type : XPS
Region Cr $2p_3$
Sensitivity factor : 1.5
number of peaks : 3

Cr(0) : Energy position : -576.84
FWHM : 3.00
Area : 18878.0
Relative area : 0.8518

Cr : Energy position : -574.48

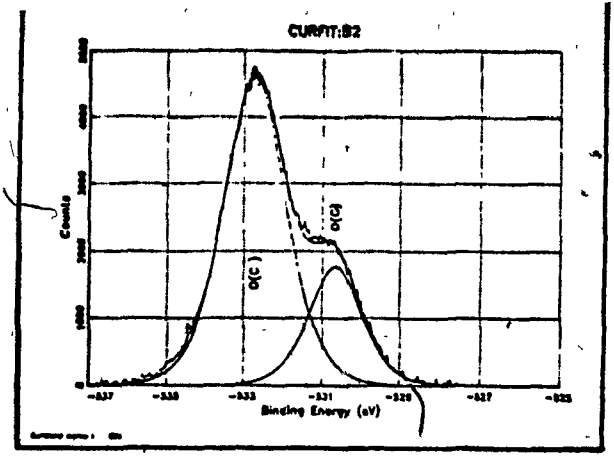

Figure 2.12a

ESCA Scan of Oxygen Region of Cr on Ceramic.

Experiment type : XPS
Region : O 1s
Sensitivity factor : 0.66
number of peaks : 2

O(C) : Energy position : -532.62
FWHM : 1.81
Area : 9429.8
Relative area : 0.7475

O(O) : Energy position : -530.58
FWHM : 1.59
Area : 3185.1
Relative area : 0.2525

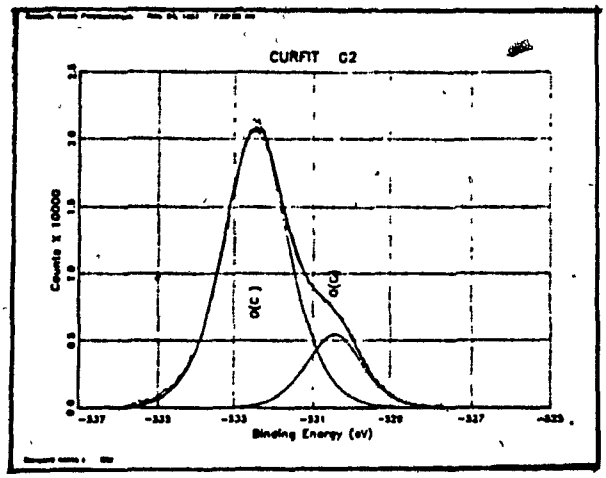

Figure 2.12b

ESCA Scan of Oxygen Region of Cr on Glass.

Experiment type : XPS
Region : O 1s
Sensitivity factor : 0.66
number of peaks : 2

O(C) : Energy position : -532.56
FWHM : 1.98
Area : 64881.6
Relative area : 0.8183

O(O) : Energy position : -530.55
FWHM : 1.64
Area : 8967.7
Relative area : 0.1817

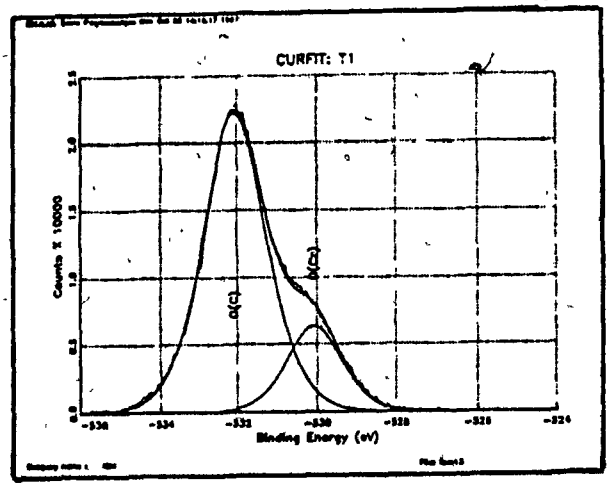

Figure 2.12c

ESCA Scan of Oxygen Region of Cr on Tile

Experiment type : XPS
Region: O 1s
Sensitivity Factor: 0.66
number of peaks : 2

O(C) : Energy position : -532.52
FWHM : 1.97
Area : 46172.5
Relative area : 0.8048

O(Cr) : Energy position : -530.32
FWHM : 1.60
Area : 11210.8

dependent on the substrate being used. Metallization on a smooth substrate will have a lower surface roughness than that on a rougher substrate. With respect to thickness variations the most uniform thickness is observed with copper. This result insures that the circuit dimensions on a ceramic substrate will be uniform.

The top chrome shows a large variation in its thickness which may cause dimensional problems of the copper layer. Thus the etching of this layer must be sufficiently overdesigned to take into account this large thickness range of metal on the part. Finally the thickness of the base chrome shows less variation than that of the top chrome layer.

The ESCA results show that on the chromium surface there exists a layer of chromium oxide of the form Cr_2O_3. The thickness of this layer is deduced to be at least 50Å. Thus the oxygen from the air must react with the metallic chromium to form this continuous oxide layer.

CHAPTER 3

A KINETIC STUDY OF CHROMIUM ETCHING

3.1 Introduction

The purpose of this chapter is to study in detail the mechanism and kinetics of the dissolution of chromium metal in alkaline potassium permanganate. As mentioned previously, the etching of chromium is not only important to the processing of metallized ceramics but also important in the manufacturing processes related to the production of chromium photomasks and in the etch -back processes for metal finishing. For the objectives of this thesis, the chromium etching mechanism and kinetics will be discussed as they relate to the etching of metallized ceramic substrates.

Thus the major objectives of the experimental work described in this chapter are:

a. To determine the intrinsic rate law for the dissoluton of chromium as a function of temperature, $[KMnO_4]$, $[Cr^{+6}]$, $[NaOH]$.

b. To formulate a reaction mechanism to describe the interactions between chromium metal and the alkaline potassium permanganate etchant solution.

c. To compare the etch rates obtained by a laboratory scale etcher to the etch rates obtained from a commercial scale spray etcher.

3.2 Materials and Methods

A. Preparation of the Etchant Solution.

To insure a consistent etchant solution for each experimental run, a standardized procedure was established and followed for all experiments. A specific amount of $KMnO_4$ crystals (reagent grade) was weighed to the nearest 0.1 g. The powder was dispensed into a 2 L Erlenmeyer flask. A desired amount of NaOH pellets (reagent grade) was weighed out and placed into the flask. The solids were dissolved in 1 L of distilled water. The mixture was shaken to start the dissolution of the crystals. Once the dissolution was complete, the solution was heated until the desired reaction temperature was reached. The exact concentrations of $KMnO_4$ and NaOH were determined as described in 3.2B.

The etchant solution was then carefully poured into the reaction vessel which is described in 3.2D. The temperature of the etchant in the reaction vessel was controlled to within 2 C and the solution was well stirred at a predetermined agitation rate. To prevent the build-up of the dissolved chromium from affecting the the etch rates, the etchant was used for a maximum of 5 experimental runs which is roughly equivalent to 75 mg/L chromium ion build-up.

B. Analysis of Etchant Concentration.

The concentrations of the dissolved Cr^{+6}, $KMnO_4$, and NaOH were were measured using standard analytical techniques described in [9]. The concentration of chromium was determined by measuring the oxidation-reduction potential (ORP) of the solution at a specific temperature and concentration of $KMnO_4$ and NaOH. The measured ORP was compared to a calibration curve

of ORP vs concentration of Cr^{+6} for the calibration curve shown in figure A.2.1 in the Appendix the concentration of chromium in the etchant solution was measured using Atomic Absorption Spectroscopy. The chromium powder used for the calibration procedure and in several rate experiments to be described later, was dissolved in a separate solution of $KMnO_4$ / NaOH before it was added to the etchant solution. The ORP method was used as a measure of the Cr^{+6} concentration because of its simplicity, and its fast response time. This method is presently being used in the manufacturing line at IBM Bromont as a measure of the Cr^{+6} build-up in the etchant baths.

The concentration of MnO_4^{-1} in solution, was determined by titration with a standardized solution of $FeSO_4 \cdot 7H_2O$ until the end-point was reached (a change in colour from purple to pale yellow). The titrant was prepared by dissolving 140.05 g $FeSO_4 \cdot 7H_2O$ in 750 ml of distilled water and 30 ml of 7N H_2SO_4. The solution was then diluted to 1 L in a volumetric flask which was then allowed to stand at room temperature for 24 hours before use. Since Fe^{+2} is oxidized by oxygen, the titrant was standardized with a standard 0.100 M $KMnO_4$ (acidic) solution, purchased from Canlab, before it was used in any titration.

The concentration of MnO_4^{-1} in the etchant was calculated from the following equation.

$$MnO_4^{-1}\ (g/L) = 3.16 \times (\text{Volume of titrant (mL)}) \qquad (3.1)$$

To determine the concentration of OH^{-1} and CO_3^{-2} the solution was titrated with a solution of 1.00N HCl until the equivalence points were reached. The equivalence points were measured using a pH meter calibrated with pH buffers at pH 10

and pH 2. The concentration of OH^{-1} and CO_3^{-2} are calculated from the following equations:

$$OH^{-1}(g/L) = (2A - B)x(1.6) \quad (3.2)$$
$$CO_3^{-2}\ (g/L) = (B - A)x(4.2) \quad (3.3)$$

where ; A = mL of 1.00N HCl used to attain pH 8.
B = mL of 1.00N HCl used to attain pH 4.

The accuracy of these titration methods are within ± 1 g/L which is adequate for the experimental objectives of this thesis.

C. Determination of the Dissolution Rates.

In a typical experiment, one or two tiles were placed in a plastic frame which held the chromium tiles by their edges only. The frame then was dipped into the etchant solution in the rotational etcher and held there for a predetermined time, after which it was removed and dipped immediately in 85 g/L oxalic acid to quench the reaction. The tiles were patted dry to remove excess water and then were stored in a dessicator at all times. In all rate experiments, the reaction times were 0.5, 1, 1.5, 2, 2.5, 3, 4, 5, minutes. It should be noted that different tiles were used for each reaction time. The change in the mass per unit surface area for each tile was then plotted against reaction time to derive the etch rate (section 2.3A).

Tiles of 2cm x 2cm x 0.3cm of 99.99% Cr metal were passivated with Apeizon wax on all sides except one to prevent the dissolution of chromium from more than one side. To obtain a surface roughness of the tile equivalent to that of a ceramic substrate, the active side of the tile was polished with 280 grit paper to get a surface roughness of 0.46 ± .05 μm.

The chromium dissolution experiments for the determination of the rates were performed in a temperature controlled CPVC (Chlorinated Polyvinyl Chloride) reaction vessel. CPVC was used for its relatively good chemical resistance to the etchant. The solution whose volume was maintained at 1L ± 5mL in the reactor was continuously agitated at 1500 rpm (section 2.3B). A laboratory scale mixer was used and the agitation speed was measured using a tachometer. The reaction vessel henceforth will be called a rotational etcher because of the high rate of impingement of the etchant on the substrate surface.

The etching time was kept to a maximum of 5 minutes because it was found that the surface roughness would not change significantly within this time range. To insure that the surface roughness was constant from each experimental run and comparable to the roughness of a ceramic substrate, the tiles were repolished before a new experiment was performed.

3.3. Results and Discussion

A. Calculation of the Etch Rate.

When the amount of chromium etched per unit surface area was plotted against time, a curve such as the one shown in figure 3.1 was obtained. In over 55 different experiments carried out at various etchant conditions, the same type of dual sloped curve was obtained as the one in figure 3.1. In general the change in the slope of the lines occurred within the first 120 seconds.

These results and further experimental evidence described

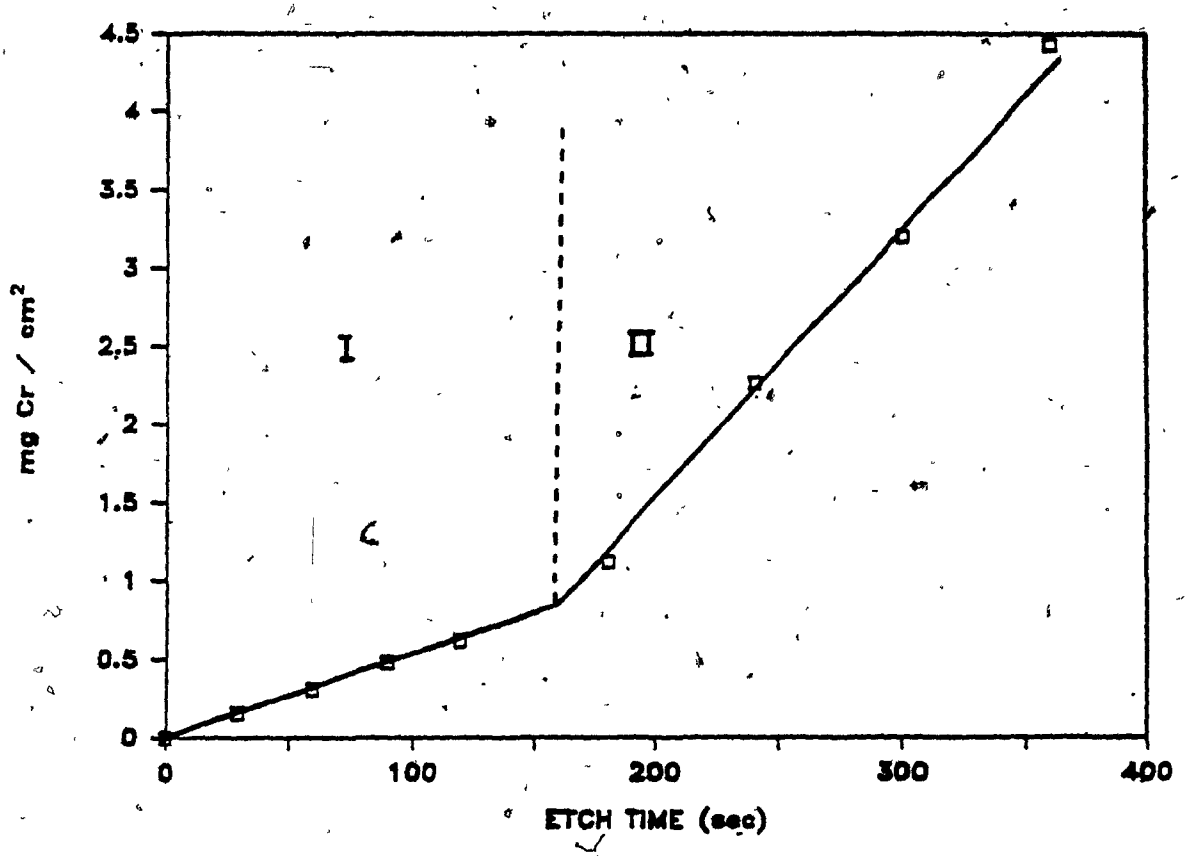

Figure 3.1 Variation in Quantity of Cr Etched with Etch Time.
($KMnO_4$ =0.41 mol/L, NaOH = 0.50 mol/L, Cr = 0.29 mmol/L, 43°C)

in this chapter suggest that two different heterogeneous reactions are occurring. The first is related to the dissolution of the Cr_2O_3 oxide layer and the second reaction is the oxidation and dissolution of the underlying chromium layer. Thus the etch rate was calculated for all rate experiments in two steps. The intital rate (r_i) was calculated from the slope of region I in figure 3.1 and the second rate (r) was calculated from the slope of region II in figure 3.1. Both rates are expressed in mmol Cr/ m^2-s.

B. Determination of the Conditions for Kinetic Control.

(i) Results

It is a well known fact that with any heterogeneous reaction, and in particular chemical etching methods, there is a boundary layer between the fluid and the surface of the solid [3,4,5]. In order for the metal to react with the oxidizing agent, the latter must diffuse through the boundary layer, react with the metal to cause its dissolution, and then the spent reactant and the dissolved metal must diffuse through the layer to mix with the bulk etchant phase. If the rate of mass transport through the boundary layer is much smaller than the rate of the surface reaction, the process is mass transfer controlled and the measured rates are not the intrinsic rates of the reaction. Since in the rotational etcher, the rate of mass transport from the liquid to the solid surface increases with increasing rotational speed of the impeller, it is expected that the rate will be invariant above a certain the rotational speed.

In this first series of experiments the chromium etch rate (region II) was determined by the procedure in 3.2D. The chromium tiles were etched in the rotational etcher at various agitation

rates of the etchant solution. The results are plotted in figure 3.2. At zero agitation the rate is mass transfer controlled thus the etch rate is observed to be the lowest at 0.83 mmol Cr / m^2-s. As the rate of agitation increases, the thickness of the boundary layer is decreased which in turn increases the rate of mass transfer. Statistically the mean etch rates at 0, 700, 900 and 1100 rpm are different at a 95 % confidence level. However the mean rates at 1100, 1500, 1700 rpm are statistically equivalent. Thus there is a point after 1100 rpm agitation where the physical etching system has no longer a significant effect on the etch rate. This indicates that at an agitation rate greater than 1100 rpm, kinetic control of the etching reaction is occurring. This also means that the bulk concentrations being measured by titration are the same as the concentration of the etchant at the substrate surface.

(ii) Discussion

In diffusional controlled etching the surface concentrations are far less than the measured bulk concentrations thus the observed etch rates are lower. In an industrial scale etcher such as the one used at IBM Bromont, two types of nozzles are used: full flow fan nozzles; and conical nozzles. The spray pressure is between 120 and 160 KPa at a nozzle -to- substrate distance of 18 cm. For the same reactant concentrations (0.41 mol/L $KMnO_4$, 0.50 mol/L NaOH and 39 °C) used to obtain the data shown in figure 3.2 bulk etch rates for chromium are known to be 1.22 mmol Cr / m^2- s , and .98 mmol Cr / m^2-s respectively for conical and fan nozzles. Fan nozzles yield better etch uniformity than conical nozzles but

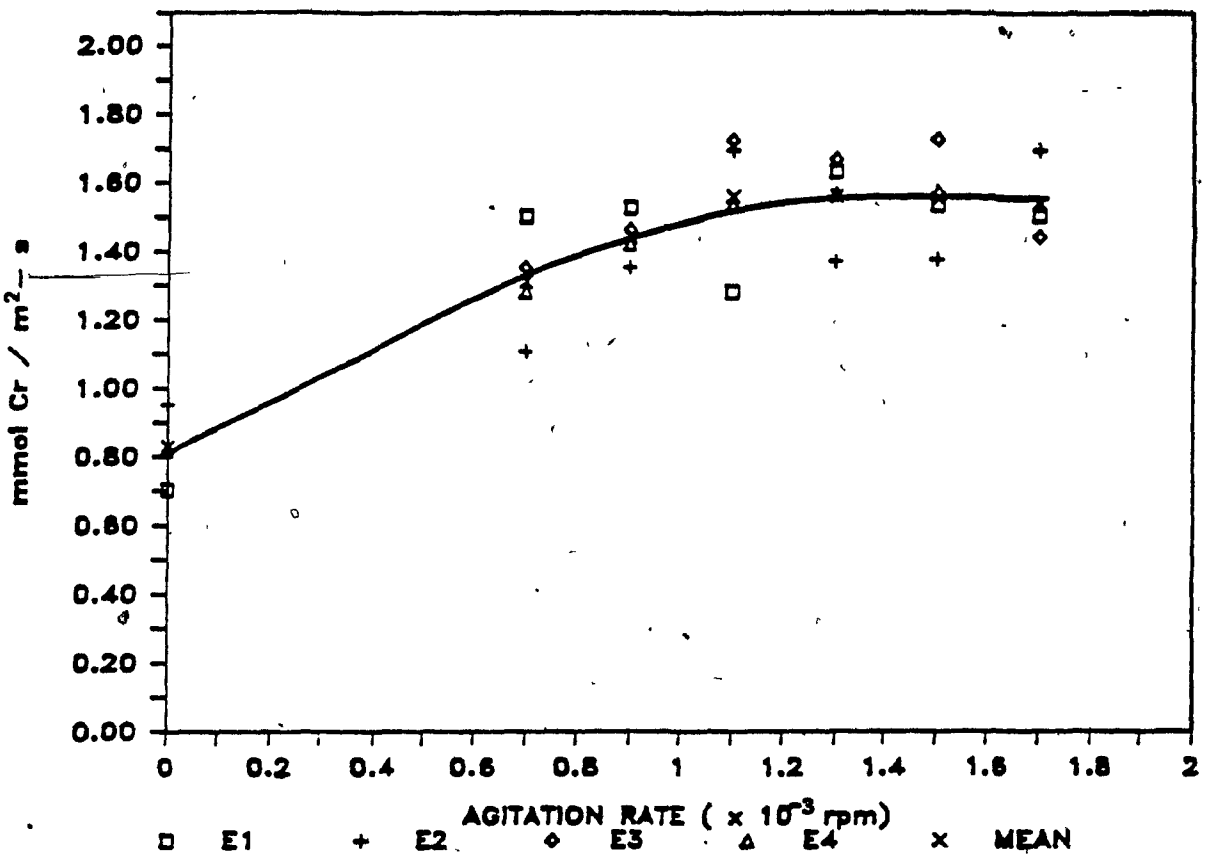

Figure 3.2 Variation of Cr Etch Rate with Etchant Agitation Rate. ($KMnO_4$ = 0.41 mol/L, NaOH = 0.50 mol/L, Cr = 0.29 mmol/L, 39°C)

the etchant flow to the surface is less. Thus the boundary layer is thicker on the substrate surface.

By comparing the two spray etch rates mentioned above to the etch rates obtained by rotational etching shown in figure 3.2 one observes that the rate of etching with fan nozzles is equivalent to a rotational etch rate at 250 rpm. Similarly with conical nozzles, the equivalent etch condition is at 620 rpm with rotational etching. In both cases one sees that the etch rates are in the region of the curve where transport effects control the etch rate.

C. Surface Roughness and Etching.

(i) Results

The effect of surface roughness on the rate of the dissolution of chromium will be discussed in this section. Figure 3.3 shows the rate of etching at various surface roughnesses. For this experiment, chrome tiles were polished at various paper grits (table A.2.3), then the roughness was measured according to the procedure in 2.2B. The rates were measured according to procedure 3.1C. The rates expressed in figure 3.3 and all subsequent figures is the rate per unit apparent surface area which is the geometric surface area of the tile and does not include the effect of porosity nor surface roughness.

The results show that the rate of the reaction depends on the surface of the chromium sample. As the roughness increases, the etchant becomes exposed to more reactant and consequently the rate of etching increases. The significant etch rate increase occurs between 0.05 μm and 0.13 μm roughness. After this jump, the rate remains relatively constant and is not

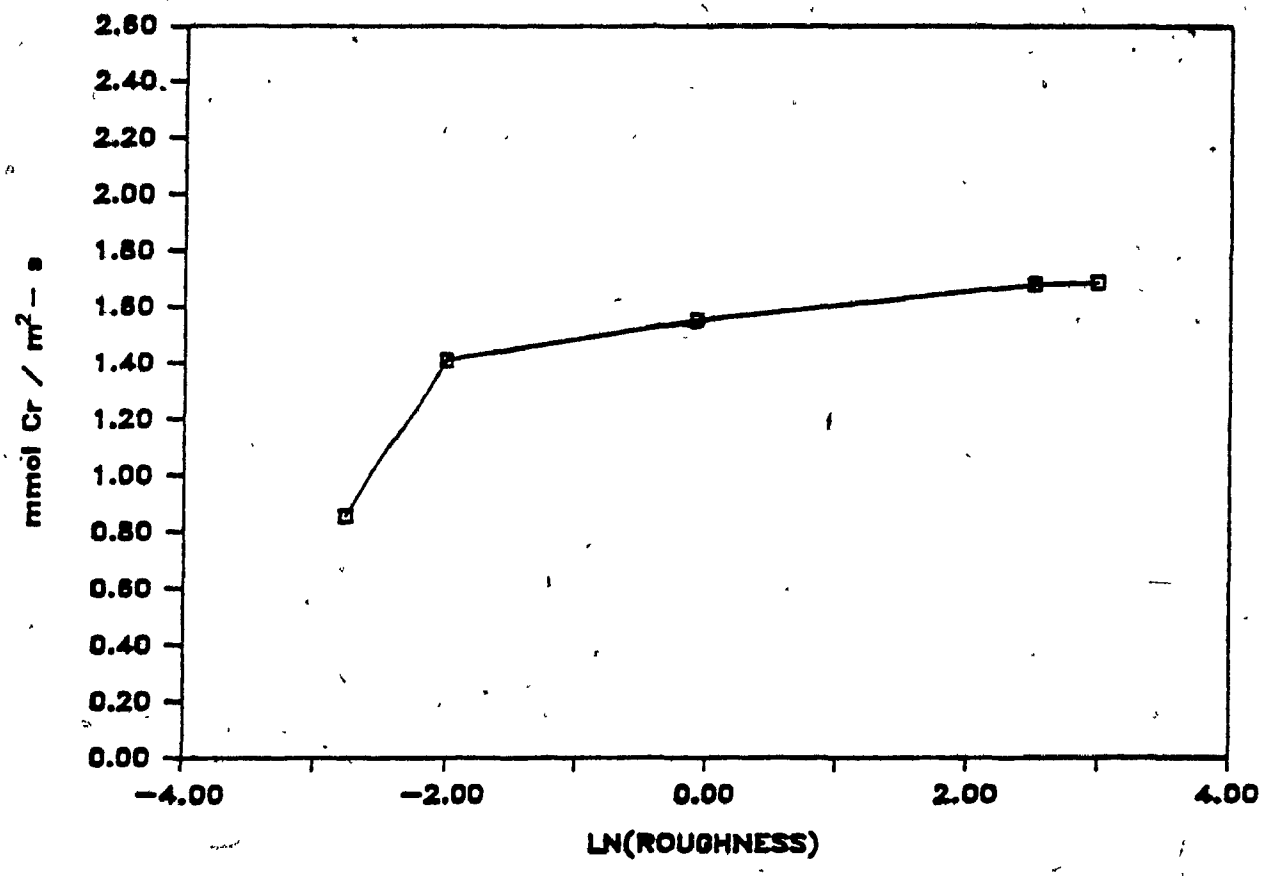

Figure 3.3 Variation of Cr Etch Rate with Surface Roughness. ($KMnO_4$ =0.41 mol/L, NaOH = 0.50 mol/L, Cr = 0.29 mmol/L, 43°C,

affected by the surface roughness. This last result indicates that there is point where the etch rate is not a strong function of the effective surface roughness and other limitations to the system such as etchant concentration and temperature become overriding factors.

(ii) Discussion

In Chapter 2, a comparison between the surface roughness of chromium on glass slides and ceramics was made in figure 2.9. Using this data and that of figure 3.3, the rate of etching of top chrome is 75% higher on ceramics over glass slides. Similarly the etch rate of base chrome on ceramics is 63% higher than on glass slides. Thus a substantial decrease in etch rate will be observed if glass is used as a substrate medium rather than alumina ceramics. In the manufacturing of ceramics, there is usually a thin glass laminate placed on the active surface. If this glass layer is so thick that the roughness of the ceramic is reduced , there will be residual metal defects on the product due to reduced etch rates. Thus the thickness of the glass laminate below the base chrome has to be carefully controlled.

The surface roughness of ceramics at 0.47 μm lies in the plateau region of figure 3.3. To eliminate one more variable from the kinetic study the surface roughness of the tiles was adjusted to 0.47 μm prior to the rate experiments. It should also be pointed out that the surface roughness during a 5 minute dissolution experiment remains the same. Figure 3.4 reveals the effect of etch time on the surface roughness of the substrate. The roughness change between 0 and 5 minutes etch time is 8 % which is a statistically insignificant change.

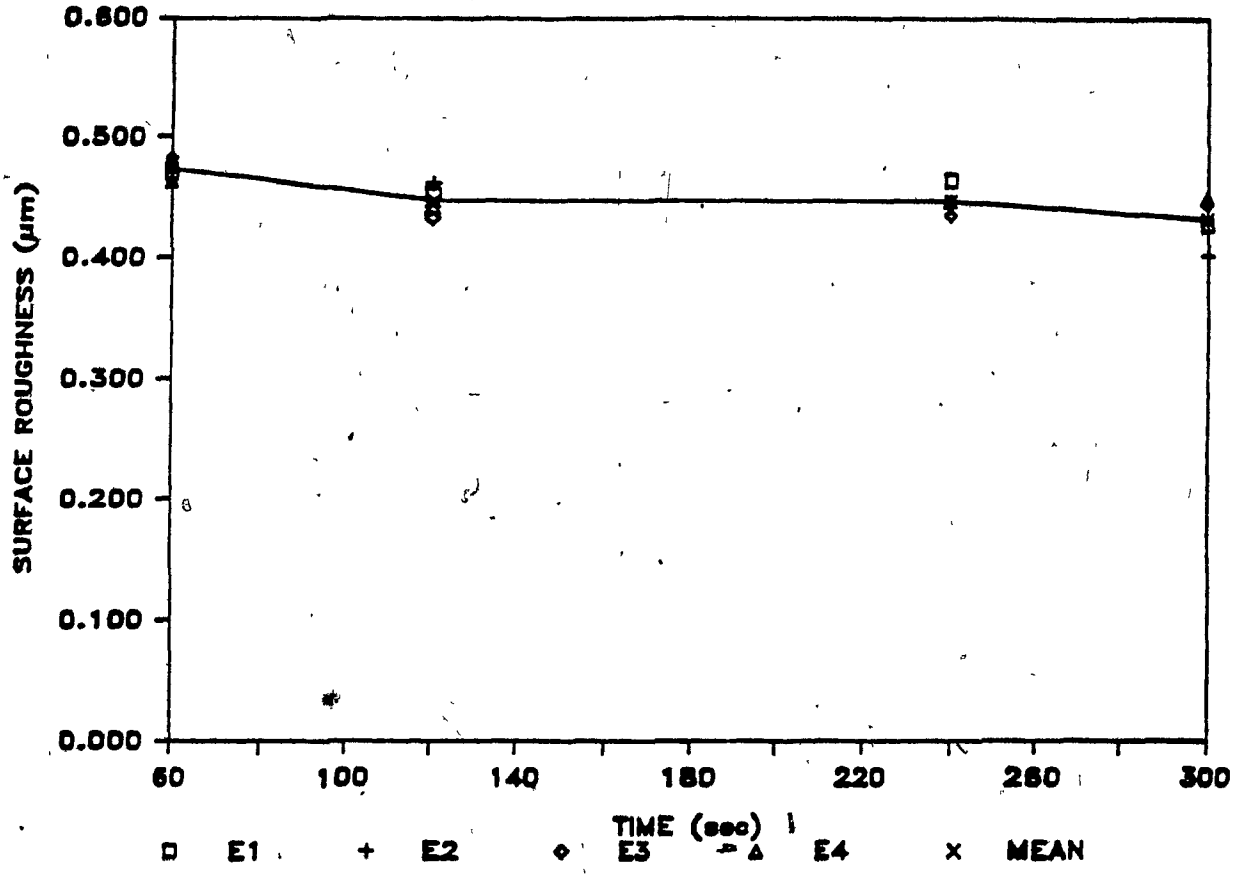

Figure 3.4 Variation of Surface Roughness with Cr Etch Time. ($KMnO_4$ =0.41 mol/L, NaOH = 0.50 mol/L, Cr = 0.29 mmol/L, 43°C)

Plates 3.1 and 3.2 show qualitatively that there is no change in the appearance of the surface of the same tile etched at 1 and 5 minutes.

D. Proposed Mechanism for Chromium Etching.

The etching of chromium with an alkaline potassium permanganate solution depends on the completion of a heterogeneous solid liquid reaction which causes the dissolution of the chromium metal. Previous work in this area has led to the formulation of two reaction pathways none of which have been proven experimentally to represent the etching of chromium metal by a solution mixture of $KMnO_4$ / NaOH. In the first hypothesized mechanism in [11], the first step of the reaction is the oxidation of $Cr_{(s)}$ to chromium hydroxide:

$$Cr_{(s)} + MnO_4^{-1}{}_{(aq)} + 2H_2O \rightleftharpoons Cr(OH)_{3(s)} + MnO_{2(s)} + OH^{-1}$$

In step 2, the oxidation of Cr^{+3} to Cr^{+6} and dissolution of Cr^{+6} in base takes place.

$$Cr(OH)_{3(s)} + MnO_4^{-1}{}_{(aq)} + OH^{-1} \rightleftharpoons CrO_4^{-2}{}_{(aq)} + 2H_2O$$

Thus the overall reaction is given by:

$$Cr_{(s)} + 2MnO_4^{-1}{}_{(aq)} \rightleftharpoons 2MnO_{2(s)} + CrO_4^{-2}{}_{(aq)}$$

The second mechanism studied in [5] is similar to the first mechanism however instead of the oxidation of Cr^{+3} to Cr^{+6} before dissolution in step two, the hydrate of chromium Cr(OH)3 is dissolved in base as Cr^{+3} and then oxidized from Cr^{+3} to CrO_4^{-2} (Cr^{+6}). However the overall reaction and the stoichiometry in both mechanisms is the same.

Plate 3.1 Chrome Tile Surface After 60 sec Etching.

Plate 3.2 Chrome Tile Surface After 300 sec Etching.

Initial experiments which consisted of the ESCA analysis of the surface of chromium tiles (section 2.3D) showed that there exists a layer of oxide in the form of Cr_2O_3 on the surface of chromium. Thus the above mechansims are deficient in that they do not take the dissolution of the Cr_2O_3 layer into account. Moreover when a Cr tile was placed in an etchant solution at pH 7.2 with out any NaOH, no dissolution of chromium was observed for a 5 minute reaction time. The ORP of the etchant solution under those conditions was measured at about 800 mV. A consultation of the Pourbaix diagrams (figure 3.5) indicated that the aqueous chromium species present under these conditions is $CrO4^{-2}$ indicating that the dissolution of the chromium should take place. However the presence of the oxide layer retards the dissolution of the chromium within the experimental time.

Finally, the effect of the oxide layer is seen in figure 3.1 where two distinct kinetic regions are observed. Kinetic experiments in each region (to be discussed later) reveal that the rate of chromium dissolution in region I is dependent on the concentration of NaOH only and the etch rate in region II is dependent on the MnO_4^{-1} and dissolved Cr^{+6} concentrations only. As predicted by the Pourbaix diagrams [12], the presence of CrO_4^{-2}, Cr^{+3}, and MnO_4^{-1} were confirmed by ion chromatography analysis of the etchant solution.

Based on the data, the observations and the consultation of the chromium and manganse chemistry in [12], the following reaction pathway is proposed. The etching of chromium follows two solid -liquid reactions : the first is related to the dissolution of the oxide film and the second reaction is related to the oxidation and dissolution of the underlying Cr

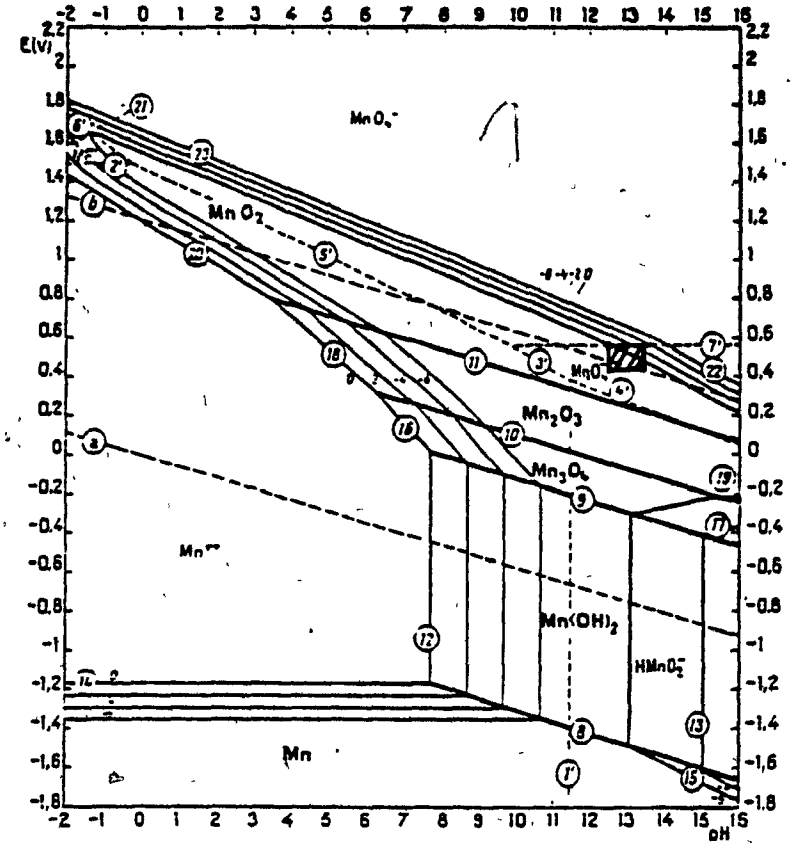

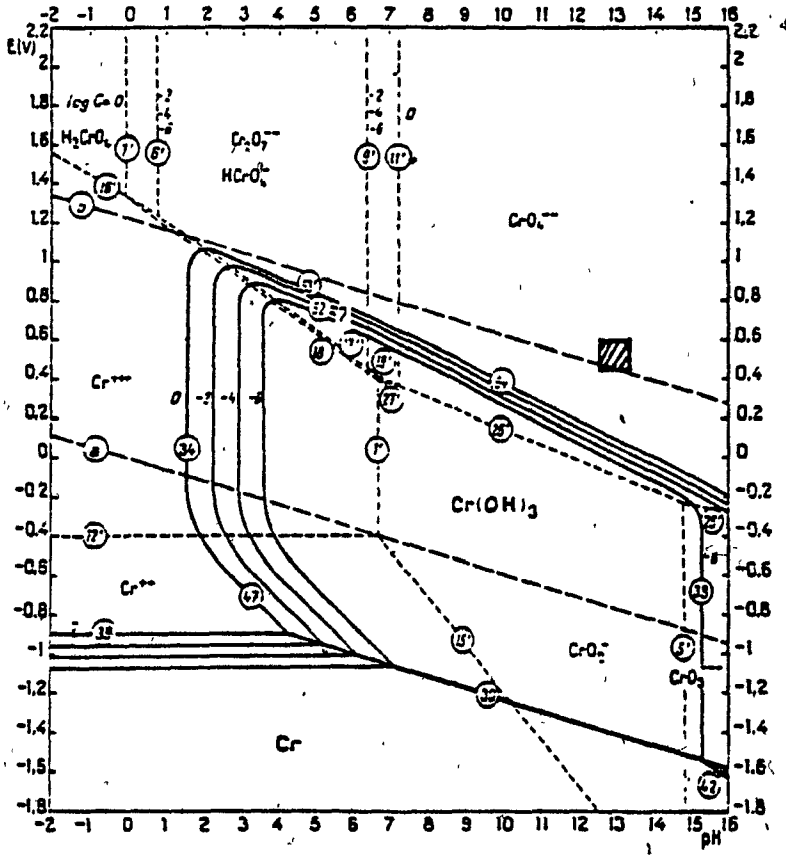

EXPERIMENTAL CONDITIONS

Figure 3.5 Pourbaix Diagrams of MnO_4^{-1} / Cr systems.

metal. The first heterogeneous reaction is:

$$Cr_2O_{3(s)} + 5H_2O \rightarrow 2H^{+1} + 2Cr(OH)_{4(aq)}^{-1}$$

The second solid /liquid reaction involves the oxidation of the Cr metal and its dissolution. The final stoichometry is the same as that proposed in [5] and [11].

$$Cr_{(s)} + 2MnO_{4(aq)}^{-1} \rightleftharpoons 2MnO_{2(s)} + CrO_{4(aq)}^{-2}$$

Now that the basic interaction between chromium and potassium permangnate and sodium hydroxide has been established, the rest of the chapter will be devoted to determining the factors that affect the rate of reaction in the two etching regions.

E. Effect of [NaOH], [$KMnO_4$], [Cr] on r_i and r.

The data from the first set of experiments was used to determine the effect of the concentration of OH^{-1}, MnO_4^{-1}, and dissolved CrO_4^{-2} expressed as Cr^{+6} on the initial rate r_i and r. A 2- level Box-Behnken experimental design was used to determine the significance of the concentrations mentioned above on the initial rate r_i and r. The range of concentrations of the reactants were :

NaOH : 0.25 - 0.75 mol/L.

$KMnO_4$: 0.32 - 0.45 mol/L.

Cr : 0 - 0.019 mol/L.

These particular concentration ranges were chosen since they are applicable to the etching process at IBM Bromont. The

detailed experimental conditions for each run and the calculated rates (r_i and r) are tabulated in A.2.9 in the Appendix.

Using the data from the Box-Behnken experimental design a linear 1st order model for the initial rate r_i was fitted in the form :

$$r_i = 0.11 + 1.86\ C_a + 0.11\ C_b + 0.97\ C_c \qquad (3.4)$$

where : r_i = initial rate (mmol / m^2-s).
C_a = concentration of NaOH in mol/L.
C_b = concentration of $KMnO_4$ in mol /L.
C_c = concentration of CrO_4^{-2} expressed as Cr^{+6}

An analysis of variance (ANOVA) was performed on the fitted data and is outlined in Appendix 4. The result of the ANOVA revealed that the linear model fit the experimental data but the only significant coefficient was that for the concentration of NaOH.

Since reaction rates normally follow a power law relationship with reactant concentrations a non-linear model of the form $r_i = k\ C_a^{\alpha}\ C_b^{\beta}\ C_c^{\gamma}$ was also fitted resulting in the following linearized relationship:

$$\ln r_i = 0.63 + 0.79\ \ln C_a + 0.03\ \ln C_b \quad 0.003\ \ln C_c \qquad (3.5)$$

As in the previous case, the non-linear model did fit the data but the only significant coefficient at 95% confidence interval was that of C_a.

A similar statistical procedure was performed on the rate data for r. A linear model was fitted in the form :

$$r = 0.16 + 0.34\ C_a + 3.41\ C_b - 54.80\ C_c \qquad (3.6)$$

A t-test for the significance of the coefficients revealed that the coefficient for C_a was insignificant at 95 % confidence level but the coefficients for C_b and C_c were found to be significant. A non-linear model of the form $r = k\, C_a^{\alpha} C_b^{\beta} C_c^{\gamma}$ was also tried but the statistical analysis revealed that the model did not fit the data.

Based on the Box-Behnken experimental design and statistical analysis of data, the initial rate r_i has been shown to depend only on the NaOH concentration while r depends only on the concentration of $KMnO_4$ and Cr.

F. Determination of the Intrinsic Rate Laws.

The Box-Behnken experimental design can only be used to determine which independent variable has a significant effect on the dependent variables. This experimental design cannot be used to determine a rate law. Thus the next set of experiments were performed by varying the concentration of one species while maintaining the other two concentrations constant.

Since r_i depends only on the concentration of NaOH, The rate was measured at various concentrations of NaOH at 43°C in the rotational etcher. The results are shown in figure 3.6. The plot shows a linear variation in r_i with NaOH concentration. To confirm this observation a linear regression of the data was performed resulting in the following relation:

$$r_i = 1.97\ C_a + 0.04 \quad (r=.99) \qquad (3.7)$$

A non- linear model of the form $r_i = k\, C_a^{\alpha}$ was also fitted to determine the order of the reaction. The resulting relation is :

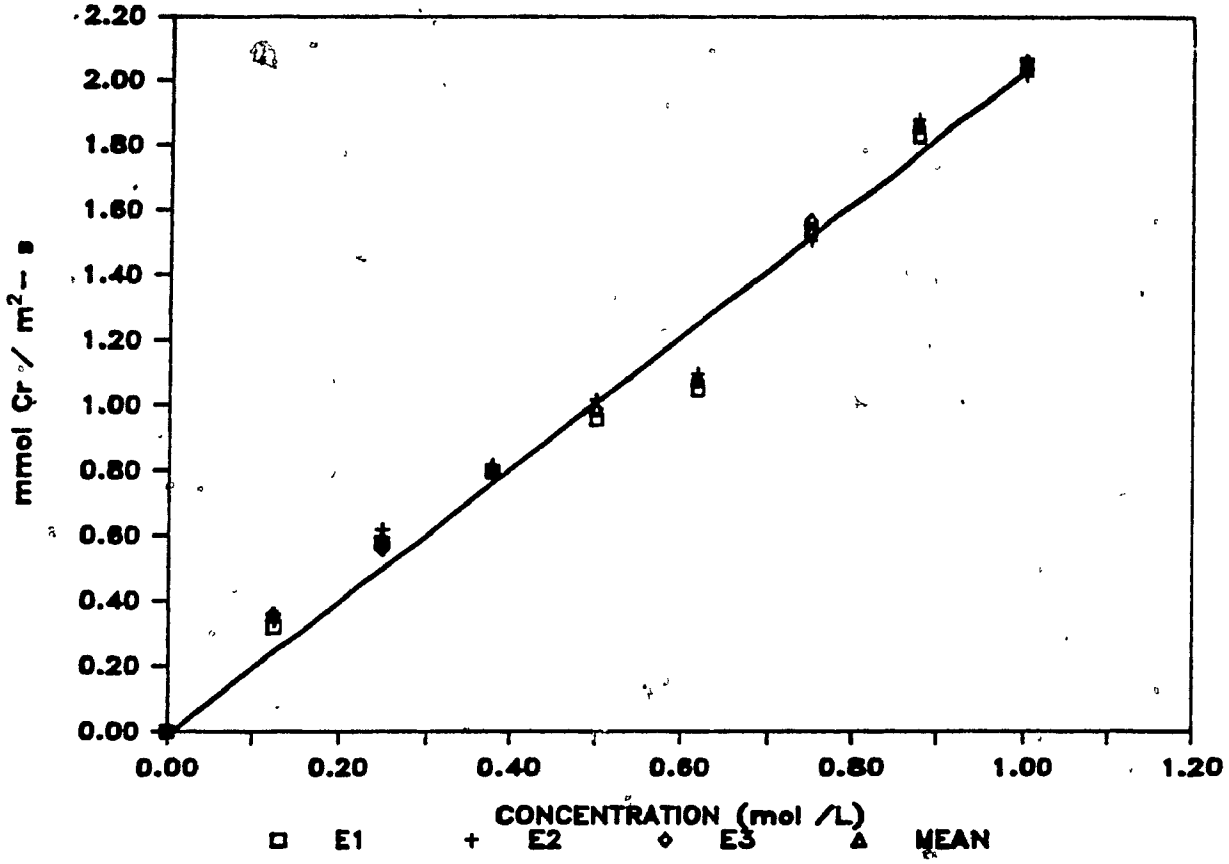

Figure 3.6 Variation in Initial Rate with Concentration of NaOH. ($KMnO_4$ =0.41 mol/L, Cr = 0.29 mmol/L, 43°C, 1500 rpm)

$$r_f = 1.88\ Ca^{0.83} \quad (r=.98) \qquad (3.8)$$

The t-test showed that the coefficient was significant at a 95% confidence level. The confidence interval was calculated for the coefficient in equation 3.8 and was found to be between 0.66 and 1.04. One also observes in equations 3.7 and 3.8 that the rate constants do not differ much.

Figure 3.7 compares the experimental data to both the linear model in equation 3.7 and the non-linear model in equation 3.8. An inspection of the two curves shows that the linear model fits the experimental data better than the non-linear model. Therefore the intrinsic rate expression for oxide dissolution is expressed as :

$$r_1 = 1.97\ C_a \qquad (3.9)$$

where: k_1 : 1.97 (L/ mol)(mmol Cr / m^2 - s) @ 43 °C.

To determine the rate expression for r, experiments were performed where the concentration of $KMnO_4$ was varied at constant NaOH and dissolved Cr concentrations. In the second series of experiments the concentration of Cr was varied at constant NaOH and $KMnO_4$ concentrations. The results for the two series of experiments are shown in figures 3.8 and 3.9 respectively.

In figure 3.8 a linear increase in r with increasing concentration of $KMnO_4$ is observed. In figure 3.9 a linear decrease in rate with increasing dissolved Cr concentration is observed. The linearity is seen between chromium concentration of 0 to 0.020 mol/L. After this point the rate levels off at 0.023 mol/L.

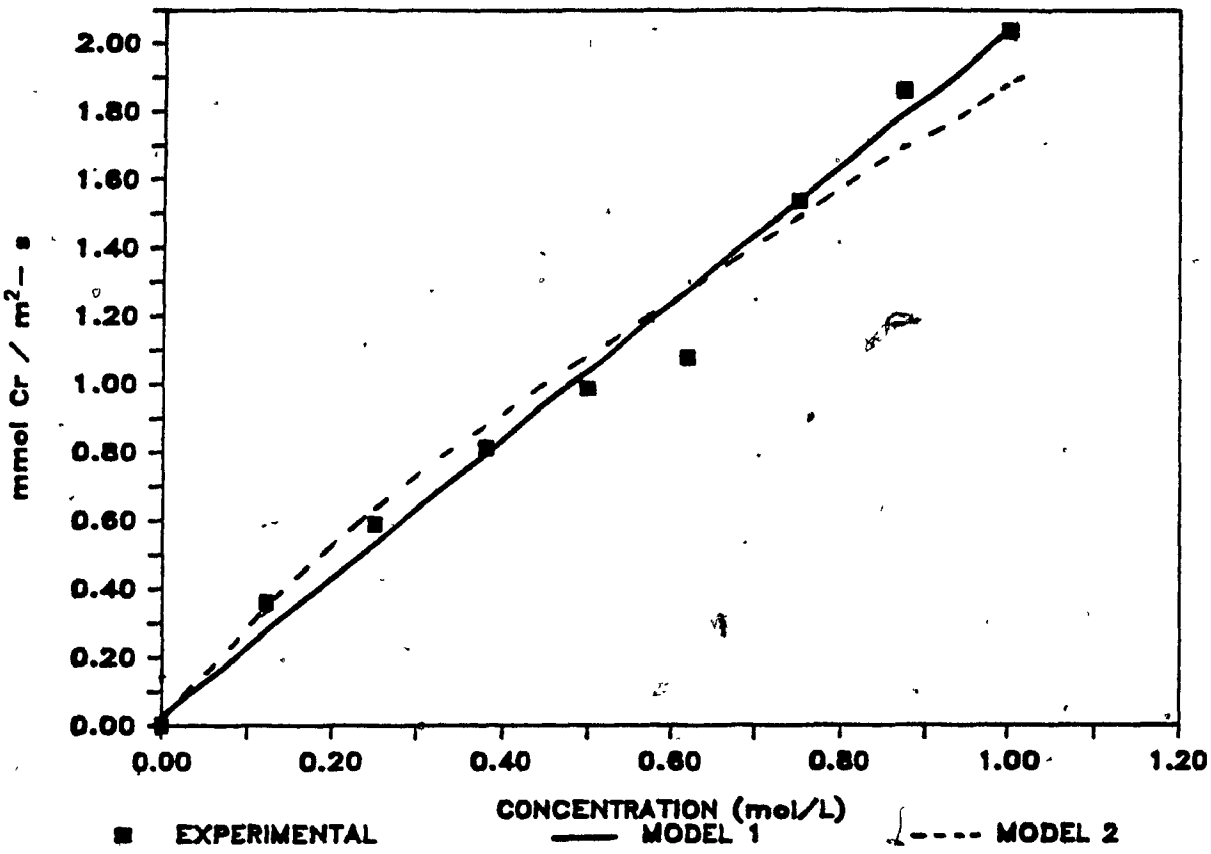

Figure 3.7 Variation of Initial Rate with Concentration of NaOH. Experimental vs Linear Model (1), Non-Linear Model (2).

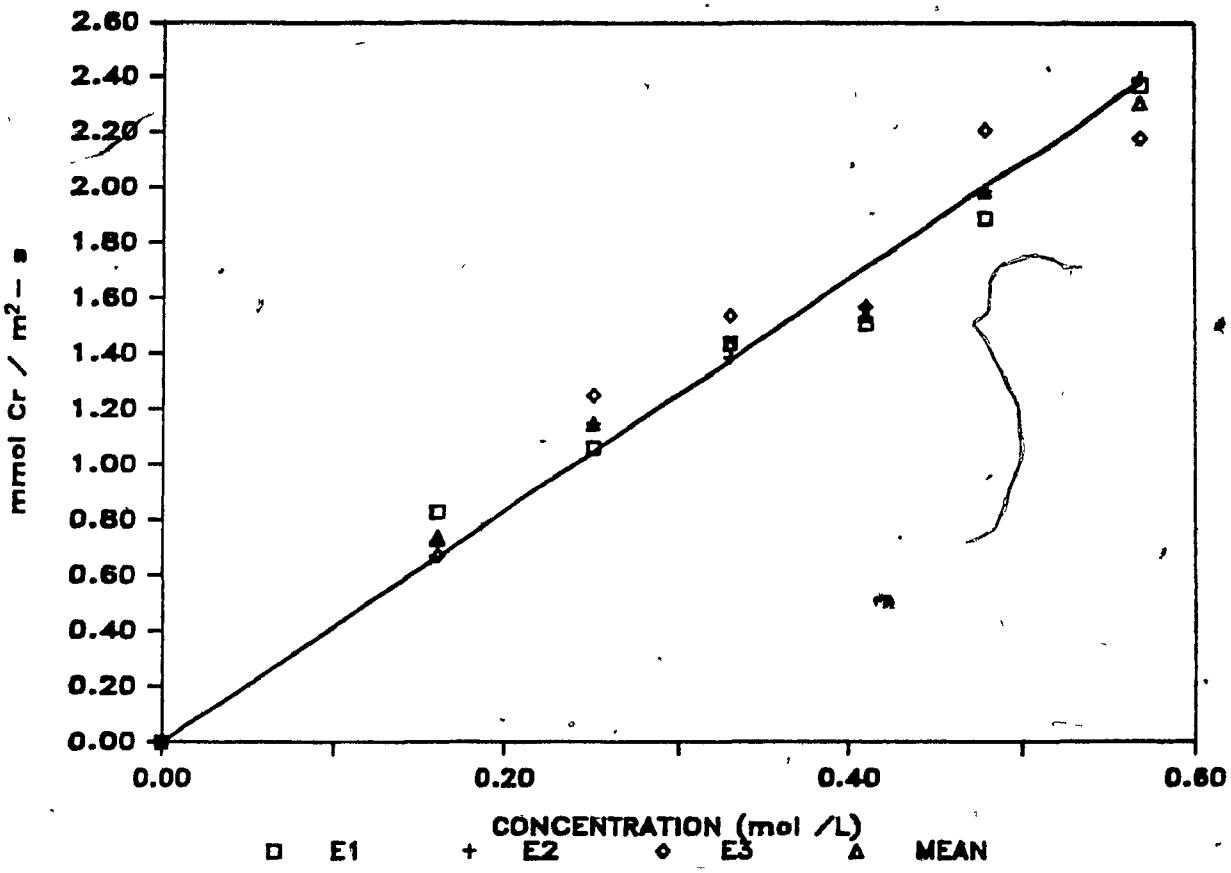

Figure 3.8 Variation in Cr Etch Rate with Concentration of $KMnO_4$. (NaOH = 0.50 mol/L, Cr = 0.29 mmol/L, 43°C, 1500 rpm)

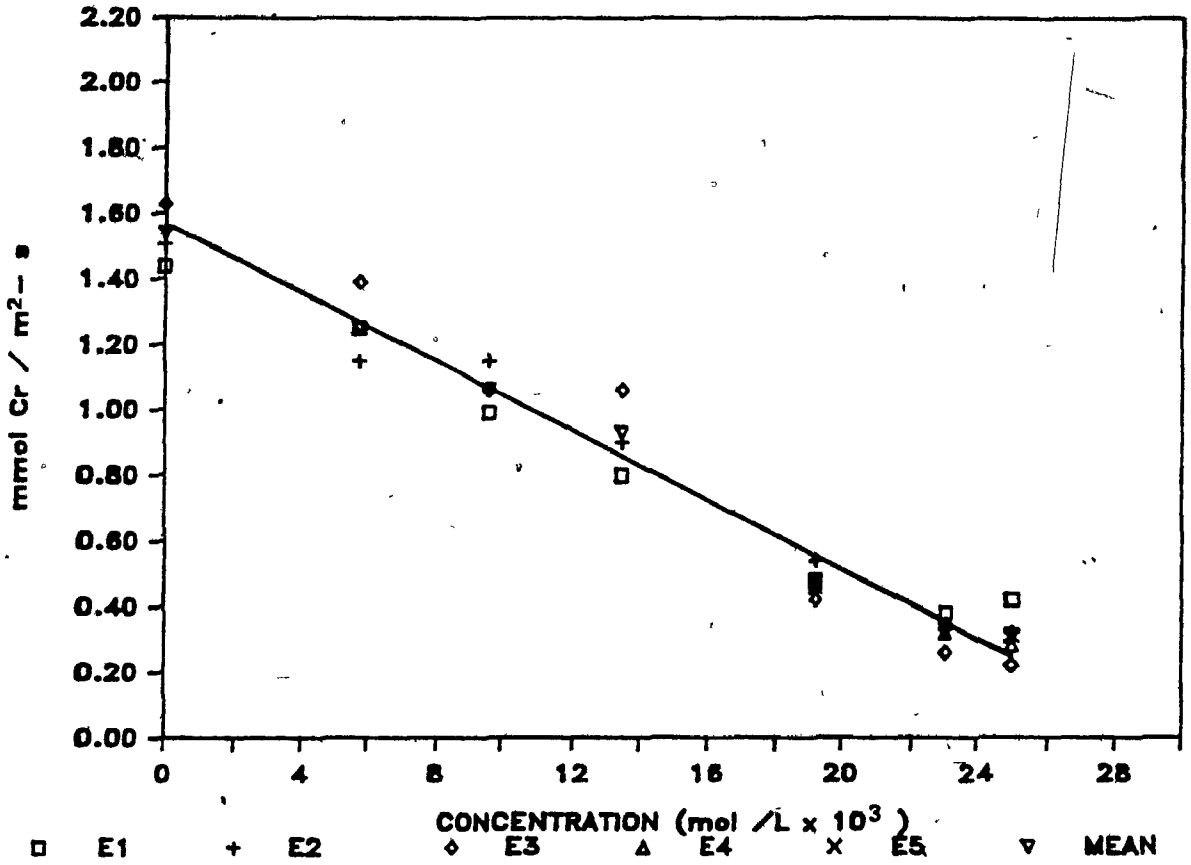

Figure 3.9 Variation in Cr Etch Rate with Concentration of CrO_4^{-2} ($KMnO_4$ =0.41 mol/L, NaOH = 0.50 mol/L, 43 C, 1500 rpm)

Using the experimental data from the two sets of isolated experiments shown in figures 3.8 and 3.9 the coefficients for the rate expression were estimated. A fit of a first order model of the form:

$$r = k_2 C_b + k_3 C_c$$

and a non-linear model of the form:

$$r = k C_b^{\beta} C_c^{\gamma}$$

was attempted. The linear expression is as follows:

$$r = 3.91 C_b - 53.61 C_c \qquad (3.10)$$

Similarly the non-linear model is :

$$r = 1.08 C_b^{0.33} C_c^{-0.07} \qquad (3.11)$$

Statistical analysis of the variance for each model showed that the linear model fit the experimental data but the non-linear model did not. In the linear model both coefficients were found to be significant at 95% confidence interval. The reaction is first order with respect to $KMnO_4$ and first order with respect to Cr. The resulting rate expression applicable to the concentration range of $KMnO_4$ from 0.16 to 0.57 mo/L and to the concentration range of Cr from 0 to 19 mmol /L is :

$$r = 3.91 C_b - 53.61 C_c \qquad (3.13)$$

where: $k_2 = 3.91$ (L/mol) (mmol /m^2-s)
$k_3 = 53.61$ (L/mol) (mmol /m^2-s) @ 43 °C

The estimated rate from this model along with the non-linear model is plotted in figures 3.10 and 3.11 along with the experimental data. One observes in both plots that the linear

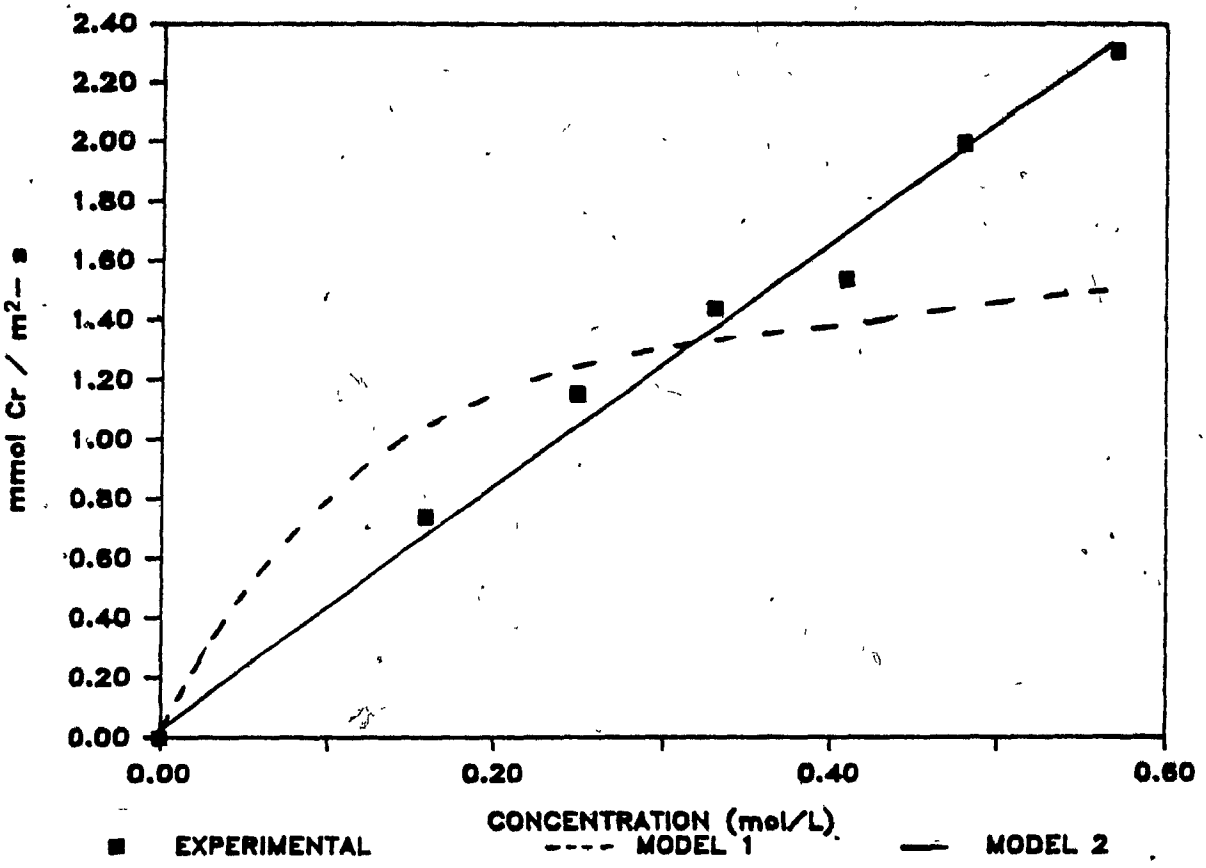

Figure 3.10 Variation of Cr Etch Rate with Concentration of $KMnO_4$. Experimental vs Linear Model (2), Non-Linear Model (1).

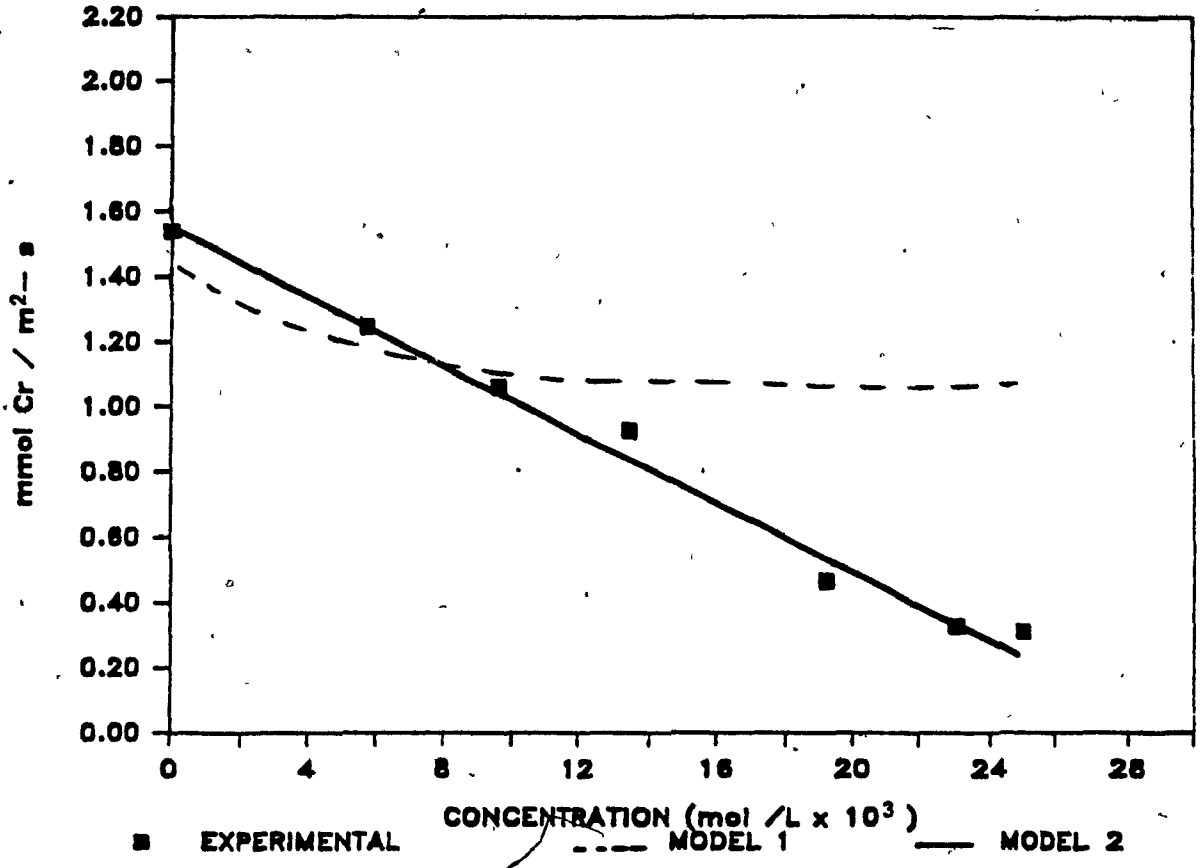

Figure 3.11 Variation of Cr Etch Rate with Concentration of CrO_4^{-2}
Experimental vs Linear Model (2), Non-Linear Model (1).

expressions fit the exerimental data noticeably better than the non-linear expressions over the entire concentration range of $KMnO_4$ and CrO_4^{-2}.

G. Effect of Temperature on the Rate.

Assuming that the temperature dependencies of the rates of the reactions taking place in the dissolution of the oxide and Cr follow the Arrhenius law, Arrhenius plots were made based on experimental data where r_1 and r was measured for temperatures in the range of 20 to 60°C.

Figure 3.12 shows that the relation between ln k_1 and 1/T is linear. From the data, a linear regression was performed to estimate the apparent activation energy E_1' from the slope of figure 2.12 and the apparent frequency factor A_1' from the 'y' intercept. For the rate constant k_1 the expression relating k_1 to temperature is :

$$k_1 = A_1' \exp [-E_1' / RT] . \qquad (3.14)$$

$$k_1 = 4.05 \times 10^8 \exp [-5.01 \times 10^4 / RT] \qquad (3.14a)$$

$A_1' = 4.05 \times 10^8$ (L/mol(mmol Cr /m^2-s) ;
$E_1' = 5.01 \times 10^4$ (J/mol)

For the reaction rate r , the expression relating k_2 to temperature was determined from the data plotted in figure 3.13. One observes in this figure a linear variation in ln(k_2) with 1/T. The Arrhenius equations for k_2 is :

$$k_2 = 4.64 \times 10^3 \exp[1.86 \times 10^4 / RT] \qquad (3.15)$$

$A_2' = 4.64 \times 10$ L/mol (mmol Cr / m^2-s)
$E_2' = 1.86 \times 10$ J/mol

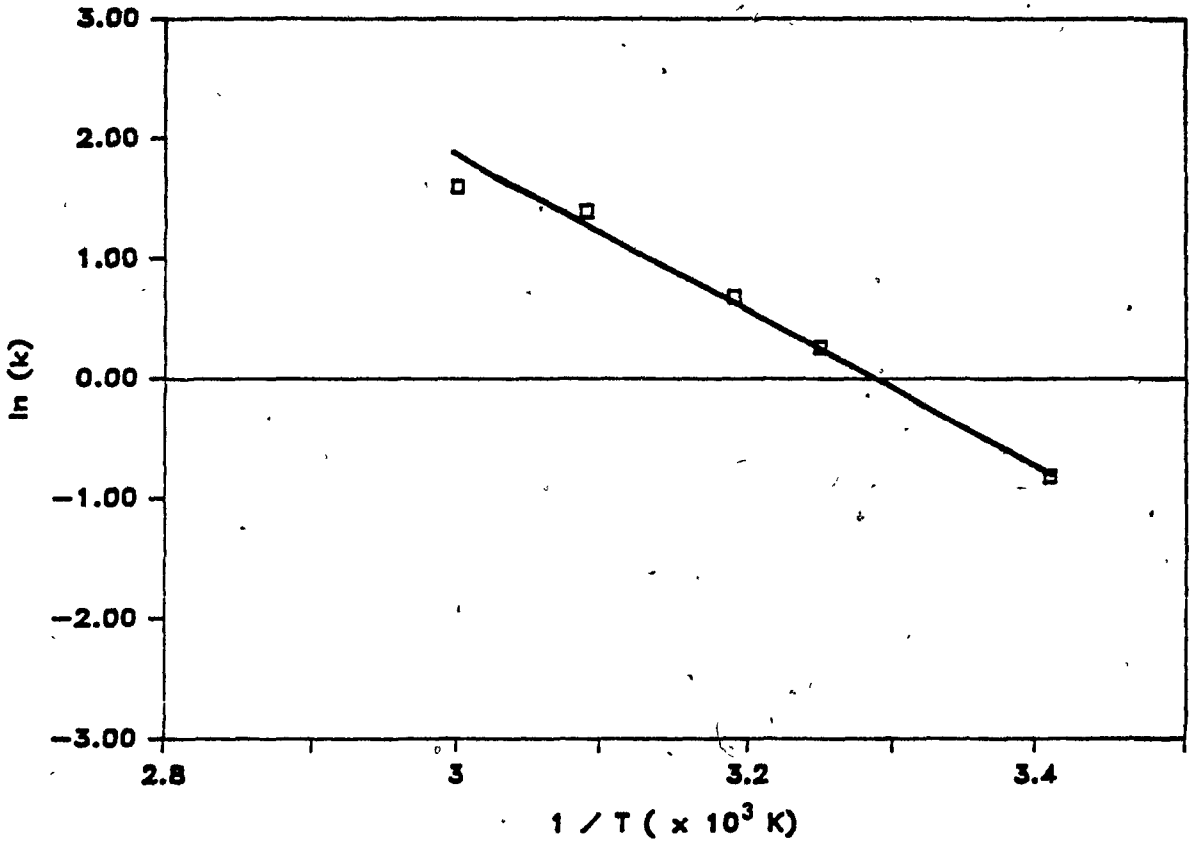

Figure 3.12 Arrhenius Plot of k1 - Rate Constant for ri.
($KMnO_4$ = 65 g/L, NaOH = 20 g/L, Cr = 0.015 g/L, —— 1500 rpm)

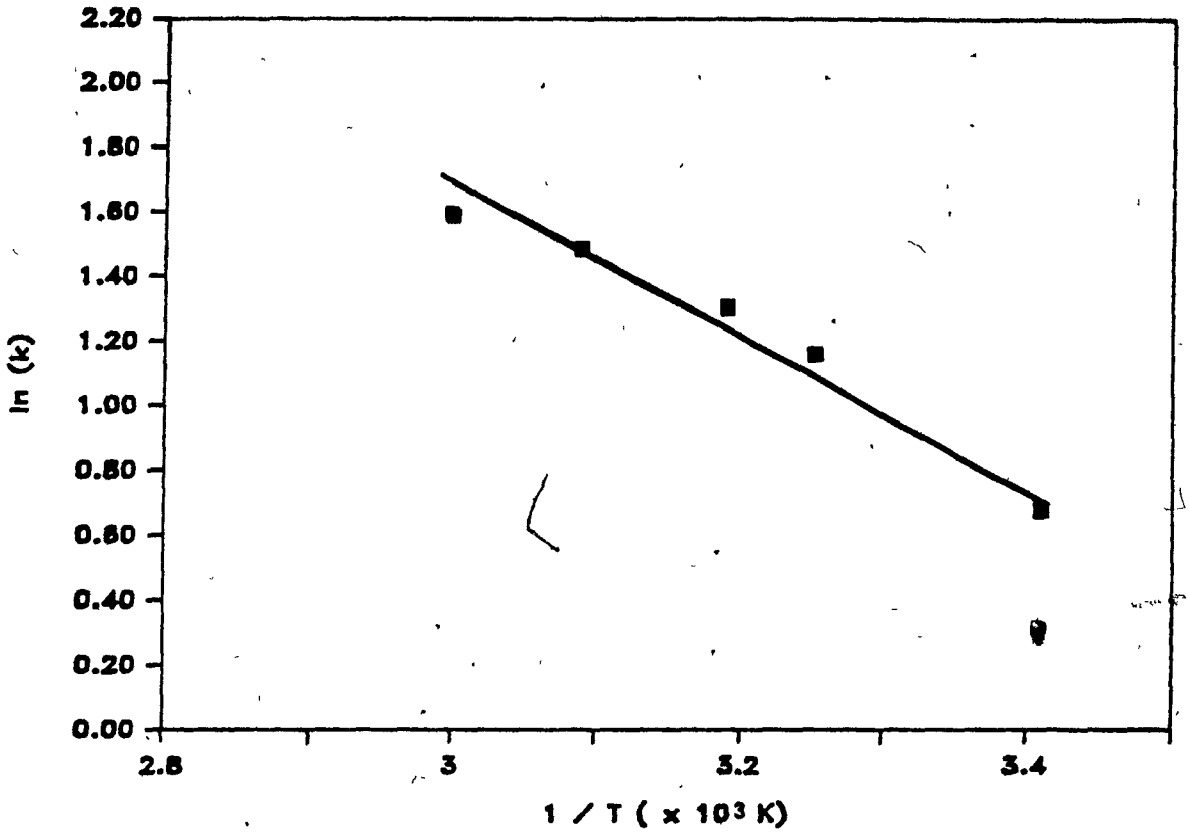

Figure 3.13 Arrhenius Plot of k2 -Rate Constant for r.
($KMnO_4$ =0.41 mol/L, NaOH = 0.50 mol/L, Cr = 0.29 mmol/L, 1500 rpm)

2.4 Conclusions

The development and use of the rotational etcher has apparently increased to rate of mass transfer of the etchant to the chromium Cr surface to the point where the rates that are being measured are actually the intrinsic rates of reaction.

The surface roughness of the metal does have an effect on the rate of Cr dissolution. The significant effect of surface roughness on the etch rates occurs at roughnesses between 0.05 and 0.13 μm. At higher surface roughnesses of the chromium tile the effect is less significant and other limitations to the etching system become the overriding factors that affect the etch rate.

From the experimental data one observes two separate solid -liquid reactions occurring during the etching of Chromium. The initial rate which is related to the dissolution of the oxide layer is a first order reaction with respect to NaOH concentration and follows the following rate law:

$$r_1 = 4.05 \times 10^{8} \exp[-5.01 \times 10^{4}/RT]\ C_a \qquad (3.16)$$

The experimental data has shown the the dissolution of the Cr^0 with MnO_4^{-1} is influenced both by $KMnO_4$ and dissolved Cr as CrO_4^{-2}. The rate law for (r) is expressed in the following relation which is valid for concentration of $KMnO_4$ between 0.13 mol/L and 0.60 mol/L and Cr concentrations between 0 and 19 mmol /L.

$$r = 3.91\ C_b - 53.61\ C_c \quad \text{at } 43^{\circ}C. \qquad (3.17)$$

The activation energy and pre-exponential factor for k_2 (the coefficient of C_b) are 5.01×10^3 J/mol and 4.64×10^4 (L/mol) (mmol Cr/m^2-s) respectively.

CHAPTER 4

CHROMIUM AND COPPER ETCH PROFILES

4.1 Introduction

The purpose of etching chrome and copper from metallized ceramics is to produce a circuit pattern that will conform to certain dimensional specifications for the final product. The range of electrode dimensions of particular concern to metallized ceramics is 25 - 50 μm. However in integrated circuit manufacturing the electrode dimensions are typically in the range of .1 - 1 μm. With this type of resolution, wet chemical etching methods are not used.

To achieve the one micron and sub-micron circuitry, dry, plasma assisted techniques such as sputter etching, plasma etching and reactive ion etching are used [13]. The advantages of these techniques are in the control of the etch profile and in the control of resist undercut. Chemical etching techniques such as dip etching, bubble etching and spray etching lead to similar etch profiles due to the diffusion and reaction mechanisms occurring at the metal surface causing equi-directional (isotropic) etching. In commercial applications, spray etching has the fastest rates and the best control of undercutting among the chemical etching methods mentioned above. The reason for the higher rates is the high impingement of the etchant on the metal surface and the high rate of solution replenishment [14]. However the boundary layer on the metal surface is not completely removed at normal operating pressures (120-160 KPa).

In this chapter various etch profiles common in the microelectronics industry will be discussed. A comparison of the etch profiles produced by spray etching and the etch profiles produced by rotational etching (a method developed during the course of this research) will be made. The effect of the etch times of top chrome, copper, and base chrome on the undercut of the resist will be studied. In this study, metallized ceramic substrates with nominal electrode widths of 25 μm were used. Finally the three common etch profiles produced by wet and dry etching methods are described. The objectives of this chapter are summarized below:

a. To determine the inter-relationship between Cr/Cu/Cr etch times on the resist undercut.

b. To describe qualitatively the possible etch profiles that can occur and compare the profiles obtained between spray etching and rotational etching.

4.2 Material and Methods

A. Etching of Copper and Chrome - Effect on Undercut.

The etchant solutions for chrome ($KMnO_4$ / NaOH) and copper ($FeCl_3$ / HCl) were prepared according to procedure 3.2A. The concentrations of the etchants were as follows:

Chrome etchant	Copper etchant
$KMnO_4$ = 0.41 mol/L	$FeCl_3$ = 35%/w
NaOH = 0.50 mol/L	HCl = 3 %/w
T = 43°C	T = 29 °C

pH = 13.3 pH = 0.5

Agitiation = 1500 rpm Agitation = 1800 rpm

Ceramic substrates were used from IBM Bromont's substrate manufacturing line. The metal thickness, resist thickness and expose energy were all within the process specifications. The parts were etched in the rotational etcher using the procedure outlined in 3.2B. The agitation rate of the etchants in the reactor and the positioning of the parts in the reactor were adjusted to reduce transport effects to the surface.

To determine the effect of the etch times of top chrome, copper and bottom chrome (which will henceforth be denoted as Cr/Cu/Cr etch time) on the electrode width and undercut, a three level 3^3 full factorial design with four replicates at the center was used. The three levels of the Cr/Cu/Cr etch times were 30, 60, 90 seconds. The details of each experimental run are tabulated in table A.3.1 in the appendix.

The dimensions of the circuit lands were measured under indirect light at 400X using a Nikon Optihot metallurgical microscope. An xyz table attached to the microscope stage was used to measure the land widths to 3.0 μm accuracy. The actual measurement of the undercut involved measurment of the resist width at prescribed locations on the part. The resist was then stripped off in order to measure the top chrome and copper electrode width using direct lighting in the microscope. To measure the base chrome undercut the top chrome and copper layers were etched from the electrodes to expose the underlying base chrome layer.

4.3 Results and Discussion

A. Modeling of the Cr/Cu/Cr Undercut

The results of the three level 3^3 factorial experimental design were used to fit three linear models relating undercut of top chrome, Copper, and base chrome to the Cr/Cu/Cr etch times. Undercut is defined as the difference between the resist width after exposure and the actual metal land width after etch.

The top chrome undercut (U_1) is given by :

$$U_1\ (\mu m) = 0.13\ T_1 + 0.36\ T_2 + 0.03\ T_3 - 0.93 \quad (4.1)$$

Where T_1 = Etch time of Top Chrome (s)
T_2 = Etch time of Copper (s)
T_3 = Etch time of Bottom Chrome (s)

The model statistically fits the experimental data and all three coefficients are significant at the 95% confidence level. This indicates that the top chrome dimension depends on the copper being efficiently etched underneath. The effect of base chrome etch is to attack not only the horizontal base Cr^0 surface but also the top chrome surface. The top chrome is easier to undercut because the resist layer is weak at the metal edges. Also, the copper surface residing on top of the base chrome is 100 times thicker and inert to the chromium etchant. If the base chrome etch time is too long, a phenomenon called copper striping occurs (to be discussed later).

The model for the copper undercut (U_2) is :

$$U_2\ (\mu m) = -5.91 + -0.09\ T_1 + 0.51\ T_2 - 0.06\ T_3 \quad (4.2)$$

ANOVA of the statistical data found that the model fit the

experimental data but the coefficient of T_2 was the only one found to be significant at 95% confidence level. Thus the resulting model for (U_2) with T_1 and T_3 dropped is:

$$U_2 = -5.91 + 0.51\ T_2 \qquad (4.2a)$$

This result indicates the obvious dependence of the copper layer and its etch time on the overall circuit dimension. During the etch experiments for the copper layer it was noticed that if a thin layer of top chrome remained, the $FeCl_3$ at a pH of 0.5 was aggressive enough to dissolve the chromium. If the residual chromium layer is thin, its effect on copper undercut is minimal because of the etchant aggressivity, but if a substantial layer of chromiumremains such as in the case after 15 s Cr etch time, then residual copper will remain on top of the base chrome. This etch time is lower than the minimum time (30 s) used in the experimental design thus the residual chrome effect is not reflected in the model (equation 4.2a).

The last model relates the base Cr^0 undercut to the Cr/Cu/Cr etch times :

$$U_3 = 0.03\ T_1 + 0.45T_2 + 0.33\ T_3 - 29.10 \qquad (4.3)$$

The model fit the experimental data but the coefficient of T1 was found to be insignificant thus was dropped from the model. The final expression is therefore :

$$U_3 = 0.45\ T_2 + 0.33\ T_3 - 29.10 \qquad (4.3a)$$

The above relation showing that U_3 is influenced by T_2 emphasizes the difficulty of the etchant to penetrate under the Cu^0 layer. As mentioned earlier the thickness of the copper is

100 times the thickness of the base chrome. This difference is the reason for the dependence of copper undercut on base chrome undercut.

B. Qualitative Discussion of Cr/Cu/Cr Undercut.

Plates 4.1 to 4.8 show the type of electrode patterns that can occur at various Cr/Cu/Cr etch times, as well as the appearance of the metal layers under the photo resist at various etch times. With spray etched parts, the expected undercut at Cr/Cu/Cr etch times of 60/30/60 seconds is 13.0 μm (plate 4.1a) The photo mask which defines the circuit pattern, is designed to take into account a loss in the electrode width during etching. This additional amount of land width is called the etch factor of the mask and its objective is to assure that all the electrodes on the part are within a certain dimensional range after etching.

Comparison of plates 4.1a, showing an example of a spray etched electrode and plate 4.1b a rotationally etched electrode reveals that for the same etch times of Cr/Cu/Cr, the rotationally etched part has less undercut of the resist (2 μm) than the spray etched which has an undercut of 13 μm. This indicates that at these etch times there is very little etching in the horizontal direction in the rotational etcher. This further supports the claim that rotational etching results in anisotropic etching.

Plate 4.2 shows the effect of an increased Cu etch time in the rotational etcher on the circuit undercut. It is observed that the undercut has increased to 13 μm which is comparable to spray etched undercut at Cr/Cu/Cr etch times of 60/30/60

Plate 4.1a Spray Etched Electrodes at Etch Times of Cr/Cu/Cr of 60/30/60 sec. (400x)

Plate 4.1b Etched Electrodes at Etch Times of Cr/Cu/Cr of 60/30/60 sec. (400x)

Plate 4.2 Etched Electrodes at Etch Times of Cr/Cu/Cr of 60/60/60 sec. (400x)

Plate 4.3 Etched Electrodes at Etch Times of Cr/Cu/Cr of 30/90/30 sec. (400x)

seconds.

Plate 4.3 shows that at low base Cr^0 etch times, a small film of Cr^0 remains on the ceramic surface, however at the same time the Cu^0 has been etched to 38 μm undercut. This phenomenon is called 100% overetch which is defined as the amount of undercut below the nominal land width.

Plates 4.4 and 4.5 show the effect of base chrome etch on top chrome undercut. A close inspection of the electrodes show that the top chrome layer has a smaller width than the uncerlying copper which is seen as the dark region around the electrode. This exposure of copper from the overetching of top chrome is called copper striping. Plate 4.6 shows a more detailed example of copper striping which has been produced by extended top Cr^0 and base Cr^0 etch times.

Plates 4.7 and 4.8 show the effect of high Cu^0 etch times at any Cr^0 etch times. In both cases 100% overetch or total undercutting of the resist has occurred. This type of undercutting causes open circuits as well as adhesion problems at the various metal interfaces as well as at the ceramic/metal interface.

C. Discussion of the Etch Profiles.

In the previous section we saw the electrode patterns as viewed from above. This method of observation in some cases does not effectively represent the actual electrode geometry and the true lateral dimension of the electrode. In this section a more detailed look at the electrode profiles will be done from a cross sectional point of view.

The three typical etch profiles that can be produced by various etching techniques both dry and wet are depicted in

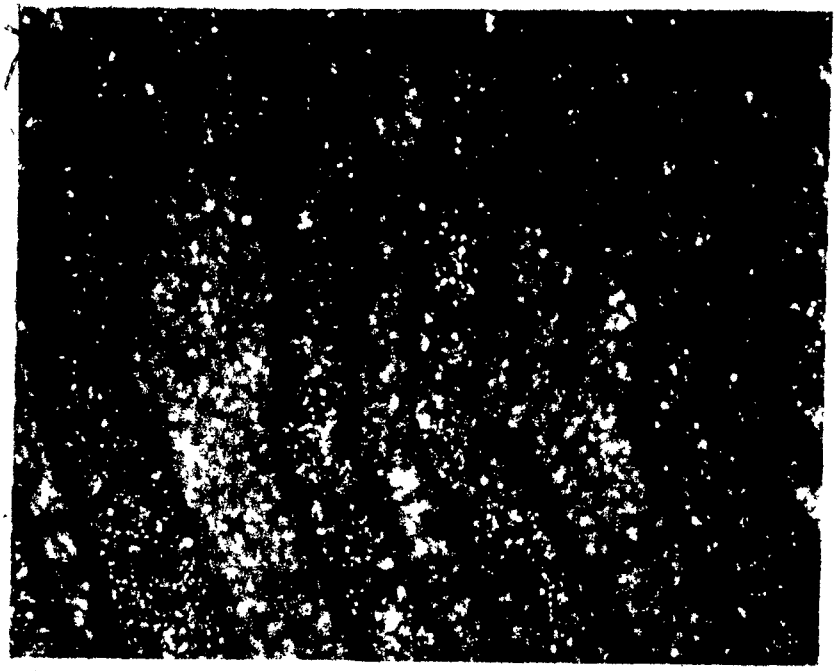

A. Base chrome

Plate 1 1 Etched Electrodes at Etch Times of Cr/Cu/Cr of 30/30/30 sec. (400x)

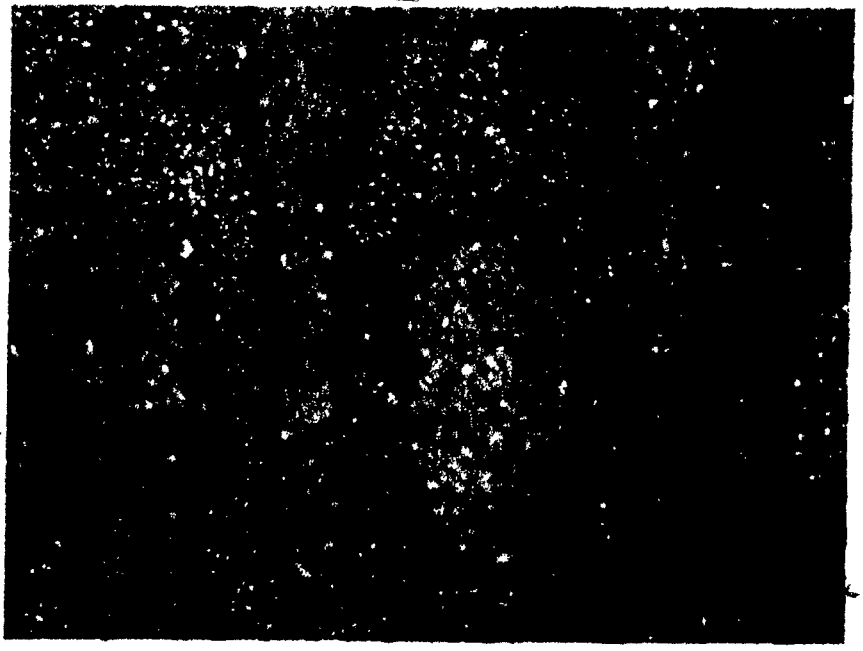

A. Ceramic
B. Copper

Plate 4.5 Etched Electrodes at Etch Times of Cr/Cu/Cr of 30/30/60 sec. (400x)

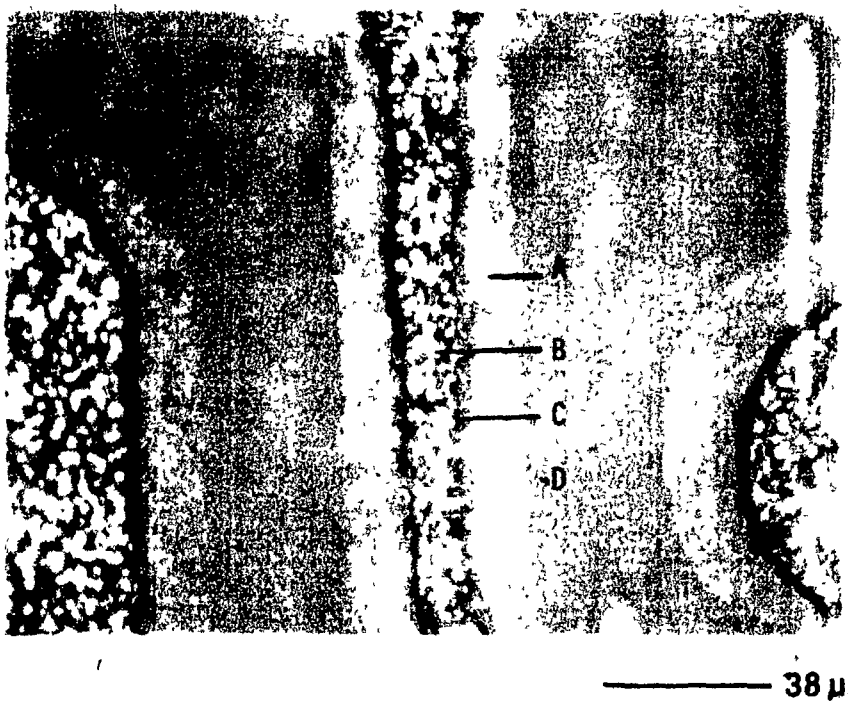

A. Photoresist
B. Top chrome
C. Copper
D. Ceramic

Plate 4.6 Etched Electrodes at Etch Times of Cr/Cu/Cr of 90/60/90 sec. (600x)

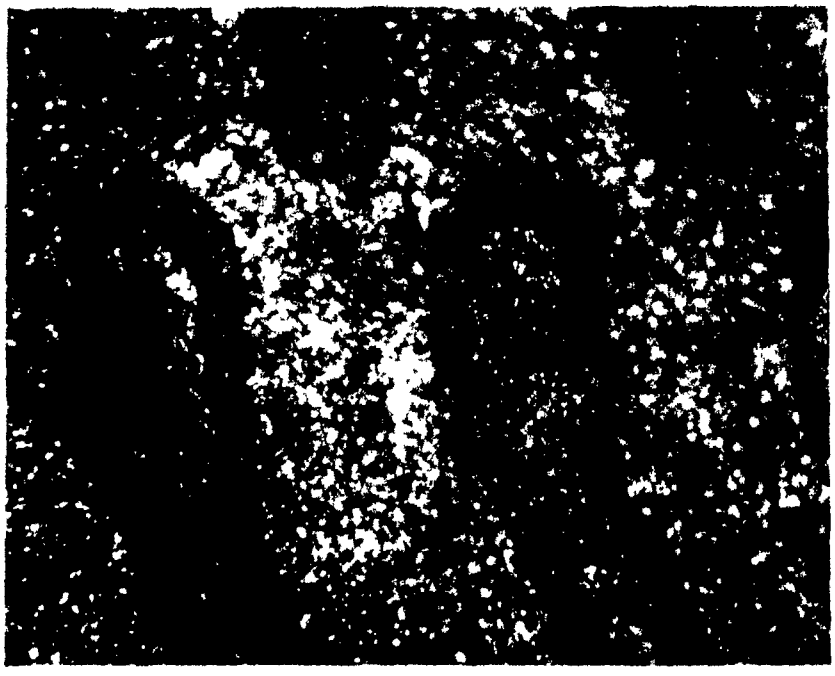

A. Base Chrome

Plate 4.7 Etched Electrodes at Etch Times of Cr/Cu/Cr of 90/90/30 sec. (400x)

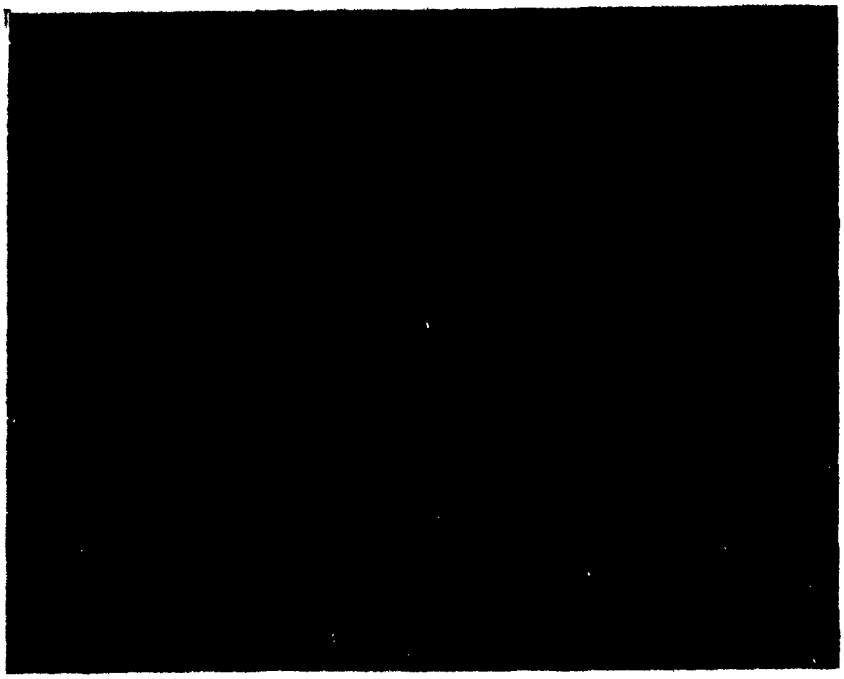

A. Photoresist
B. Ceramic

Plate 4.8 Etched Electrodes at Etch Times of Cr/Cu/Cr of 90/90/90 sec. (400x)

figure 4.1. The etched profile in figure 4.1a is typical of wet chemical etching and those in figure 4.1b and 4.1c are typical of plasma assisted etching techniques. The main objective of this section is to show that profiles in 4.1b and 4.1c were produced by wet chemical techniques in a rotational etcher. The profiles in 4.1b and 4.1c, can be produced by controlling the direction at which the the ions bombard the surface during sputter or reactive ion etching. With this type of control anisotropic etching (4.1c) or 80% anisotropy (4.1b) can be obtained.

The profile in 4.1b which is a steep wedged profile is caused by the failure of the resist to adhere at the edges. During etching the metal atoms on the horizontal surface unprotected by the resist are removed first. As etching continues, the resist at the edges of the land break off causing the horizontal surface under the broken resist area to be exposed and eventually etched. The radial profile in figure 4.1a is a result of isotropic etching. The reactants that diffuse through the boundary layer react equally in all directions thus the global rate of reaction is equal in both the horizontal and vertical direction.

To determine the actual geometry of the electrode, S.E.M. (Scanning Electron Microscope) cross sections were taken of the etched Cr/Cu/Cr electrodes. It is difficult to discern the top chrome and base chrome layers because of their small thickness. Thus the cross section in plates 4.9 to 4.13 are of 8 μm thick copper electrodes.

Plate 4.9 shows a 25μm wide copper electrode spray etched at IBM Bromont's spray etcher at 60/30/60/ seconds Cr/Cu/Cr/ etch times. The profile observed with S.E.M. is similar to the

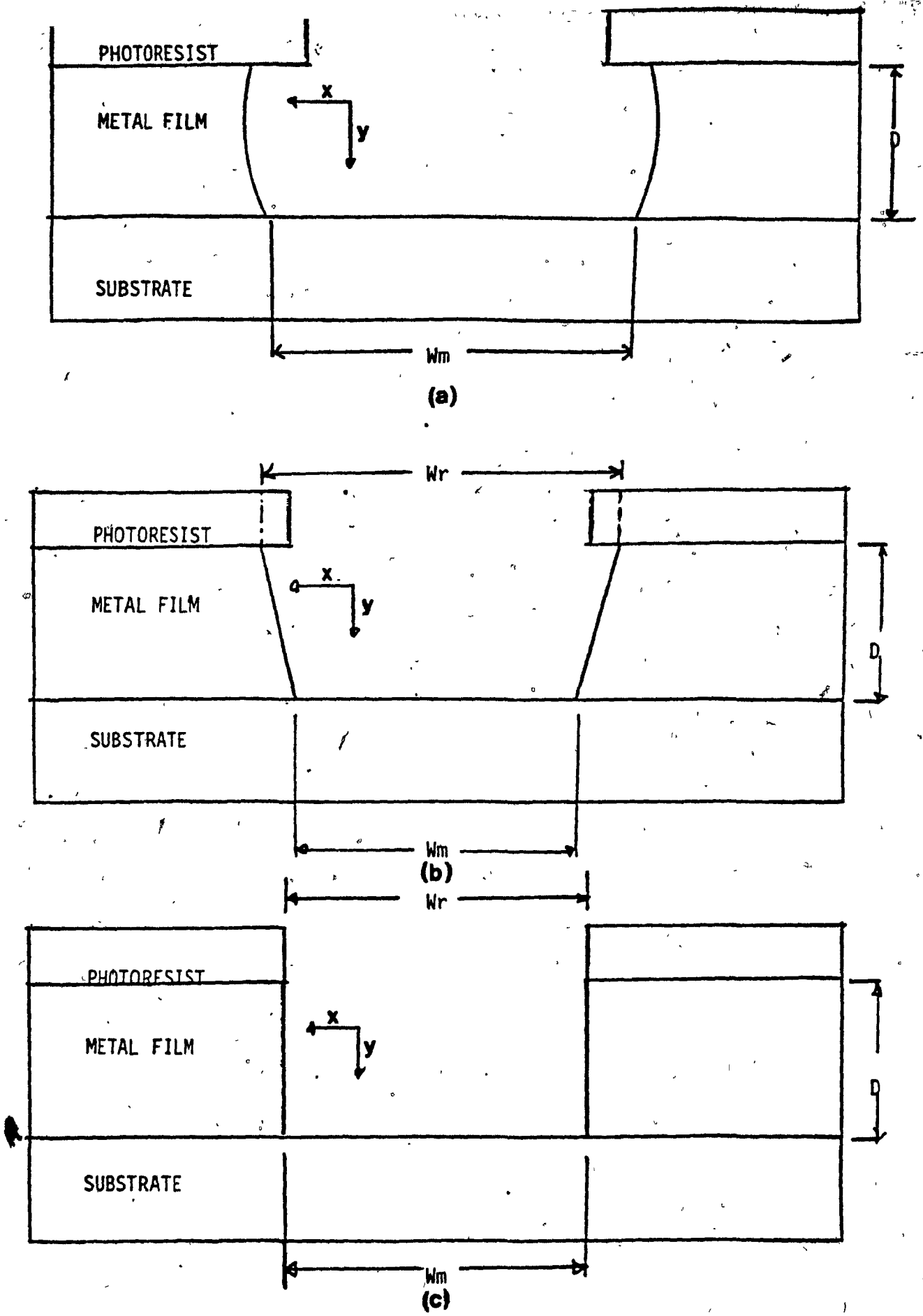

Figure 4.1 Comparison of Etch Profiles: a) Isotropic, b) Steep Wedge, c) Anisotropic

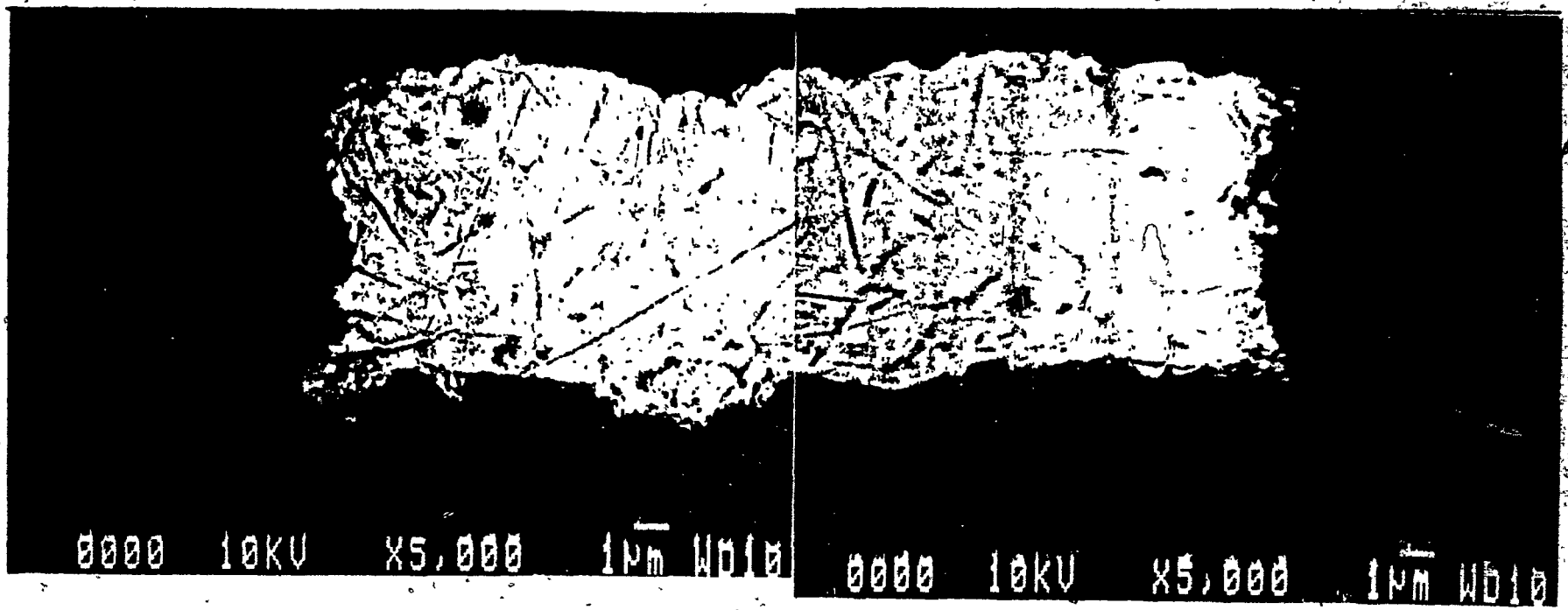

Plate 4.9 S.E.M. Cross Section of 25 um Electrode Spray Etched at Cr/Cu/Cr Etch Times of 60/30/60 sec.

profile depicted in figure 4.1a which is an isotropic etch profile. As mentioned earlier, spray etching results in isotropic etching, that is the etch rate is the same in the vertical and horizontal direction. Initially very little metal is removed from the vertical surface of the electrode. As time proceeds more and more of the vertical surface is being exposed leading to an increase in the rate of metal removal from the vertical surface. This results in a concave profile as seen in plate 4.9.

Plates 4.10 and 4.11 show S.E.M. cross sections of copper electrodes of 25 μm and 50 μm width respectively. In both cases, an anisotropic etch profile similar to figure 4.1c is observed. This further supports the claim that with rotational etching, one can obtain anisotropic etch rates.

Plates 4.12 and 4.13 show rotationally etched 25 and 50 μm electrodes that have respectively undergone resist failure at the edges. The etch profile is still linear (80% anisotropic) but the top edges near the failed resist have been etched more than the bottom edges of the electrodes. In the last four plates depicting the anisotropic etch profiles, the dimensions measured by a microscope can be used to determine the true dimensions of the electrode since the profiles are linear.

4.3 Conclusions

From the experimental data one sees that the undercut of the top chrome is dependent on top chrome, base chrome and copper etch times. However the copper undercut is dependent on the copper etch time only. This leads to the conclusion that even if some residual top chrome remains on the copper surface,

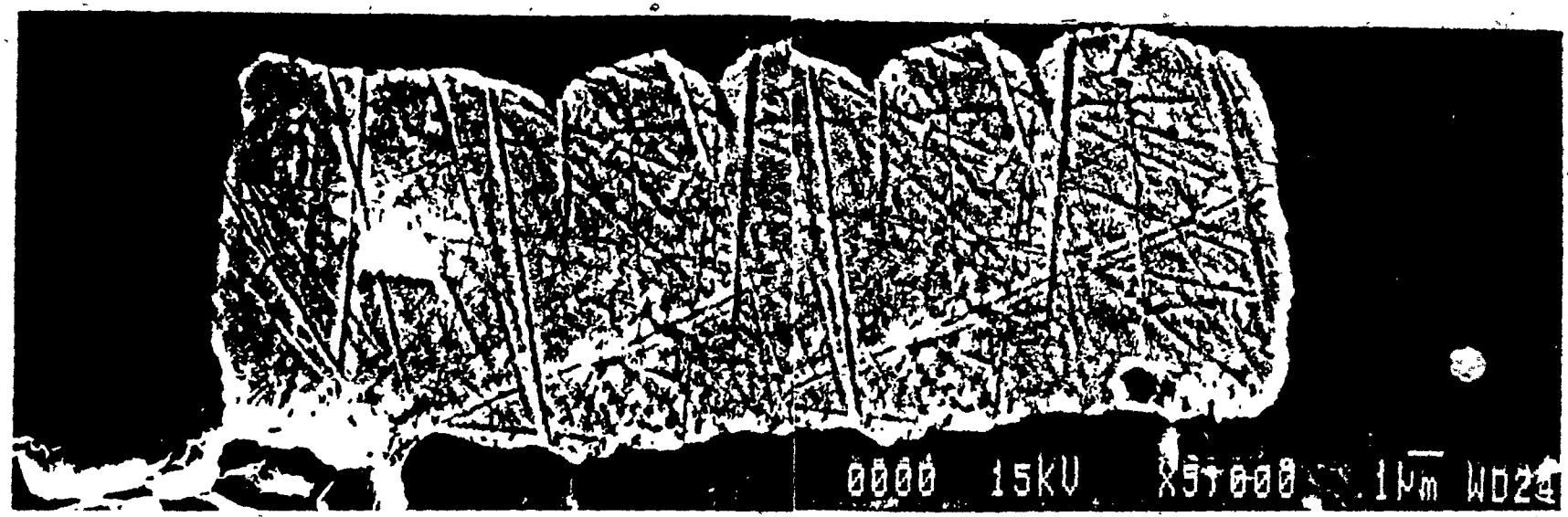

Plate 4.10 S.E.M. Cross Section of 25 um Electrode Rotationally Etched at Cr/Cu/Cr Etch Times of >30/>30/>30 sec.

Plate 4.11 S.E.M. Cross Section of 50 um Electrode Rotationally Etched at Cr/Cu/Cr Etch Times of >30/>30/>30 sec.

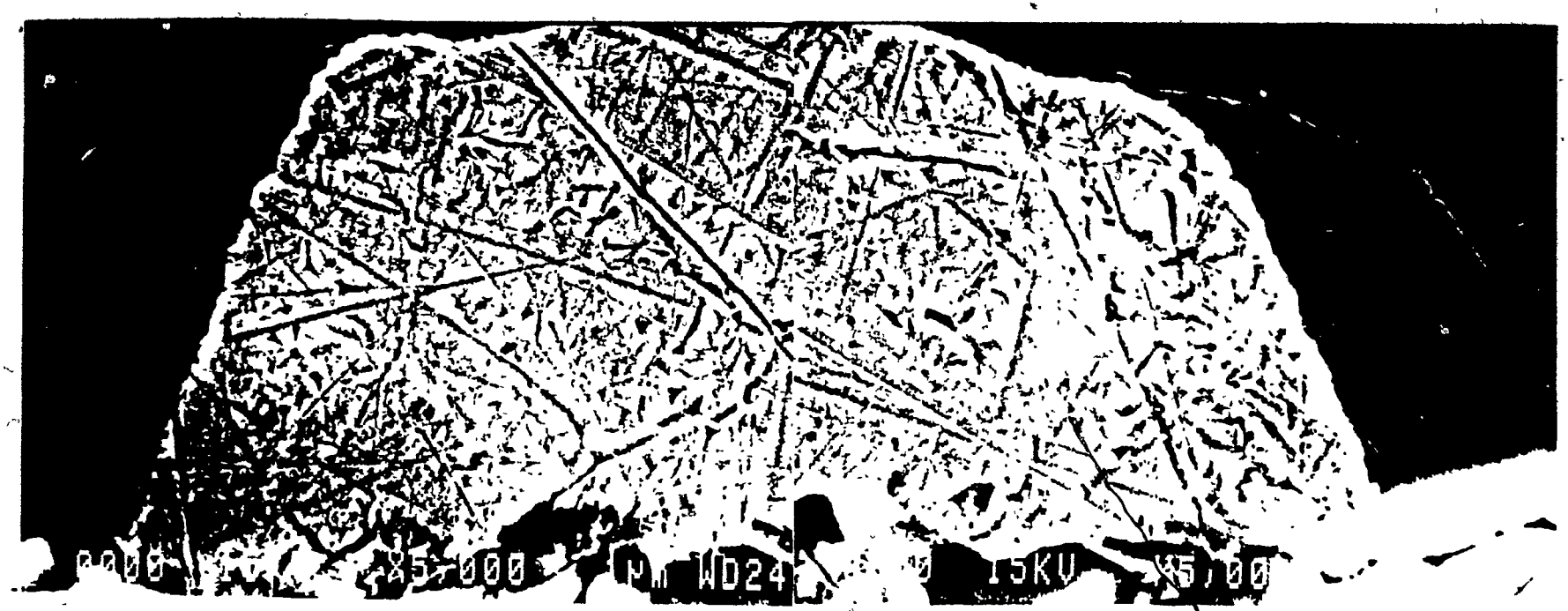

Plate 4.12 S.E.M. Cross Section of 25 um Electrode Rotationally Etched at Cr/Cu/Cr Etch Times of >30/>60/>30 sec.

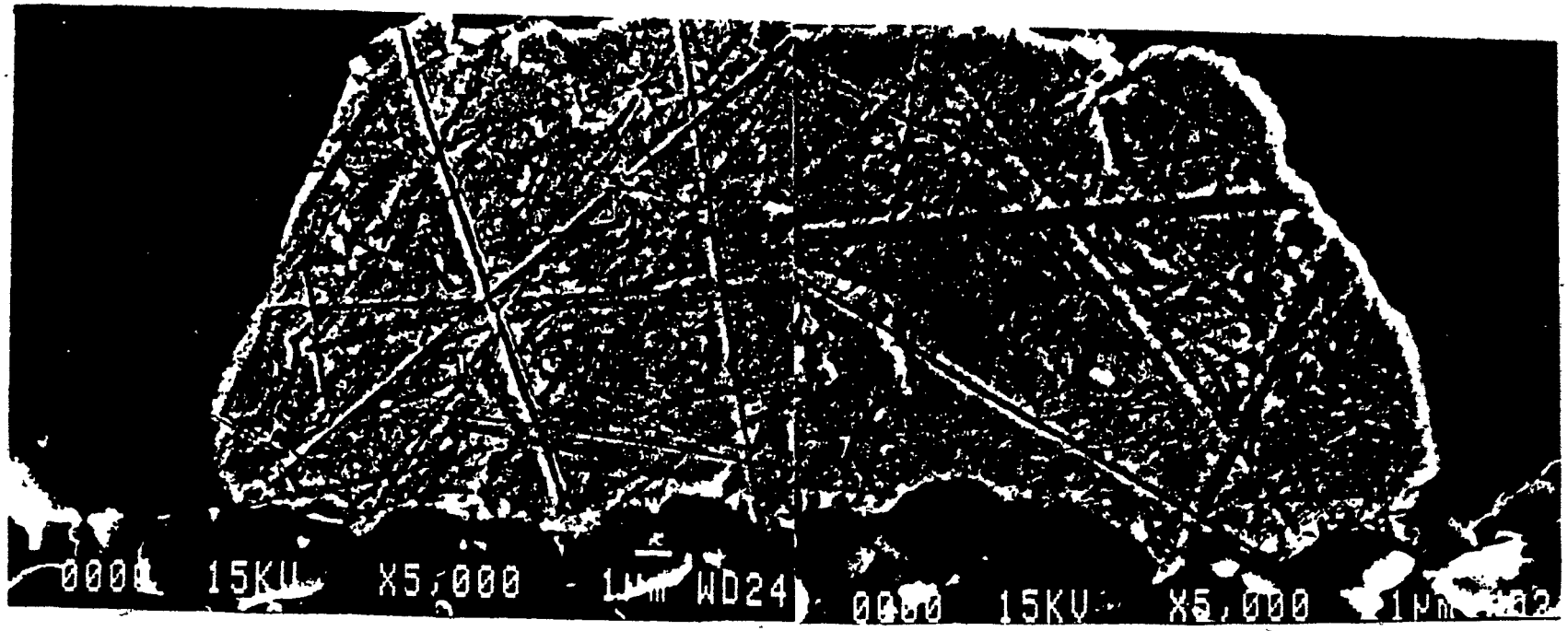

Plate 4.13 S.E.M. Cross Section of 50 μm Electrode Rotationally Etched at Cr/Cu/Cr Etch Times of >30/>60/>30 sec.

the $FeCl_3$ etchant is agressive enough to dissolve this metal film. One also observes that copper striping is a results of top chrome attack during base chrome etch. Base chrome etch seem to be heavily dependent on the efficiency of the top copper etch.

One can conclude from the S.E.M. cross sections that the rotational etcher that was developed for this research project does indeed reduce transport effects at the surface. The linear edged profiles that were obtained show that anisotropy is being attained with a chemical etching method.

CHAPTER 5

GENERAL CONCLUSIONS AND RECOMMENDATIONS

The purpose of this thesis work was to study the kinetics of chromium etching in order to be able to understand this phenomenum that is occurring in the present etching process at IBM. With a better understanding of the reaction mechanisms, one can investigate further process improvements.

5.1 Conclusions

1. The surface roughness of the substrate is important to efficient etching. Thus a close control on ceramic quality is warranted to insure consistent etching.

2. The range in metal thickness on a substrate was assumed to be small but the data shows that a large variation in the chromium layer can exist on one substrate. Thus during thickness measurement of the samples to determine if a particular sputter run is within specifications, it is important to be consistent in the areas being measured for metal thickness. More than one area of the substrate should be measured to insure that the thickness of the whole suface is within the process specifications.

3. From the kinetics data one sees that the etching of chromium follows two reaction steps. The first step which is related to the dissolution of the oxide film is governed by the

following rate law:

$$r_1 = 4.05 \times 10^8 \exp[-5.01 \times 10^4 / RT]\, C_a \qquad (3.18)$$

The second reaction step is the dissolution of the chromium metal and is governed by the following rate law:

$$r = 3.91\ C_b - 53.61\ C_c \qquad @\ 43\,^{\circ}C \qquad (3.17)$$

The activation energy and pre-exponential factor for k_2 (the coefficient of C_b) are 5.01×10^3 J/mol and 4.64×10^4 (L/mol) (mmol Cr/m^2-s) respectively.

5.2 Significance and Recommendations

1. The knowledge of the etching mechanism indicates that in the commercial etching process the time spent to etch to chromium layer is divided into two parts. About 60 % of the etch time is used to dissolve the oxide layer and 40% of the time is spent dissolving the underlying Cr metal. The benefit of the oxide layer is that it promotes good resist - chrome adhesion but if the oxide layer is too thick (caused by an air leak in the sputter chamber) the chrome becomes difficult or impossible to etch. A possible rework procedure to be investigated when the oxide layer is too thick is a possible pre-dip of the parts in a concentrated NaOH before the parts are applied with photoresist.

2. The determination of the rate laws and rate constants for the chromiumetch process allows the implementation of P.I.D. control of the chemical bath adjustments. Present work on the etch process was to automate the bath adjustments using a

controller. However only - On/Off control could be achieved since no kinetics data existed for the chromiumetching process. Now that the rate constants are known, the controller transfer functions can be written and implemented into the control loop.

3. The intrinsic rate laws that were developed show that there is room for improvement in the etching rates. The bulk etch rates measured in the spray etchers are at least 20% lower than the intrinsic etch rates. Thus modifications to the spray system in terms of new nozzle configurations or new nozzle type should be investigated to reduce transport effects at the surface.

4. Modifications to the bulk chemical concentrations should be investigated since the bulk concentrations in the spray etcher are not representing the concentrations of the etchant at the substrate surface.

5. The etch profiles obtained by rotational etching are advantageous in that:

i) The electrode dimensions measured by a microscope are representative of the actual etched electrode dimension. In the case of the spray etched parts, the concavity of the electrode makes it difficult to determine the true dimension of the electrode when focusing from above;

ii) The reduced undercutting of the etched electrodes means that the mask etch factor can be reduced thus previous space on the mask that was used to add width to the electrodes because of etch aggresivity could be used for additional electrodes. That is, the circuit density could conceivably be increased if rotational etching is employed.

6. The models developed to show the inter-relationship between the various etch times on final circuit dimensions, with some additional experiments, can be use to predict the circuit dimensions at a given etch condition before the actual parts are passed through the commercial spray etcher. This could reduce or eliminate the need for send-ahead samples to be passed before the entire lot is etched. The benefit of this change would be increased throughput of the machine and reduced inspection of the product.

REFERENCES

1. Keizer, A, and Brown, D., "Bonding Systems for Microelectronic Tape Technology" Solid State Technology, 21 (1978) p.54

2. Howell, J.R., "Relaibility Study of Plastic Encapsulated Copper Lead Frame Epoxy Die Attach Packaging System" Proc Int Rel Phy. Symp. (1981) p 104.

3. Habu, Shinichi., "Study of Copper Etching in Ferric Chloride Solutions" J. Ind. End Chem Process Des Dev. 5 (1982) pp. 511- 514.

4. Dedrick J.W., "Determination of Ferric Chloride Etch Function" IBM Technical Report 01.2597 (1982) pp.1-15.

5. Simons, J., "Improvement of Chromium and Copper Etching Baths In Metallized Ceramic Line", IBM Technical Report 49131 (1980) pp. 1-30.

6. Raniseski, J.W., Chromium Photomasks. IBM Technical Report 22.1027 (June 17,1980).

7. Whyzmuzis, P.J., and Interchemical Corp.," Etch offset plates", U.S.Patent 2,572,228, (Oct. 23 1951).

8. Alph Step 200 Profiler Manual - Tencor Instruments Corp 2400 Chesterton Road Mt. View California.

9. Hamilton & Simpson, Quantitative Chemical Analysis, The McMillan Company N.Y., 12 ed., (1965).

11 Bendz,D.J., "Alkaline Etchant for Chromium Compatible with Positive Resist" IBM Technical Report 22.1822 (1979), pp.1-26.

12. Pourbaix, Marcel., Atlas of Electrochemical Equilibria in Aqueous Solution. Permagon Press (1966) pp.259-293.

13. Sze,S.M., VLSI Technology, Chapter 8 "Dry Etching", McGraw Hill Book Co. N.Y. (1983) p. 303.

14. Duffek, E.F. & Armstrong E., Hanbook of Circuits Manufacturing - Etching McGraw Hill Co. N.Y.(1980) pp.8-1-8.45

15. Himmelblau, David. Process Analysis by Statistical Methods, Sterling Swift Co.Texas, (1970), pp. 51-160.

APPENDIX

TABLE A.1.1 BASE CHROME METAL THICKNESS MEASURMENTS

GRID POSITION	N	MEAN THICKNESS (Å)	ST.DEV
-1, 1	5	628	5
-.5, 1	5	818	7
0, 1	5	865	4
.5, 1	5	740	11
1, 1	5	800	15
1, .5	5	705	6
1, 0	5	815	11
1,-.5	5	785	16
1,-1	5	815	2
.5,-1	5	685	5
0,-1	5	710	5
-1,-1	5	737	13
-1,-.5	5	630	2
-1, 0	5	640	7
-1, .5	5	670	2
-.5, .5	5	865	4
0, .5	5	875	6
.5, .5	5	890	5
.5, 0	5	810	7
.5,-.5	5	815	3
0,-.5	5	895	2
-.5,-.5	5	862	5
-.5, 0	5	795	8
0, 0	5	860	3

TABLE A.1.2 COPPER METAL THICKNESS MEASURMENTS

GRID POSITION	N	MEAN THICKNESS (KÅ)	ST.DEV
-1, 1	5	69.84	.54
-.5, 1	5	42.40	1.78
0, 1	5	65.52	2.34
.5, 1	5	60.90	3.86
1, 1	5	62.30	.34
1, .5	5	82.09	1.68
1, 0	5	82.63	1.88
1, -.5	5	79.95	2.34
1, -1	5	81.55	3.45
.5, -1	5	80.60	.68
0, -1	5	81.80	.24
-1, -1	5	77.62	.36
-1, -.5	5	74.95	.12
-1, 0	5	63.04	1.87
-1, .5	5	58.12	2.24
-.5, .5	5	63.44	1.56
0, .5	5	84.15	1.32
.5, .5	5	83.20	2.04
.5, 0	5	79.66	.78
.5, -.5	5	84.95	.45
0, -.5	5	75.85	.12
-.5, -.5	5	76.80	1.23
-.5, 0	5	82.39	.56
0, 0	5	82.12	.43

TABLE A.1.3 TOP CHROME METAL THICKNESS MEASURMENTS

GRID POSITION	N	MEAN THICKNESS (Å)	ST.DEV
-1, 1	5	945	3
-.5, 1	5	1020	8
0, 1	5	1605	14
.5, 1	5	2015	11
1, 1	5	1440	13
1, .5	5	1425	6
1, 0	5	1565	13
1,-.5	5	1008	16
1,-1	5	1162	10
.5,-1	5	1070	15
0,-1	5	1105	16
-1,-1	5	945	5
-1,-.5	5	1025	6
-1, 0	5	1140	2
-1, .5	5	1145	4
-.5, .5	5	1075	13
0, .5	5	1228	5
.5, .5	5	1130	2
.5, 0	5	1358	9
.5,-.5	5	1178	3
0,-.5	5	1068	2
-.5,-.5	5	1040	15
-.5, 0	5	1160	6
0, 0	5	1131	3

TABLE A.1.4 SURFACE ROUGHNESS MEASUREMENTS

SURFACE	# OF MEASUREMENTS	MEAN ROUGHNESS (μm)	ST .DEV
RAW CERAMIC	10	0.520	0.009
BASE Cr/CERAMIC	10	0.534	0.007
COPPER / CERAMIC	10	0.449	0.010
TOP CR / CERAMIC	10	0.454	0.006
GLASS SLIDE	10	0.009	0.005
BASE Cr /GLASS	10	0.034	0.008
COPPER / GLASS	10	0.024	0.012
TOP Cr / GLASS	10	0.026	0.010

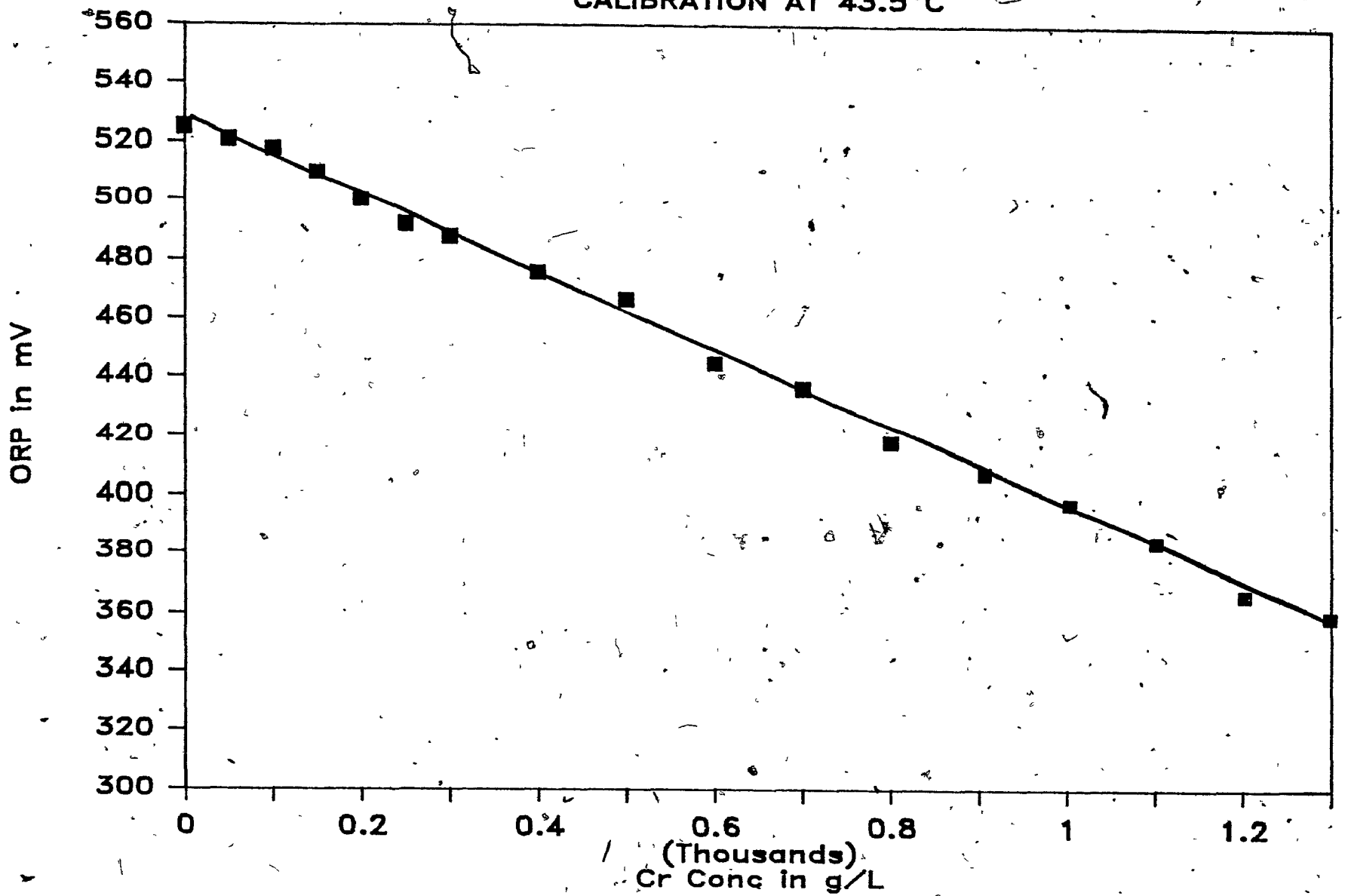

Figure A.2.1 ORP CALIBRATION CURVE @ $KMnO_4$ = 65 g/L, NaOH = 20 g/L

TABLE A.2.1 QUANTITY OF METAL ETCHED IN A GIVEN TIME

TIME (s)	mg Cr etched / cm^2				
	E1	E2	E3	$\bar{x}$	s
0	0.00	0.00	0.00	0.00	0.00
30	0.16	0.15	0.15	0.15	0.00
60	0.31	0.31	0.30	0.31	0.01
90	0.46	0.48	0.49	0.48	0.01
120	0.62	0.62	0.63	0.62	0.01
180	1.10	1.12	1.15	1.12	0.01
240	2.28	2.20	2.30	2.26	0.05
300	3.21	3.22	3.18	3.20	0.02
360	4.37	4.50	4.41	4.43	0.04

ETCHANT CONDITIONS:

$KMnO_4$ = 65 g/L
NaOH = 20 g/L
43 ± 2C
AGITATION = 1.500 RPM

ROTATION SPEED (RPM)	OVERALL ETCH RATE (mmol / m^2 - s)					
	T1	T2	T3	T4	MEAN	ST.DEV
0	0.71	0.95	0.81	0.82	0.83	0.10
700	1.50	1.11	1.35	1.28	1.31	0.16
900	1.52	1.34	1.47	1.43	1.44	0.07
1100	1.28	1.69	1.71	1.53	1.56	0.20
1300	1.63	1.37	1.67	1.56	1.56	0.13
1500	1.53	1.37	1.73	1.58	1.57	0.14
1700	1.51	1.69	1.44	1.53	1.54	0.11

ETCHANT CONDITIONS : $KMnO_4$ = 65 g/L
NaOH = 20 g/L
Cr = .015 g/L
39°C ± 2°C

TABLE A.2.3 SURFACE ROUGNESS FOR VARIOUS POLISHING GRITS

GRIT SIZE	SURFACE ROUGHNESS (μm)	N	ST. DEV
600	0.062	5	0.004
400	0.133	5	0.019
280	0.468	5	0.018
180	0.938	5	0.017
UNPOLISHED	13.100	5	0.235

TABLE A.2.4 SURFACE ROUGHNESS VERSUS ETCH TIME

TIME (SECONDS)	SURFACE ROUGHNESS (μm)					
	T1	T2	T3	T4	MEAN	ST.DEV
60	0.470	0.478	0.483	0.464	0.474	0.008
120	0.453	0.462	0.433	0.442	0.448	0.013
240	0.465	0.433	0.436	0.448	0.448	0.012
300	0.428	0.402	0.445	0.451	0.432	0.022

ETCHANT CONDITIONS: $KMnO_4$ = 65 g/L
NaOH = 20 g/L
40 ± 2°C
AGITATION : 1500 RPM

TABLE A.2.5 Cr ETCH RATE VERSUS SURFACE ROUGHNESS.

SURFACE ROUGHNESS (μm)	N	MEAN OVERALL ETCH RATE (mmol / m^2 - s)	ST.DEV
0.064	5	0.86	.08
0.135	5	1.41	.09
0.923	5	1.55	.11
12.180	5	1.68	.07
13.845	5	1.69	.34

ETCHANT CONDITIONS : $KMnO_4$ = 65 g/L
NaOH = 20 g/L
43°C ± 2°C
AGITATION = 1500 RPM

TABLE A.2.6 INITIAL ETCH RATE vs CONCENTRATION OF NaOH

CONCENTRATION (g/L)	INITIAL RATE (mmol / m^2 - s)				
	E1	E2	E3	MEAN	ST.DEV
0	0	0	0	0	0
5	0.32	0.34	0.36	0.36	0.02
10	0.58	0.62	0.56	0.59	0.03
15	0.80	0.82	0.80	0.81	0.01
20	0.96	1.02	0.99	0.99	0.03
25	1.05	1.10	1.08	1.08	0.02
30	1.54	1.51	1.57	1.54	0.03
35	1.83	1.88	1.86	1.86	0.02
40	2.05	2.02	2.06	2.04	0.02

ETCHANT CONDITIONS : $KMnO_4$ = 65 g/L
Cr= .015 g/L
43 ± 2 °C
AGITATION RATE = 1500 RPM

TABLE A.2.7 ETCH RATE vs CONCENTRATION OF $KMnO_4$

CONCENTRATION (g/L)	ETCH RATE (mmol / m^2 - s)				
	E1	E2	E3	MEAN	ST.DEV
0	0	0	0	0	0
25	0.83	0.71	0.67	0.74	0.08
40	1.06	1.15	1.25	1.15	0.09
52	1.44	1.39	1.54	1.44	0.08
65	1.51	1.57	1.57	1.54	0.04
76	1.89	1.99	2.12	1.99	0.12
90	2.37	2.40	2.18	2.31	0.12

ETCHANT CONDITIONS: NaOH = 20 g/L
Cr = 0 g/L
43°C
AGITATION RATE :1500 rpm

CONCENTRATION (g/L)	ETCH RATE (mmol / m^2 - s)						
	E1	E2	E3	E4	E5	MEAN	ST.DEV
0.0	1.44	1.51	1.63	-	-	1.54	0.09
0.3	1.25	1.15	1.39	-	-	1.25	0.10
0.5	0.99	1.15	1.06	-	-	1.06	0.08
0.7	0.80	0.90	1.06	-	-	0.93	0.13
1.0	0.48	0.54	0.42	0.47	0.46	0.47	0.04
1.2	0.38	0.35	0.26	0.32	0.35	0.33	0.04
1.3	0.42	0.32	0.22	0.28	0.31	0.31	0.07

ETCHANT CONDITIONS: $KMnO_4$ = 65 g/L
NaOH = 20 g/L
43°C
AGITATION: 1500 rpm

TABLE A.2.9 RESULTS OF BOX-BEHNKEN DESIGN

[NaOH]	[$KMnO_4$]	[Cr]	RATE (mmol / m^2- s)	
			r_i	r
0.75	0.45	0.0096	1.58	1.56
0.75	0.32	0.0096	1.55	1.43
0.25	0.45	0.0096	0.62	1.50
0.25	0.32	0.0096	0.61	0.82
0.75	0.38	0.0190	1.54	0.47
0.75	0.38	0.0000	1.62	1.59
0.25	0.38	0.0190	0.65	0.48
0.25	0.38	0.0000	0.69	1.52
0.50	0.45	0.0190	1.03	0.69
0.50	0.45	0.0000	1.04	1.90
0.50	0.32	0.0190	1.02	1.08
0.50	0.32	0.0000	1.04	1.46
0.50	0.38	0.0096	1.03	1.09
0.50	0.38	0.0096	1.03	1.07
0.50	0.38	0.0096	1.04	1.07

ETCHANT CONDITION:
AGITATION 1500 RPM
43 ± 2°C

TABLE A.2.10 INITIAL ETCH RATE vs TEMPERATURE

TEMPERATURE (°C)	INITIAL RATE (mmol / m^2 - s)				
	E1	E2	E3	MEAN	ST.DEV
20	0.22	0.24	0.21	0.22	0.02
35	0.65	0.68	0.62	0.65	0.02
40	0.99	0.97	1.03	0.99	0.03
50	2.08	1.99	2.02	2.03	0.04
60	2.37	2.32	2.29	2.33	0.03

TABLE A.2.11 FINAL RATE vs TEMPERATURE

TEMPERATURE (°C)	FINAL RATE (mmol / m^2 - s)				
	E1	E2	E3	MEAN	ST.DEV
20	0.78	0.92	0.80	0.82	0.07
35	1.32	1.28	1.35	1.32	0.03
40	1.54	1.56	1.53	1.54	0.02
50	1.80	1.88	1.82	1.83	0.02
60	2.07	2.04	1.95	2.03	0.09

ETCHANT CONDITIONS : $KMnO_4$ = 65 g/L
NaOH= 20 g/L
Cr = 0.015 g/L
AGITATION= 1500 rpm

TABLE A.2.12 INITIAL RATE CONSTANT vs TEMPERATURE

$1/T \times 10^3$ (K)	k_1 (mmol / m^2 - s) *(L/ mol)
3.41	0.44
3.25	1.30
3.19	1.98
3.09	4.06
3.00	4.66

TABLE A.2.13 RATE CONSTANT vs TEMPERATURE

$1/T \times 10^3$ (K)	(mmol/ m^2-s)*(L/ mol)
	k_2
3.41	1.98
3.25	3.19
3.19	3.72
3.09	4.42
3.00	4.90

TABLE A.3.1 3 -LEVEL 3^3 FACTORIAL DESIGN RESULTS

RUN #	ETCH TIME (SEC)			AVERAGE UNDERCUT (N=3) (μm)					
	TCr	Cu	BCr	TCr	s	Cu	s	BCr	s
1	30	30	30	2.5	0.0	0.0	0.0	0.0	0.0
2	30	30	60	5.1	1.3	0.0	0.0	5.0	1.3
3	30	30	90	7.6	1.5	0.0	0.0	0.0	0.0
4	30	60	30	25.4	1.5	25.4	1.5	0.0	0.0
5	30	60	60	25.4	2.5	25.4	2.5	25.4	2.5
6	30	60	90	33.5	2.5	30.5	0.0	30.5	0.0
7	30	90	30	38.1	0.0	38.1	0.0	0.0	0.0
8	30	90	60	38.1	0.0	38.1	0.0	38.1	0.0
9	30	90	90	38.1	0.0	38.1	0.0	38.1	0.0
10	60	30	30	22.9	2.5	22.9	2.5	0.0	0.0
11	60	30	60	22.9	0.0	15.2	0.0	15.2	0.0
12	60	30	90	33.5	2.5	7.6	0.5	7.6	0.7
13	60	60	30	30.5	1.3	30.5	1.3	0.0	0.0
14	60	60	60	33.2	0.0	33.2	0.0	33.2	0.0
15	60	60	90	33.2	0.0	25.4	1.3	25.4	1.3
16	60	90	30	38.1	0.0	38.1	0.0	38.1	0.0
17	60	90	60	38.1	0.0	38.1	0.0	38.1	0.0
18	60	90	90	38.1	0.0	38.1	0.0	38.1	0.0
19	90	30	30	20.3	1.5	20.3	30.5	0.0	0.0
20	90	30	60	7.6	2.5	0.0	0.0	0.0	0.0
21	90	30	90	17.6	2.5	2.5	1.2	2.5	1.2
22	90	60	30	38.1	2.5	38.1	2.5	0.0	0.0
23	90	60	60	33.0	1.2	30.1	1.2	30.1	1.2
24	90	60	90	38.1	0.0	38.1	1.2	38.1	1.2
25	90	90	30	38.1	1.2	38.1	2.2	0.0	0.0
26	90	90	60	38.1	1.2	38.1	2.2	38.1	1.2
27	90	90	90	38.1	0.0	38.1	0.0	38.1	0.0
28	60	60	60	33.1	1.2	33.1	1.2	33.1	0.8
29	60	60	60	30.5	1.2	30.5	1.2	30.5	1.2
30	60	60	60	28.0	1.2	28.0	1.3	28.0	1.2
31	60	60	60	33.0	1.2	33.0	0.7	33.	1.2

TCr : Top Chrome; BCr : Base Chrome.

ETCHANT CONDITIONS - CHROME ETCHANT :
$KMnO_4$ = 65 g/L
NaOH = 20 g/L
43 °C ± 2C
AGITATION = 1500 RPM

COPPER ETCHANT:
$FECl_3$ = 37 %
HCl = 3 %
29 °C±2°C
= 1900 RPM

A.4. STATISTICAL ANALYSIS OF EXPERIMENTAL DATA

A.4.1 Hypothesis Testing

A. Test for Equivalent Variances.

Since specific experimental runs used the same procedure a comparision of the variablity of the data for all runs will be tested at the same time using Bartlett's test for multiple variances [15]. The applicable equations are:

$$C = 1 + \frac{1}{3(n+1)} \left(\sum_{i=1}^{n} \frac{1}{pi} - \frac{1}{\sum_{i=1}^{n} pi} \right) \qquad (A4.1)$$

$$S = \frac{1}{\left(\sum_{i}^{n} pi - n\right)} \sum_{i=1}^{n} (p_i - 1)\, Si^2 \qquad (A4.2)$$

$$\Lambda = \frac{-1}{C} \sum_{i=1}^{n} pi \ln\left(\frac{Si^2}{S^2}\right) \qquad (A4.3)$$

Where : Si^2 = Variance of the ith experiment
S^2 = Pooled variance from A4.2
n = Number of experiments.
pi = Number of trials in ith experiment.

The hypothesis to be tested is :

Ho : $\sigma 0^2 \neq \sigma 1^2 \neq \sigma 2^2 \neq \sigma n^2$
Hl : $\sigma 0^2 = \sigma 1^2 = \sigma 2^2 = \sigma n^2$
α = .05
Stat : = Λ
C.V.: = Chi Square at (α, n-1).

Conclusion : If Stat > C.V. Accept Ho - Variances not equal.

B. Test for Equivalence of Means.

The mean value for each experimental run will be tested for some experiments to determine if the difference between specific experimental runs are significant The applicable equations are :

$$\text{Stat} = t_{(1-\frac{\alpha}{2})} \; Sp \left[\frac{nA - nB}{nAnB} \right]^{\frac{1}{2}} \qquad (A4.4)$$

ν = Degrees of freedom = nA + nB - 2.

Sp = Square root of the pooled variances =

$$\frac{\nu a Sa^2 + \nu b Sb^2}{\nu a + \nu b} \qquad (A4.5)$$

The hypothesis to be tested is :

Ho : $\mu A \neq \mu B$
Hl : $\mu A = \mu B$
α : .05

C.V.: $|\overline{X}A - \overline{X}B|$
Stat: A4.4

Conclusion : Accept Ho if C.V. > Stat. Means are not equal.

C. Test for Surface Roughness Experiments (table A.1.4)

Definition of the terms :

	Ceramic	Glass
Unmetallized	$\overline{X}1$, $S1^2$	$\overline{X}5$, $S5^2$
Base Cr	$\overline{X}2$, $S2^2$	$\overline{X}6$, $S6^2$
Cu	$\overline{X}3$, $S3^2$	$\overline{X}7$, $S7^2$
Top Cr	$\overline{X}4$, $S4^2$	$\overline{X}8$, $S8^2$
	n = 4	n = 4
	pi = 10	pi = 10

The results for the Bartlett's test are:

Ceramics	Glass
C = 1	C = 1
S^2 = .000067	S^2 = 6.2
Λ = 3.4	Λ = 2.9
Stat = 7.81	Stat = 7.81
Conclusion : Ho Rejected	Ho Rejected

Thus the variance in the experimental data is equivalent within 95 % confidence level.

The results for the t-test for equivalent means are:

$\mu 1 \neq \mu 2$, $\mu 2 \neq \mu 3$, $\mu 3 = \mu 4$, $\mu 5 \neq \mu 6$, $\mu 6 \neq \mu 7$, $\mu 7 = \mu 8$.

Thus the surface roughness of each layer is different within 95 % confidence.

D. Test for the Agitation Rate experiments: (table A.2.2)

The test for equivalent variances and means was performed to determine stastically if the rate data at an rpm less than 1100 was different from the rate data above 1100 rpm. If the data is different then it would indicate that the system is in kinetic control at an rpm greater than 1100.

The various conditions are defined as follows:

rpm = 0	$\bar{X}1$, $S1^2$
= 700	$\bar{X}2$, $S2^2$
= 900	$\bar{X}3$, $S3^2$
= 1100	$\bar{X}4$, $S4^2$
= 1300	$\bar{X}5$, $S5^2$
= 1500	$\bar{X}6$, $S6^2$
= 1700	$\bar{X}7$, $S7^2$

For the Bartlett's test the following resulted:

C = 1.07
S^2 = .018
Λ = 9.8

Stat = 12.59 @ 95%
Conclusion: Ho rejected- the variances are equal.

The results for the t-test are as follows:

$\mu 1 \neq \mu 2$, $\mu 2 \neq \mu 3$, $\mu 3 \neq \mu 4$, $\mu 4 = \mu 5$, $\mu 5 = \mu 6$, $\mu 6 = \mu 7$.

This indicates that there is kinetic control at an rpm after 1100 since the rates are equivalent at 1100, 1300, 1500 rpm respectively and are different at 0, 700, 900 and 1100 rpm respectively.

E. Test for the Surface Roughness vs Rate Experiments. (table A.2.4)

The test for equivalent variances and means was performed to determine if the rate data at various surface roughnesses are different. The various conditions are defined as follows:

Ra = .064	$\bar{X}1$,	$S1^2$
= .135	$\bar{X}2$,	$S2^2$
= .923	$\bar{X}3$,	$S3^2$
= 12.2	$\bar{X}4$,	$S4^2$
= 13.9	$\bar{X}5$,	$S5^2$

For the Bartlett's test the following resulted:

$c = 1.2$
$S^2 = .013$
$\Lambda = 7.5$
Stat = 13.70 @ 95%
Conclusion: Ho rejected- the variances are equal.

The results for the t-test are as follows:

$\mu 1 \neq \mu 2$, $\mu 2 \neq \mu 3$, $\mu 3 \neq \mu 4$, $\mu 4 = \mu 5$.

This indicates that at high surface roughness the rates are equivalent and thus surface roughness is not an important factor influencing the etching rate.

A.4.2 Analysis of Variance for Statistical Models

A. General Terms and Hypothesis to be Tested.

In all cases in the following analysis, the hypothesis to be tested is one where the lack of fit of the model (MSr) is compared to the error in the data (MSe) due to the regression equation. The hypothesis is as follows:

$$\text{Ho} : \theta_r^2 < \theta_e^2$$
$$\text{Hl} : \theta_r^2 \geq \theta_e^2$$
$$\text{Stat} : \text{MSr} / \text{MSe}$$
$$\text{C.V.}: F(\nu r, \nu e) \text{ at } .05/2$$
$$\text{Conclusion} : \text{If stat} < \text{C.V. Then the model fits.}$$

To test the significance of the coefficients, the t-sig value given in the ANOVA table is compared to alpha = .05. If t-sig is greater than .05 the coefficient is insignificant and should be dropped from the model.

B. Experiment to Determine the Effect of [NaOH], [$KMnO_4$] and [Cr] on the rates.

The effect of the above concentration variables on the rates ri and r were determined from the experimental data. A 3 variable , 2 level Box-Behnken design with three replicates at the center was used at the experimental design. The conditions for each concentration are as follows:

		Range in mol / L		
		-1	0	+1
Ca	[NaOH] =	.25	.50	.75
Cb	[$KMnO_4$] =	.32	.38	.45
Cc	[Cr] =	0.00	.0096	.019

i. Model for r_i :

A linear model of the form :

$$r_i = b_0 + b_1 C_a + b_2 C_b + b_3 C_c \qquad (A4.6)$$

was fitted for the experimental data. The resulting relationship is :

$$r_i = 0.11 + 1.86 C_a + 0.11 C_b - 0.97 C_c \qquad (A4.7)$$

The ANOVA table for this model is as follows:

SOURCE	SUM OF SQUARES	DF	MEAN SQUARES
REGRESSION	1.73	3	0.577
LACK OF FIT	0.02	8	0.0025
ERROR	0.01	3	0.0033
TOTAL	1.75	14	

The hypothesis to be tested is therefore :

$$Ho : \theta r^2 < \theta e^2$$
$$H1 : \theta r^2 \geq \theta e^2$$

Stat : MSr / MSe = .0025/.0033 = .76

C.V.: F (8,3) at .05/2 = 8.84

Conclusion : Stat < C.V. thus the model fits.

The test for the significance of the coefficients yielded

	t-SIG	Alpha = .05
b1	0.000	keep
b2	.6959	drop
b3	.6385	drop

The data was re-run through IBM STATPAK with b2,b3 dropped. The resulting model for r_i is :

$$r_i = 1.86 C_a + 0.01 \qquad (A4.8)$$

When the model is re-run with b2,b3 dropped the coefficient of Ca is the same indicating that the data is orthogonal.

ii. Non-linear Model for r_i.

A non linear model of the form :

$$r_i = k\, C_a^{\alpha}\, C_b^{\beta}\, C_c^{\gamma} \qquad \text{(A4.9)}$$

The resulting model for r_i of a non linear forms is:

$$\ln r = 0.63 + .79\ \ln C_a + .031 \ln C_b - .011 \ln C_c \qquad \text{(A4.10)}$$

An analysis of variance was perforemed on the model similar to that in i. The ANOVA showed that the model fit the data and the coefficients b2 and b3 were insignificant. The final model with the b2 and b3 dropped is :

$$r_i = 1.87\ C_a^{0.79} \qquad \text{(A4.11)}$$

To check whether the coefficient of Ca spanned unity the confidence interval was claculated to be:

$$0.66 \leqslant b1 \leqslant 1.004$$

Therefore the order of the first reaction was taken to be unity. To further confirm this hypothesis, the predicted data for the two models was plotted and indeed the linear model fit the experimental data better.

iii Linear Model of r.

A linear model of the form in equation A4.6 was fitted to the data. The resulting relation :

$$r = .16 + .34 C_a + 3.4 C_b - 54 C_c \qquad \text{(A4.12)}$$

The resulting analysis of variance table is :

SOURCE	SUM OF SQUARES	DF	MEAN SQUARES
REGRESSION	1.58	3	0.527
LACK OF FIT.	0.03	8	0.0038
ERROR	0.01	3	0.0033
TOTAL	1.62	14	

The hypothesis to be tested is therefore :

$$Ho : \theta_r^2 < \theta_e^2$$
$$H1 : \theta_r^2 \geq \theta_e^2$$

Stat : MSr / MSe = .0025/.0033 = 1.13

C.V.: F (8,3) at .05/2 = 8.84

Conclusion : Stat < C.V. thus the model fits.

The test for the significance of the coefficients yielded :

	t-SIG	Alpha = .05
b1	.2814	drop
b2	.0144	keep
b3	.0000	keep

The last result indicates that the rate in region II of figure 3.1 is only dependent on the $[KMnO_4]$ and [Cr] concentrations.

iv Non- linear Model for r.

A non-linear model of the form in equation A4.9 was run with the experimental data. The resulting equation is :

$$r = 1.08\ C_a^{0.14}\ C_b^{0.33}\ C_c^{-0.07} \qquad (A4.13)$$

The ANOVA table for this model is :

SOURCE	SUM OF SQUARES	DF	MEAN SQUARES
REGRESSION	0.71	3	0.238
LACK OF FIT	1.67	8	0.209
ERROR	0.19	3	0.021
TOTAL	2.57	14	

The hypothesis to be tested is therefore :

$$Ho : \theta_r^2 < \theta_e^2$$
$$Hl : \theta_r^2 \geq \theta_e^2$$

Stat : MSr / MSe = .209/.02 = 10.45

C.V.: F (8,3) at .05/2 = 8.84

Conclusion : Stat > C.V. thus the does not fit.

The analysis of variance has shown that the model did not fit the data nor were any of the coefficients significant. Thus the linear first-order model seems to represent the data for the rate of Cr dissolution.

C. Statistical Modeling of the Cr/Cu/Cr Undercut.

A. Description of Experimental Design.

The effect of Cr and Cu etch times on the top chrome, copper, and base chrome undercuts was determined experimentally. The data for the experiments and the etchant conditions are tabulated in table A.3.1.

A 3 level -3^3 factorial experimental design with four replicates at the center was used to derive stastical models from the experimental data which can be used to predict the resist undercut of the three levels of metallurgy based on the knowledge of the etch time. The nomenclature that will be used for the following statistical analysis is:

U_1 = Top Chrome undercut. (μm)

U_2 = Copper undercut. (μm)

U_3 = Base Chrome undercut (μm).

T_1 = Top Chrome etch time (sec).

T_2 = Copper etch time (sec).

T_3 = Base chrome etch time (sec).

The range in the independant variables for the experiments are :

	-1	0	+1
T_1 :	30	60	90
T_2 :	30	60	90
T_3 :	30	60	90

i) Model for U_1.

A linear first order model for U1 was fitted to the data. The resulting equation for U1 is :

$$U_1 = -0.93 + 0.12T_1 + 0.36T_2 + 0.03T_3 \qquad (A4.14)$$

The ANOVA table for this model is :

SOURCE	SUM OF SQUARES	DF	MEAN SQUARES
REGRESSION	2314	3	771.0
LACK OF FIT	948	23	41.2
ERROR	146	4	36.5
TOTAL	3408	30	

The hypothesis to be tested is therefore :

$$Ho : \theta^2_r < \theta^2_e$$
$$Hl : \theta^2_r \geq \theta^2_e$$
$$Stat : MSr / MSe = 41.2 / 36.5 = 1.13$$
$$C.V.: F(23,4) \text{ at } .05/2 = 5.77$$

Conclusion : Stat < C.V. thus the model fits.

The test for the significance of the coefficients yielded

	t-SIG	Alpha = .05
b1	.02	keep
b2	.00	keep
b3	.01	keep

Since all the coefficients are significant the model shown in equation A4.14 is the final model for U1.

ii) Model for U_2.

A linear first order model for U_2 was fitted to the data. The resulting equation for U_2 is :

$$U2 = -5.91 + 0.09T_1 + 0.51T_2 + 0.06T_3 \qquad (A4.15)$$

The ANOVA table for this model is :

SOURCE	SUM OF SQUARES	DF	MEAN SQUARES
REGRESSION	4371	3	1457.0
LACK OF FIT	1026	23	44.6
ERROR	200	4	20.0
TOTAL	5597	30	

The hypothesis to be tested is therefore :

$$H_o : \theta^2_r < \theta^2_e$$
$$H_1 : \theta^2_r \geq \theta^2_e$$
$$\text{Stat} : MS_r / MS_e = 44.6/50 = .89$$
$$\text{C.V.}: F(23,4) \text{ at } .05/2 = 5.77$$

Conclusion : Stat < C.V. thus the model fits.

The test for the significance of the coefficients yielded :

	t-SIG	Alpha = .05
b1	.11	drop
b2	.00	keep
b3	.26	drop

Since b1 and b3 are insignificant the final model for U2 relating copper undercut to etch time is therefore:

$$U_2 = -5.91 - 0.51T_2 \qquad \text{(A4.16)}$$

iii) Model for U_3.

A linear first order model for U_3 was fitted to the data. The resulting equation for U_3 is :

$$U_3 = -29.1 + 0.03T_1 + 0.45T_2 + 0.39T_3 \qquad \text{(A4.17)}$$

The ANOVA table for this model is :

SOURCE	SUM OF SQUARES	DF	MEAN SQUARES
REGRESSION	5506	3	1835.0
LACK OF FIT	1882	23	81.8
ERROR	1061	4	265.3
TOTAL	8849	30	

The hypothesis to be tested is therefore :

$$Ho : \theta_r^2 < \theta_e^2$$
$$H1 : \theta_r^2 \geq \theta_e^2$$

Stat : MSr / MSe = 81.8/265.3 = .31
C.V.: F (23,4) at .05/2 = 5.77
Conclusion : Stat < C.V. thus the model fits.

The test for the significance of the coefficients yielded :

	t-SIG	Alpha = .05
b1	.76	drop
b2	.00	keep
b3	.01	keep

The resulting model for U3 is a function of T2 and T3 only thus resuling in the final equation relating base Cr undercut to etch time:

$$U_3 = -29.1 + 0.45T_2 + 0.33T_3 \qquad (A4.18)$$